博士学位論文

Research on Smart Condition Diagnosis System of Production Equipment - Intelligent Vibration Signal Processing Method for Condition Diagnosis of Rotating Machinery –

（生産設備のスマート状態診断システムに関する研究 −回転機械状態診断のための知的振動信号処理方法−）

三重大学大学院　生物資源学研究科
共生環境学専攻　環境・生産科学講座
環境情報システム工学教育研究分野
宋 雪瑋

Abstract

Rotating machinery is an important and indispensable engineering equipment in industries such as electric power, petrochemical, metallurgy, rail transit and marine ships. Once fault occurs, not only the rotating machinery itself is damaged, so serious that it led to economic losses, major accidents, and life-threatening. With the development of the industrial intelligence, the fault diagnosis of rotating machinery based on vibration signal is becoming more and more extensive application. However, due to the complication of rotary machinery, bad working environment, and variable operating conditions, the vibration signal acquired by the acceleration sensor has the characteristic of non-stationarity, non-linearity, and complexity. At the same time, affected by factors such as transmission loss, signal attenuation, and strong background noise, the regularity fault impact contained in the vibration signal is further weakened. The fault characteristic frequency in the spectrum is more difficult to extract, and it is more difficult to realize the accurate fault diagnosis of rotating machinery. Therefore, the research on effective vibration signal processing method for rotating machinery fault diagnosis has important engineering application significance.

Aiming at the key problems that urgently need to be solved in the signal processing of rotating machinery fault diagnosis, such as suppressing background noise and enhancing fault feature information, the thesis carried out the research about signal fault impact enhancement, signal non-stationarity decomposition, signal adaptive filtering and signal image conversion. By analyzing the rotating machinery vibration signals under different working conditions, the characteristics of the signal are deeply studied, and the corresponding signal processing methods are proposed in a targeted manner. The specific research contents are as follows:

(1) Aiming at the problems of strong background noise and submerged regular impact in vibration signals, a signal processing method based on weighted kurtosis variational modal decomposition (VMD) and improved frequency-weighted energy operator (IFWEO) is proposed. Firstly, the raw signal is decomposed by VMD, and the weighted kurtosis is employed to select the intrinsic mode function (IMF) optimally to reconstruct the signal. The reconstructed signal will carry abundant fault information. Secondly, a third-order cumulant method is introduced to improve the frequency-weighted energy operator (FWEO), which could strengthen the signal impulse and enhance the fault feature. The IFWEO could better effectively reduce the noise impact. Finally, the method is validated in low-speed bearing fault diagnosis.

(2) Aiming at the non-stationary and non-linear of vibration signal, this chapter proposed a signal filtering and fault characteristic enhancement method based on reconstruction adaptive determinate stationary subspace filtering (Rad-SSF) and enhanced third-order spectrum to address the above-mentioned problems. In particular, Rad-SSF reconstructs an adaptive self-determined and decomposed vibration signal trajectory matrix to obtain the non-stationary signals. Thereafter, the filtered signal with the best fault characteristics is extracted according to the kurtosis. Meanwhile, a 1.5-dimensional third-order energy spectrum is performed to enhance the fault characteristics by strengthening the fundamental frequency and eliminating non-coupling harmonics. Finally, the method is validated in high-speed bearing fault diagnosis.

(3) To solve the problem where the actual rotating frequency and its harmonics cannot be accurately extracted in engineering applications, an improved adaptive multi-band filtering method is designed. This method takes the theoretical rotating frequency as the search center, extracts the maximum within the positive and negative deviation as the actual rotating frequency, and sets a threshold according to the actual value to realize

multi-band filtering. This method can effectively remove background noise and accurately extract the actual rotating frequency and its harmonics. This model can automatically extract the in-depth features of the filtered signal and improve the fault classification accuracy. Finally, the method is validated in rotating machinery abnormal structure fault diagnosis.

(4) Aiming at the problem that the discrimination between fault categories is not obvious after one-dimensional vibration signal is converted to two-dimensional image, an incrementally accumulated holographic symmetrical dot pattern (SDP) characteristic fusion method is proposed in this chapter. The current study simultaneously extracts the time- and frequency-domain characteristic parameters of vibration signal based on the incremental accumulation method to avoid inconspicuous difference and small discrimination generated by a single parameter. Subsequently, the extracted characteristic signals are transformed into a 2D image based on the SDP method to enhance the differences between signals. Finally, the method is validated in rotating machinery bearing fault diagnosis.

The vibration signal processing methods of rotating machinery proposed in this thesis have been verified by simulation experiments and engineering experiments, and the verification results prove that the proposed methods can realize effective and targeted signal processing.

The main contribution of this thesis is to propose the corresponding signal processing method according to the unique characteristics of vibration signals under different operating conditions and the actual engineering application of rotating machinery fault diagnosis, which effectively suppresses the background noise, enhances the fault characteristic signal, and increases the discrimination between fault types.

Concent

Chapter 1 Introduction

1.1 Background and significance of rotating machinery fault diagnosis

Rotating machinery is usually composed of bearings, gears, transmission mechanisms, and motors, with the advantage of integration, complexity, and stability [1-3]. As the most widely used mechanical equipment in industry, it plays an important role in aerospace, energy, electric power, transportation, petrochemical, and other industrial fields [4-6]. In recent decades, with the rapid development of science and technology, rotating machinery is developing towards large-scale, precision, automation, and intelligence [7, 8]. However, in the harsh working environment of high-speed, high-load, and high-temperature, the number of faults of rotating machinery is much higher than that of other industrial equipment [9-12]. As the key equipment of large-scale industry, once fault occurs to rotating machinery, it will cause sudden shutdown and stoppage of the whole production line, resulting in huge economic losses, even serious cause the tragedy of machine destruction and human death [13-15]. Most rotating machinery has complex structures, and the fault is often the result of the joint action of many factors [16], all of which increase the difficulty of fault diagnosis. At present, regular maintenance of rotating machinery is a common method to ensure the normal operation of equipment. However, this method causes excessive maintenance in the early stage of the rotating machinery life cycle and insufficient maintenance in the later period. At the same time, the regular maintenance based on disassembly method not only consumes time and energy, but also may cause rotating machinery abnormalities. Therefore, it is of great significance to carry out intelligent diagnosis of rotating machinery.

In recent years, many scholars have carried out scientific research in the fault diagnosis of rotating machinery, and successfully designed some condition monitoring and fault diagnosis systems dedicated to engineering application. Those methods play a positive role in guaranteeing the healthy operation of rotating machinery, reducing regular maintenance costs, and enhancing production efficiency of industry. Those fault diagnosis research is mainly divided into two categories:

1) The method based on extracting the fault characteristic frequency. This method mainly studies signal filtering, signal decomposition, and the envelope spectrum, among others [17-20]. In reference [21], considering the rotating machinery has the characteristic of non-linear working conditions and unknown background noise, a statistical filtering method for vibration signal feature extraction is designed based on the central limit theory, it can significantly improve the performance of fault classification. In reference [22], the multiscale clustering grey infogram is used to diagnose the local faults of rotating machinery, and the Fourier spectrum of vibration signal is decomposed into multiple scales with different initial resolutions. At the same time, both time- and frequency-domain spectral negentropies are taken into account to guide the clustering through grey evaluation of both negentropies. In reference [23], a time-frequency analysis method based on ensemble local mean decomposition (ELMD) and fast kurtogram (FK) is proposed for rotating machinery fault diagnosis. This method has the capability to decompose multicomponent modulation vibration signal into a series of demodulated mono-components, and the selected product functions signal is further filtered by an optimal band-pass filtering based on FK to extract impulse signal. In reference [24], a signal feature extraction and fault diagnosis method based on statistic filtering (SF) and wavelet package transform (WPT) combined with moving-peak-hold method (M-PH) is proposed. The SF is first used to adaptively cancel noises, and then fault

detection is performed by exploiting the optimum symptom parameters in a time-domain to identify a normal or fault state low-speed machinery.

2) The feature self-extraction diagnosis method based on deep learning models, such as the deep belief network (DBN), convolutional neural network (CNN), and stacked autoencoder (SAE) [25-28]. In this method, the characteristics of the input signal are adaptively extracted to achieve accurate fault diagnosis. In reference [29], the deep convolutional network (DCN) is used to establish the rotating machinery fault diagnosis model. Based on the multiscale information extraction capability of the WPT method, a vibration signal is subjected to pyramid wavelet packet decomposition, and each sub-band coefficient is used as the input for each channel of a DCN. In reference [30], it provides a comprehensive review of artificial intelligence (AI) algorithms in rotating machinery fault diagnosis, from both the views of theory background and industrial applications. This review presented a brief introduction of k-nearest neighbor, naive Bayes, support vector machine, artificial neural network and deep learning, and discussed the advantages, limitations, practical implications of different AI algorithms, as well as some new research trends. In reference [31], a new intelligent method based on deep neural networks (DNNs) is proposed to diagnose rotating machinery faults. In this method, DNNs with deep architectures, instead of shallow ones, could be established to mine the useful information from raw data and approximate complex non-linear functions. The diagnosis results show that the proposed method is able to not only adaptively mine available fault characteristics from the measured signals, but also obtain superior diagnosis accuracy. In reference [32], a CNN based fault diagnosis method for rotating machinery is proposed. Both temporal and spatial information of the raw data from multiple sensors is considered during the training process of the CNN. Representative features can be extracted automatically from the raw signals and avoids manual feature extraction or selection.

Although the abovementioned literatures have been realized the fault diagnosis of rotating machinery, with the mechanical equipment becoming larger, more continuous and more automatic, the technology of fault diagnosis has been demanded higher. In addition, under the strong background noise, the regular impact signal caused by faults in vibration signals is submerged, and the fault characteristics are difficult to accurately extract, which brings challenges to the fault diagnosis of rotating machinery [33-35]. Therefore, aiming at the problems of strong background noise, large external disturbances, and weak fault characteristics, it is of great significance for engineering applications to study signal processing methods that can effectively suppress noise, enhance fault characteristics frequency, and improve fault recognition rate.

1.2 Literature review

Rotating machinery fault diagnosis is an emerging interdisciplinary technology that integrates machinery, mechanics, mathematics, signal analysis and processing, and computer technology. It has very important engineering application value for the research of this kind of technology. The fault diagnosis of rotating machinery mainly includes signal acquisition, signal processing, feature extraction, and fault recognition [36], in which signal processing is the key to improve the diagnostic accuracy [37-39]. The premise of accurate fault diagnosis of rotating machinery is to timely acquire the current state information of the equipment, such as vibration signal [40], acoustic emission signal [41,42], and instantaneous angular speed [43]. Among them, vibration signals can provide equipment status information timely and accurately, and can be monitored permanently or intermittently, which has obvious advantages [44,45].

Traditional rotating machinery vibration signal processing methods are mainly divided into three categories: time-domain, frequency-domain, and time-frequency domain analysis [46]. The time-domain analysis method is to diagnose the fault by calculating the statistics of the vibration

signal, including dimensional parameters such as peak-value, mean-value, mean-square-value, variance, etc., and dimensionless parameters including margin, skewness, kurtosis, divergence, etc. [47,48]. Dimensionless parameters are mostly suitable for non-stationary vibration signals. In engineering applications, dimensionless parameters such as kurtosis and divergence are commonly used for fault diagnosis of signals with obvious impact characteristics of rotating machinery. However, time-domain signal statistics characters are easily affected by the changes of speed and load, so it is not suitable for quantitative analysis. The frequency-domain analysis method mainly refers to the Fourier transform of the vibration signal to obtain its spectrum [49], and it also includes the envelope spectrum, cepstrum, higher-order spectrum and holographic spectrum. Among them, envelope spectrum analysis is the most widely used in vibration signal fault diagnosis [50, 51]. The time-frequency domain analysis [52, 53] is mainly based on short-time Fourier transform (STFT), Wigner-Ville distribution (WVD), wavelet transform (WT) and Hilbert-Huang transform. This time-frequency analysis method provides the joint distribution information of time domain and frequency domain of vibration signal, and can clearly describe the relationship between the frequency and the time change.

The vibration signals acquired under different engineering working conditions usually contain multiple resonance frequency bands and complex frequency components, the global characteristics of Fourier transform have certain limitations in such signals [54, 55]. Therefore, it is necessary to reduce the influence of the interference frequency to effectively diagnose the rotating machinery faults.

1.2.1 Signal filtering method

Filtering methods based on setting the best center frequency and frequency band [56, 57], including a high-pass filtering, a low-pass filtering, a band-pass filtering, a kurtogram [58], and an infogram [59]. High-pass filtering, low-pass filtering and band-pass filtering are simple and effective vibration signal filtering methods. They are widely used in engineering because they have the advantages of small calculation, simple algorithm, and short running time.

Some filtering methods based on artificial intelligence algorithm, such as genetic algorithm (GA). In reference [60], the optimal cut-off frequency of the high-pass filtering is determined using a combination of GA and tabu search, and the bearing fault is properly diagnosed using the possibility theory and fuzzy reasoning. This method achieved certain results in some signal filtering, but it has disadvantages, such as difficulty in parameter adjustment and high algorithm complexity.

In order to both reflect the strength of signal transient impact and indicate the signal frequency, Dwye proposed the concept of spectral kurtosis (SK) based on the statistical signal processing method. According to this, a method, such as kurtogram, and infogram, is developed for finding the best cut-off frequency. Reference [61] proposed a filtering method based on kurtogram and frequency domain correlation kurtosis. The frequency folding problem caused by down-sampling was solved by frequency sequencing, and the maximum value in the correlation kurtogram demonstrated the best frequency band for envelope analysis. Reference [62] proposed an ALKurtogram (ALK), which aligns the traditional fast kurtogram frequency division strategy with the average local kurtosis. The ALK measures the target component local and global impulsivity and essentially makes up some shortcomings of fault feature extraction under multi-interference conditions in previous methods. However, the difficulty of those filtering method is to accurately set the cut-off frequency. Researchers need to have a priori knowledge about the characteristics of signal frequency, otherwise the inappropriate parameter setting will make the filtering result very poor.

WT [63] is widely used in frequency domain analysis of rotating machinery, mainly including wavelet transform modulus maximum denoising, wavelet coefficient correlation denoising and wavelet threshold denoising. Reference [64] used continuous wavelet transform (CWT) and sparse measurement (SM) to detect and characterize the resonance caused by gear faults.

1.2.2 Signal decomposition method

In order to realize adaptive signal filtering, a new signal processing method, empirical mode decomposition (EMD), creatively proposed by NE Huang at NASA in 1998. It is especially suitable for the analysis of non-linear and non-stationary vibration signals. EMD [65-67] and its improved algorithms complementary ensemble empirical mode decomposition (CEEMD), complete ensemble empirical mode decomposition adaptive noise (CEEMDAN), etc. are applied to decompose the bearing fault signal. The reference [68] proposed an EMD filtering based on adaptive optimization time-varying to extract clear and rich bearing early fault features. This method can remove background noise and extract the fault characteristic frequency accurately. However, the adaptiveness should be studied further. In reference [69], the EMD is used to decompose the equally-divided vibration signals into several intrinsic mode function (IMF) components, and the rolling bearing fault types classification is realized by combining the symmetrized dot pattern (SDP) image with improved Manhattan distance. In reference [70], a novel fault diagnosis method combining CEEMD, probabilistic neural network (PNN) and particle swarm optimization (PSO) algorithm is proposed. In this method, the vibration signals are decomposed into a number of IMFs by the CEEMD algorithm since it has good adaptive ability to nonstable signals and can effectively extract fault features. In reference [71], considering the non-linear and non-stationary characteristics of rolling bearing vibration signals, a signal processing method based on CEEMDAN, refined composite multi-scale fuzzy entropy (RCMFE), Laplace score (LS), and PSO-PNN is proposed. CEEMDAN is used to decompose the vibration signal, and select the IMF containing the primary fault information via the frequency domain correlation coefficient method. Those methods work well in some conditions, but the EMD uses cubic spline interpolation to fit the envelope, which has obvious shortcomings such as over-envelope, under-envelope, end effect and mode mixing, resulting in distortion of the IMF components decomposed from the original signal. Although their improved methods could alleviate the above deficiencies, they still introduce new problems, such as the white noise cannot be completely neutralized and resulting in false components, therefore, the fault feature extraction is still seriously affected under strong background noise.

Other adaptive decomposition methods, include local mode decomposition (LMD), adaptive local iterative filtering (ALIF), intrinsic timescale decomposition (ITD), variational mode decomposition (VMD) and their improvement methods，have also been well developed in rotating machinery fault diagnosis. LMD [72, 73] could self-adaptively decompose a complicated multi-component signal into a set of product function (PF) components, each of which is the product of an envelope signal and a purely frequency modulated signal. The local mean function and envelope function are calculated by the moving averaging method according to the local extreme points. Reference [74] proposed a time-frequency analytical method of ensemble LMD, which can effectively alleviate mode mixing, but it still retains a large amount of noise in the filtered signal. In reference [75], an early bearing fault diagnosis method, local mean decomposition-based multilayer hybrid denoising (LMD-MHD), is proposed for extracting the weak fault features under strong background noise. LMD is a novel self-adaptive time-frequency analysis method, and is thus particularly suitable for processing of multicomponent amplitude-modulated and frequency-modulated signals. But the construction of local mean function and envelope function in the LMD algorithm plays an important role in the accuracy of the PF components it

extracts, the moving averaging method may cause phase error of the functions after several iterations, which has an adverse effect on the accuracy of PF components.

ALIF constructs an adaptive filtering through the Fokker-Planck equation, it can effectively solve the noise sensitivity and modal aliasing problems in the adaptive decomposition algorithm. In reference [76], the ALIF is used to decompose the vibration signal, and best IMF is selected according to the multiscale entropy features to realize bearing fault diagnosis. In reference [77], the ALIF is combined with Teager energy operator (TEO) to realize the fault characteristic frequency extraction of bearing rolling elements early faults. Although the ALIF used in the bearing fault signals decomposition is more and more widespread, there still some problems need to be resolved such as large amount of calculation, unstable convergence, and easy to fall into local loops.

The ITD [78, 79] method adopts the form of linear transformation to decompose the signal, it could adaptively decompose any complex signal into a sum of several proper rotation components (PRCs) independent of each other, and its instantaneous frequency has physical meaning. In reference [80], a new method called intrinsic time-scale decomposition-based sparse coding shrinkage (SCS) (named ITD-SCS) is proposed as a sparse representation for impulse component extraction from bearing vibration signals. ITD can decompose the signal into a set of proper rotations (PRs) to enable impulse components as prominent as possible. In reference [81], based on the linear transformation and cubic spline interpolation of the ITD method, an improved intrinsic time scale decomposition method (IITD) is proposed, which is combined with spectral kurtosis to realize the intelligent diagnosis of bearing fault. The definition of the baseline in the ITD method is based on the linear transformation of the signal itself, and there is an evident signal distortion starting from the second component.

VMD [82, 83] is an effective decomposition method. VMD can complete the adaptive division of the frequency band according to the frequency characteristics of the signal itself, and it is suitable for the separation of multi-component non-stationary signals. VMD is a generalization of the classical Wiener filtering for adaptive, multiple bands and is somewhat more robust to noise. It has the advantages of high precision, fast decomposition speed and strong robustness. Reference [84] proposed an independence-oriented VMD method. The number of IMFs is determined by the approximately complete reconstruction criterion to overcome the information loss and over-decomposition. Reference [85] uses VMD to decompose the vibration signal and extracts the IMF component containing the best fault information based on the weighted kurtosis index. The spectral kurtosis filtering method can help the decomposition algorithm in extracting the best IMF, but this approach cannot work efficiently when a higher impulse is present. In Reference [86], a vibration signal-based hybrid diagnostic method is proposed to realize fault diagnosis of general gearboxes. VMD was adopted to realize adaptive signal decomposition and wolf grey optimizer (GWO) was applied to optimize parameters of VMD. However, the signal decomposition filtering has certain limitations, including breakpoint effects and modal aliasing. Although the noise can be filtered out, it also inevitably weakens the energy of useful signals, and finally the signal-to-noise ratio (SNR) is lower, which affects the fault diagnosis accuracy.

1.2.3 Signal enhancement method

The vibration signal acquired by the acceleration sensor is often a mixed signal generated and superimposed by the common vibration of rotating machinery multiple structures. After these complex vibration signals reach the rotating machinery surface through different transmission paths, the signals interfere and couple with each other. In addition, the impact signal containing fault information is often interfered by the structural vibration and background noise of the machine itself, making most of the fault signals very weak. It is difficult to ensure the accuracy

of fault identification by directly using the signal acquired by the sensor. Therefore, in engineering application, it is particularly important to enhance the fault impact signal of rotating machinery. TEO [87-90] is an effective signal feature enhancement method, and it could analyze the signal time-frequency characteristics, it is often used to analyze and track the narrowband signal energy. This method could effectively improve the signal impulse, and it has the advantages of simple algorithms and response quickly. In reference [91], TEO is used for low-speed bearing fault feature extraction, according to its good time resolution and adaptive ability of transient signal changes. Although the TEO has the advantage of enhancing the signal impulse, it also has the disadvantages of low demodulation accuracy and substantial noise interference. In order to improve the shortcomings of TEO, the central finite difference method was introduced into it [92], the improved TEO could overcome the problem of low demodulation accuracy, but it is still greatly bad affected by strong background noise. In reference [93], an alternative bearing fault extraction method based on fast iterative filtering decomposition (FIFD) and symmetric difference analytic energy operator (SDAEO) is proposed. The enhanced demodulation technology, SDAEO, is used to detect the bearing fault features from the selected IMF. In reference [94], a higher order energy operator fusion (HOEO-F) method is proposed for bearing fault detection. In this method, multiple high-order energy operators are fused to form a simple transformation to process the bearing signal obscured by noise and vibration interference. Frequency-weighted energy operator (FWEO) as an improved TEO method is proposed in [95], it can assess instantaneous energy, and improve the analytic performance, but it still imperfect when signals have strong noise.

1.2.4 Signal transition method

The time-frequency domain analysis method can characterize the relationship between the frequency of the signal and time, and is more suitable for processing non-linear and non-stationary vibration signals. The commonly used time-frequency transform methods include STFT [96, 97], CWT [98, 99] and WVD [100, 101] etc. In reference [102], a time-frequency procedure incorporating a new feature extraction step that combines the classical wavelet packet decomposition energy distribution technique and a new feature extraction technique based on the selection of the most impulsive frequency bands is proposed. In this method, the most useful sub-bands are represented in the time-frequency domain by using STFT algorithm for knowing exactly what the frequency components presented in those frequency sub-bands are. In reference [103], an optimized deep learning structure is constructed for bearing fault diagnosis based on the simple spectral matrix obtained by STFT. In this method, the sensor signal is preprocessed by STFT for effectively mining features from big data and accurately identifying the bearing health conditions. However, STFT requires researchers to manually select the window function that changes with time. Meanwhile, limited by Heisenberg uncertainty law, it has high requirements for the selection of window function, and it is more suitable for analyzing linear and slowly varying signals.

In reference [104], a data-driven intelligent fault diagnosis approach for rotating machinery based on a novel continuous wavelet transform-local binary convolutional neural network (CWT-LBCNN) model is proposed. The proposed approach builds an end-to-end diagnosis mechanism, and does not need manual feature extraction. By feeding the inputting vibration signal, features are captured adaptively and fault condition of rotating machinery is diagnosed automatically. In reference [105], the CWT and time domain signal analysis methods are used for feature extraction of the recorded acoustic emission signals. In this method, GAs in combination with artificial neural networks (ANN) are applied to select and classify the extracted features. Although CWT can take into account both time and frequency characteristics, and filter the background noise well, there is information omission in the processing of high-frequency signal. At the same time,

the selection of the wavelet basis is difficult, and different wavelet bases produce different results.

WVD is a bilinear time-frequency distribution algorithm, it has the advantages of good time-frequency resolution and concentrated energy. It is a representative algorithm in quadratic time-frequency distribution, and it can satisfy the time-frequency edge. In reference [106], a methodology based on LMD and WVD is proposed to get more reliable bearing fault diagnosis based on vibration signals. WVD has the advantages of excellent resolution and localization in time-frequency domain. In reference [107], a novel fractional-order smoothed pseudo Wigner-Ville distribution (FrSPWVD) is proposed to solve the problem of low time-frequency resolution when suppressing cross-term interference. In this method, the signals are analyzed by FrSPWVD, and the parameters of original signals are accurately extracted according to the corresponding appropriate fractional order and fractional frequency of signals. However, the cross term will interfere with it when using WVD to analyze the multi-component signals.

The SDP method can reflect the difference between signals because it can amplify fault characteristics. In the literature [108], SDP images are combined with the squeeze-and-excitation CNN classification model to visually diagnose the bearing fault. In the literature [109], vibration signal components after EMD are represented by SDP images, and image features are calculated using the improved Chebyshev distance. These studies have proven that SDP visualizes signals and amplifies their differences.

Although the abovementioned method can realize effective signal processing, the frequency components in the acquired engineering vibration signals are slightly different according to different operating conditions of rotating machinery. At the same time, the fault characteristics of rotating machinery are very different from each fault types. Therefore, it is necessary to research appropriate signal processing methods for vibration signals under different working conditions.

1.3 Research objectives

In the vibration signal under the fault state of rotating machinery, there contains a large amount of fault characteristics information. However, due to the harsh working environment and variable working conditions, the vibration signal acquired by the acceleration sensor contains strong background noise, resulting in the submersion of the fault characteristic signal. Therefore, it is of great significance to research the signal processing methods in the fault diagnosis of rotating machinery.

1.3.1 Research on signal fault characteristic enhancement method

The background noise in the vibration signal acquired by the acceleration sensor is strong, which makes the regular impact caused by the fault submerged, resulting in the difficulty of extracting the fault characteristic frequency in the spectrum. The more serious the interference of vibration signal by background noise, the higher the difficulty of fault feature extraction. How to effectively suppress the background noise in the vibration signal, improve the SNR and enhance the fault characteristics signal is a very key problem in rotating machinery fault diagnosis.

1.3.2 Research on non-stationary vibration signal filtering method

The rotating machinery itself and its transmission structure are very complex. The vibration signals acquired from the rotating machinery have the characteristics of non-linearity, non-stationarity, and complexity, resulting in fault impact signal submerged and weak fault characteristic signal. How to effectively filter the vibration signal under the complex background noise and enhance the fault characteristic is a problem worthy of research.

1.3.3 Research on adaptive filtering method specially for engineering signals

For the rotating machinery vibration signal acquired from engineering field, there is a deviation between the actual rotating frequency and the theoretical value. This deviation leads to the inability to accurately extract features in the industrial fault diagnosis. How to accurately extract the actual rotating frequency and its harmonic from the engineering signal, and to reduce the interference of background noise, is the key problem to realize the adaptive filtering of rotating machinery.

1.3.4 Research on signal image conversion method

In visual fault diagnosis of rotating machinery, the method which can clearly highlight the difference between two-dimensional images and increase the identification of fault types is the guarantee of diagnosis accuracy. In the existing time-frequency image conversion methods, there is a problem that the image discrimination is not obvious. How to effectively extract the fault feature information hidden in the vibration signal and avoid the influence of noise in signal transformation is a problem worthy of research.

1.4 Outline of thesis

This thesis focuses on the key problems of signal processing in rotating machinery fault diagnosis, such as the filtering of non-linear and non-stationary vibration signal, enhancing the weak impact characteristic based on strong background noise, accurately extracting the actual rotating frequency from engineering signal, and increasing fault image discrimination in visual fault diagnosis. The main contents of the dissertation are as follows:

In Chapter 2, it mainly reviews the signal processing methods commonly used in the rotating machinery fault diagnosis, including signal filtering method, signal decomposition method, signal enhancement method, and signal demodulation method.

In Chapter 3, aiming at the problem of large background noise and inundation of regular impact in the rotating machinery vibration signal, a signal feature enhancement method based on weighted kurtosis VMD and improved frequency weighted energy operator is proposed. After the raw signal is decomposed by VMD, several IMFs are obtained. Based on the weighted kurtosis index, the optimal IMF component with the most fault features is selected as the filtered signal. Then, the filtered signal is demodulated by the improved weighted energy operator to further suppress the noise and improve the SNR. This method is verified by the low-speed bearing fault of rotating machinery.

In Chapter 4, aiming at the problems of strong non-linearity, non-stationarity, weak fault characteristics and large noise interference of vibration signal in rotating machinery, a signal filtering method based on reconstruction adaptive determinate stationary subspace filtering (Rad-SSF) and enhanced third-order spectrum is proposed. For the raw vibration signal, the false nearest neighbor method is used to adaptively reconstruct the phase space matrix signal. Based on the stationary subspace algorithm, the reconstructed signal is divided into stationary signal and non-stationary signal, and the best filtered signal is selected from the non-stationary signal based on the maximum kurtosis values to suppress the background noise. Then the third-order calculation is integrated into the TEO to demodulate the filtered signal, and the 1.5-dimensional energy spectrum is obtained to improve the fault characteristics signal. This method is verified by the high-speed bearing fault of rotating machinery.

In Chapter 5, aiming at the problem that there is a deviation between the actual rotating frequency and the theoretical value in the engineering vibration signal, an adaptive multi-band filtering algorithm is proposed. The adaptive multi-band filtering can accurately find out the

actual rotating frequency of the vibration signal, so as to accurately extract the fault characteristics. This method is verified by the rotating machinery abnormal structure faults, including angle misalignment, coupling looseness, dynamic imbalance, pedestal looseness, and static imbalance. Combined with the intelligent classification algorithm, stack autoencoder, the adaptive diagnosis of rotating machinery abnormal structure faults is realized.

In chapter 6, aiming at the problem that the discrimination of vibration signal transformed images is not obvious in the rotating machinery visual diagnosis, an incrementally accumulated holographic SDP characteristic fusion method is proposed. The time-domain and frequency-domain characteristic parameters of vibration signals are extracted successively, and image fusion is performed based on SDP to convert one-dimensional vibration signals into two-dimensional graphics. This method is verified by the bearing fault of rotating machinery, and the experiment result proved that this method can magnify the difference between the signals.

In Chapter 7, it makes a comprehensive and systematic summary of this thesis, and points out the deficiencies in the existing research and areas for improvement. At the same time, it also forecasts the work that needs further research in the future.

Chapter 2 Review of signal processing methods for rotating machinery fault diagnosis

In this chapter, some signal processing methods used in rotating machinery fault diagnosis are summarized, which are mainly divided into four parts: signal filtering method, signal decomposition method, signal enhancement method and signal demodulation method. In each section, it detailly described the origin and development of some common signal processing methods, and their advantages and disadvantages are also summarized.

2.1 Signal filtering method

Signal filtering method can suppress noise by selecting effective frequency components, it has the advantages of significantly improve the SNR of the signal. The key to the signal filtering methods is the setting of the appropriate parameters, such as cut-off frequency and pass-through frequency band. This method mainly includes four categories: 1) the methods by manually setting the parameters of cut-off frequency and pass-through band, including high-pass filtering, low-pass filtering, and band-pass filtering; 2) the methods by using the kurtosis value to determine the optimal parameters of cut-off frequency and pass-through band, including kurtogram, autogram, etc.; 3) the methods based on intelligent algorithm that automatically searches and determines the best parameters of cut-off frequency, such as GA and PSO; 4) the methods by reasonably setting window functions, such as Kalman filtering and wavelet filtering.

2.1.1 High-pass filtering, low-pass filtering, and band-pass filtering

2.1.1.1 High-pass filtering

High-pass filtering has the characteristics of retaining high-frequency components higher than the cut-off frequency, and weakening low-frequency components lower than the cut-off frequency. However, the amplitude of suppression and attenuation varies with different filtering procedures. High-pass filtering only attenuates the frequency components below the cut-off frequency and without phase shift, which is mainly used to eliminate low-frequency noise. In the fault diagnosis of rotating machinery, it is often used to filter vibration signals and sound signals.

2.1.1.2 Low-pass filtering

Low-pass filtering is the opposite of high-pass filtering. It retains low-frequency components and suppresses high-frequency components. It is often used for filtering current signals in rotating machinery faults diagnosis.

2.1.1.3 Band-pass filtering

Band-pass filtering is used to retain the passing frequency band, and is often used to filter the vibration signal in rotating machinery abnormal structural faults.

Fig. 1 shows the signal comparison after high-pass filtering, low-pass filtering and band-pass filtering.

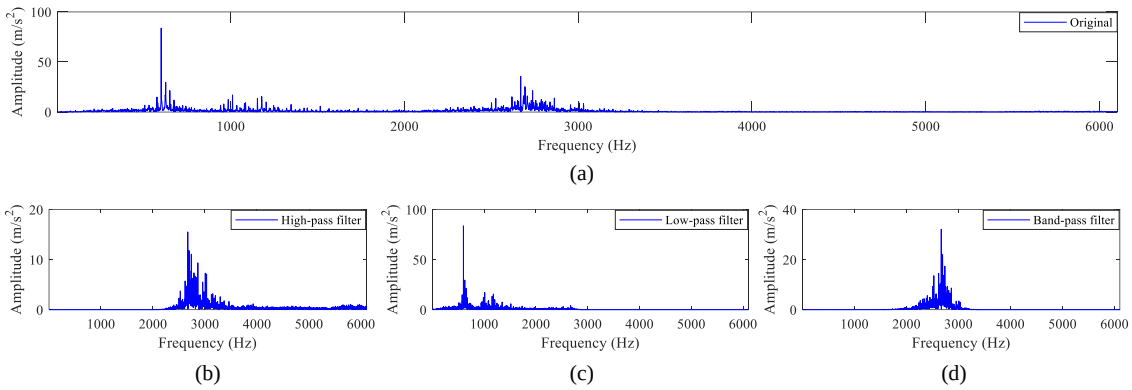

Fig.1 Comparison of the effects of high-pass filtering, low-pass filtering, and band-pass filtering

2.1.2 Kurtogram

The concept of kurtogram was originally proposed by Dwyer, and its basic idea is to determine the impact frequency band in the signal by calculating the kurtosis value on the spectral line. Fast kurtogram and autogram are the filtering methods based on the development of kurtogram. Fig. 2 shows an application example of kurtogram.

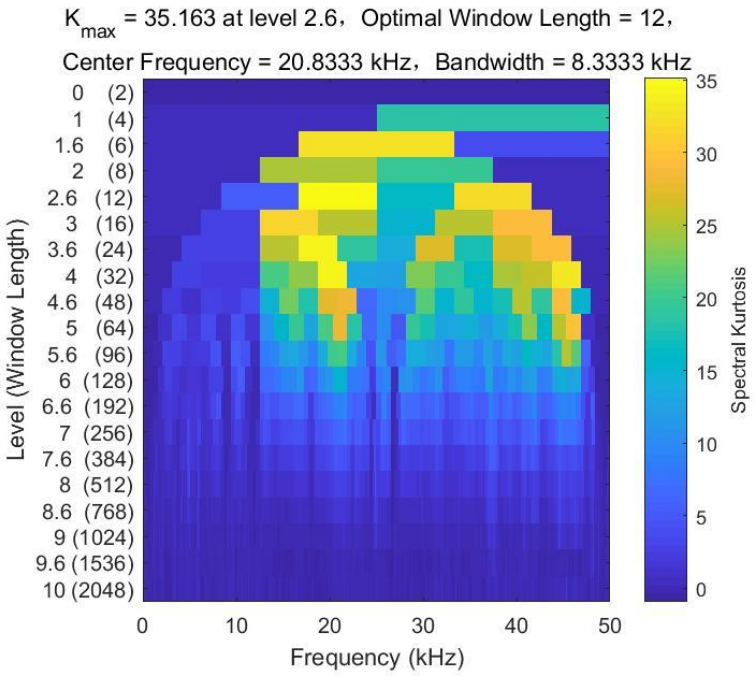

Fig. 2 Example of kurtogram

2.1.2.1 Fast kurtogram

Fast kurtogram is a two-dimensional map composed of frequency *f*, frequency resolution Δf and spectral kurtogram value, which is represented by the shade of color. It can determine the optimal parameters of band-pass filtering, so as to restore the essence of periodic impact of fault signal. The main idea of fast kurtogram algorithm is to calculate the spectral kurtosis of each sub-band (frequency) by constructing a series of 1 / 3-binary tree band-pass filtering banks with different frequency bands, and determine the optimal demodulation frequency band by comparing the spectral kurtosis of the sub-band, so as to extract the envelope corresponding to the demodulation frequency band. The fast kurtogram can determine the center frequency of the best band-pass filtering according to the spectral kurtosis.

2.1.2.2 Autogram

Moshrefzadeh and Fasana proposed the autogram method based on the maximum overlap discrete wavelet packet transform (MODWPT). In this method, the spectrum is divided by binary tree structure, and the bandwidth of each layer is fixed, so as to obtain a series of demodulation frequency bands. It can effectively suppress the influence of aperiodic components on the actual fault frequency and improve the accuracy of detecting the optimal frequency band.

2.1.3 Intelligent algorithm filtering

The filtering based on artificial intelligence methods such as GA and PSO algorithm mainly determines the optimal cut-off frequency through the automatic search principle.

2.1.3.1 GA filtering

GA filtering is an intelligent automatic signal filtering method, which can automatically suppress noise and extract fault signal. In this method, the acquired raw signal is transformed from time domain to frequency domain by fast Fourier transform (FFT), and then matches each value of the binary string to each frequency (from low to high frequencies) of the abnormal signal spectrum. Then in the found optimal binary string, 0 corresponds to the normal component and 1 corresponds to the fault component. Finally, after the raw signal is multiplied by the spectrum of the binary string, only the filtered fault component will be generated.

2.1.3.2 PSO filtering

The PSO filtering uses particles with weight values to approximate the posterior probability distribution, and is suitable for non-linear and non-Gaussian noise environments. This filtering finds the optimal value by continuously updating the speed and position of the particle in the search space, and the particle continuously updates its position and speed by chasing the individual and the global optimal value. The method has high prediction accuracy and good robustness.

2.1.4 WT filtering

The WT filtering determines the filtering bandwidth based on the characteristic frequency of typical faults, and uses the fast spectral kurtosis method for reference to find the center frequency with the largest kurtosis. By selecting the appropriate basis function to ensure the accuracy of the algorithm, it does not have self-adaptability, and there is also the problem of signal energy leakage during filtering. Dual-tree complex wavelet filtering is a new development method with many excellent characteristics, such as approximate translation invariance, good direction selectivity, complete reconstruction, limited data redundancy and efficient computing efficiency.

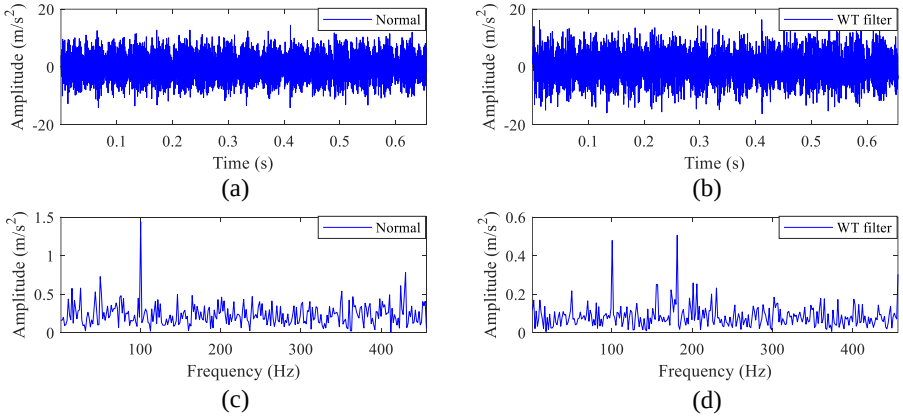

Fig. 3 Example of Wavelet filtering

2.1.5 Kalman filtering

The Kalman filtering is estimated by the minimum variance in the time domain, and each calculation only depends on the current monitoring data and the optimal estimated value at the previous moment. It is an efficient linear recursive filtering that can estimate the state of a dynamic system from a series of incomplete and noisy measurements. On the basis of the linear state space representation, the noisy input and observation signals are processed to obtain system status or real signal. For the system disturbance and observation error (i.e. noise), as long as some appropriate assumptions are made about their statistical properties, the estimated value of the real signal with the smallest error can be obtained in the sense of average by processing the observation signal containing noise.

2.2 Signal decomposition method

The signal decomposition method mainly decomposes the signal according to the time scale characteristics of the signal itself, without setting any basis function in advance. It can decompose the complex signal into finite IMFs, and the decomposed IMF components contain the local characteristic signals of different time scales of the original signal. This kind of method extracts the best IMF as the final filtered signal by calculating the kurtosis value and other parameters. Such methods include EMD and its improved algorithm, VMD, ITD, LMD, singular value decomposition (SVD) and so on.

2.2.1 EMD and its improved methods

EMD is a non-linear and non-stationary signal processing method widely used in mechanical fault diagnosis. It has good adaptability, but it has serious mode aliasing. Therefore, on this basis, researchers have proposed improved methods such as en-semble empirical mode decomposition (EEMD), CEEMD, and CEEMDAN.

2.2.1.1 EMD

EMD is an adaptive decomposition method for non-linear and non-stationary signals proposed by Huang et al. The method adaptively decomposes complex multi-component signals into a series of single-component IMFs according to the time scale of the signal itself. Since EMD is not limited by the basis function, it can accurately and effectively grasp the small characteristics of the raw signal and avoid the diffusion and leakage of signal energy. Therefore, compared with wavelet filtering, EMD method has good stability and accuracy.

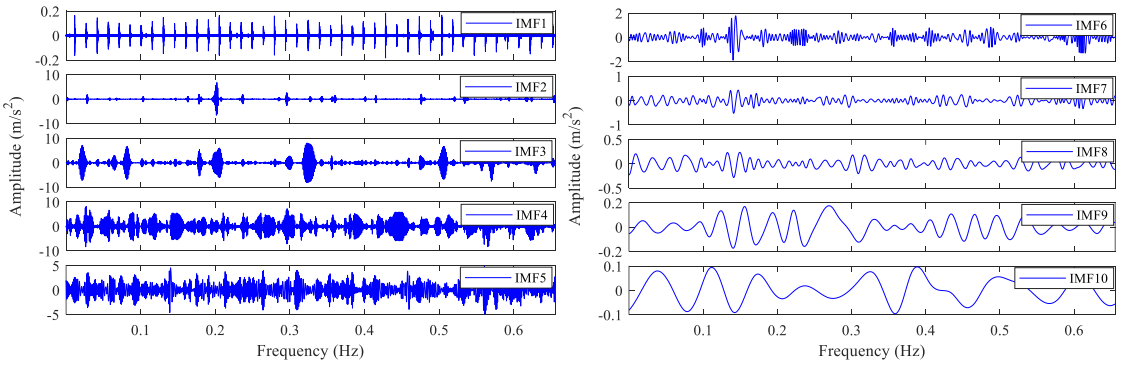

Fig. 4 Example of EMD decomposition

2.2.1.2 EEMD

EEMD is a noise-assisted signal analysis method. It uses the statistical characteristics of white noise with uniform frequency distribution, adds Gaussian white noise of the same amplitude to the raw signal, and performs multiple EMD decompositions. The decomposed IMFs are overall averaged. This method changes the characteristics of its extreme points and enhances the anti-aliasing characteristics of the signal. However, the white noise added in the signal decomposition can't be completely neutralized, so the decomposition completeness of this method is poor.

2.2.1.3 CEEMD

CEEMD adds positive and negative Gaussian white noise to the raw signal, and then perform EMD decomposition respectively. It greatly reduces the residual white noise in the EEMD reconstructed signal. The CEEMD method further improves the defect mode aliasing problem of EMD method, makes the decomposition result more thorough, and has been widely used.

2.2.1.4 CEEMDAN

Based on EEMD, the CEEMDAN is proposed. In this method, adaptive white noise is added in each stage of decomposition, and each IMF is obtained by calculating the unique residual signal. It effectively solves the problems of mode aliasing of EMD and poor completeness of EEMD.

2.2.2 VMD

VMD is an effective decomposition method. VMD can complete the adaptive division of the frequency band according to the frequency characteristics of the signal itself, and it is suitable for the separation of multi-component non-stationary signals. VMD could decompose a complex signal into the sum of its multi-scale components, and it is a non-recursive tool. VMD is a generalization of the classical Wiener filtering for adaptive, multiple bands and is somewhat more robust to noise. It has the advantages of high precision, fast decomposition speed and strong robustness.

2.2.3 ITD

The ITD method adopts the form of linear transformation to decompose the signal, it could adaptively decompose any complex signal into a sum of several PRCs independent of each other, and its instantaneous frequency has physical meaning. The definition of the baseline in the ITD method is based on the linear transformation of the signal itself, and there is an evident signal distortion starting from the second component.

2.2.4 LMD

LMD could self-adaptively decompose a complicated multi-component signal into a set of PF components, each of which is the product of an envelope signal and a purely frequency modulated signal. But the construction of local mean function and envelope function in the LMD algorithm plays an important role in the accuracy of the PF components it extracts. The local mean function and envelope function are calculated by the moving averaging method according to the local extreme points.

2.2.5 SVD

SVD can clearly and effectively detect mutation information in strong noise background, and has achieved good results in feature information separation and weak signal extraction. The SVD component signal in Hankel matrix mode has the characteristics of linear superposition. By selecting the components of interest for superposition, the signal feature information can be

extracted. Due to its good stability and invariance, SVD technology is widely used in periodic component extraction and noise reduction of mechanical fault vibration signals. It has the advantages of zero phase shift, small waveform distortion and high signal-to-noise ratio.

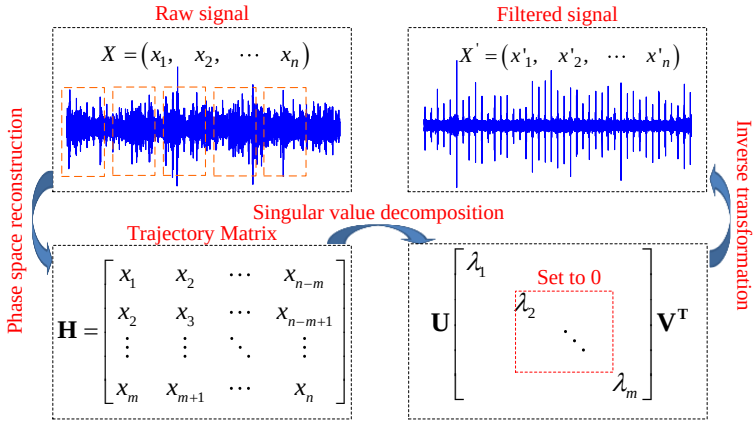

Fig. 5 The principle of SVD

2.3 Signal enhancement method

Under the strong background noise, the weak fault characteristic is often submerged and difficult to extract. Therefore, when performing signal processing on weak signals, it is necessary not only to filter the background noise, but also to enhance the fault characteristic. Commonly used methods to enhance characteristic signals include TEO and its improved methods, such as SDAEO, FWEO.

2.3.1 TEO

TEO is an effective non-linear energy operator developed by Kaiser. The operator estimates the total energy required by the signal source to produce a dynamic signal through the non-linear combination of the time-varying value of the signal and its differential. TEO can estimate the sum of kinetic energy and potential energy of signal, so it can extract relatively weak fault features, and has the advantages of strong timeliness and high time resolution. TEO is an effective signal feature enhancement method, and it could analyze the signal time-frequency characteristics, it is often used to analyze and track the narrowband signal energy. This method could effectively improve the signal impulse, and it has the advantages of simple algorithms and response quickly.

2.3.2 SDAEO

The SDAEO combines the ideas of TEO, Hilbert transform and symmetric difference, which can reflect the local variation characteristics of signal and effectively enhance the fault characteristics. In the SDAEO, Hilbert transform is used to replace the first-order differential operation in TEO to improve the transient frequency characteristics of the signal and improve the resolution of the algorithm. At the same time, the symmetrical difference method is used to smooth the signal, reduce the background noise and improve the demodulation efficiency.

2.3.3 FWEO

The FWEO is proposed by John on the basis of TEO. The intermediate difference method is used to calculate the derivative, so that there is no meaningless negative value in the calculation result. This method realizes signal demodulation by calculating the envelope of signal derivative, and has stronger anti-interference characteristics. However, when the center frequency of the demodulated signal is low, the values of its adjacent sampling points are similar, resulting in small FWEO amplitude and inundation of fault information by noise.

2.3.4 Power spectrum

Power spectrum is defined as the signal power in the unit frequency band and represents the change of signal power with frequency. The power spectrum is a description based on the signal energy or power distribution, including the self-power spectrum and the cross-power spectrum. The self-power spectrum and the amplitude spectrum contain the same amount of information, but under the same conditions, the self-power spectrum is clearer than the amplitude spectrum. The classical spectral estimation method assumes that the unknown data outside the data work area is zero, which is equivalent to data windowing.

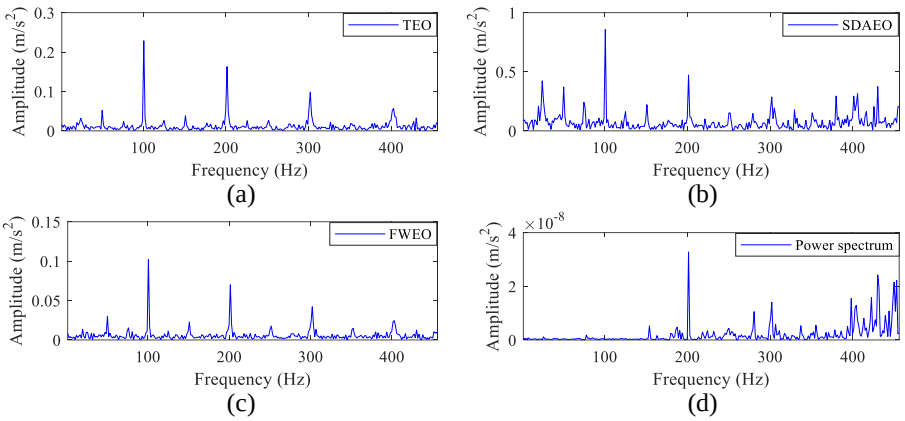

Fig. 6 Examples of TEO, SDAEO, FWEO and power spectrum

2.4 Signal demodulation method

The signal demodulation method is mainly to move the spectrum carrying characteristic information near the carrier to the baseband, and then filter out the baseband signal with the corresponding filtering. It can weaken the influence of background noise and extract the weak fault characteristic information. Compared with other methods, it has the advantages of amplification, selectivity, proportionality, low frequency, correspondence, and broadening. Common demodulation methods include resonance demodulation, Hilbert transform, envelope spectrum, 1.5-dimensional spectrum, energy spectrum and so on.

2.4.1 Resonance demodulation

The basic principle of resonance demodulation technology is that the rotating machinery fault will cause the impact sharp pulse signal. Because these impact sharp pulses have a wide frequency band, they will produce resonance after being received by the sensor, and output a reduced amplitude oscillation signal whose frequency is close to the natural frequency of the sensor. Then the band-pass filtering with high center frequency is used to effectively separate the impact fault information from the low-frequency interference signal and improve the signal-to-noise ratio. Finally, the filtered signal is demodulated, such as calculating the absolute value and taking the envelope, so as to obtain the low-frequency resonance demodulation signal.

2.4.2 Hilbert transform

Hilbert transform plays a very important role in signal processing. The vibration signal is processed by Hilbert transform, the amplitude of each frequency component remains unchanged, but the phase will shift by 90°. Through Hilbert transform, it is possible to define and calculate the instantaneous parameters of short signal and complex signal, and can realize the extraction of instantaneous signal in the real sense. Compared with the traditional amplitude spectrum, the spectrum obtained by this method is more concise in the spectral line distribution component,

which can directly find the fault frequency component of vibration signal, and improve the efficiency and accuracy of fault diagnosis process.

2.4.3 Envelope spectrum

Envelope analysis is one of the widely used vibration signal fault feature extraction method. The key of envelope analysis is to determine the appropriate filtering center frequency and bandwidth. The envelope demodulation can demodulate the fault-related information from the high-frequency modulated signal, and it has become a common method to extract the fault characteristics of rotating machinery. Envelope demodulation analysis is the most commonly used diagnostic method, but its difficulty is to find the optimal demodulation frequency band.

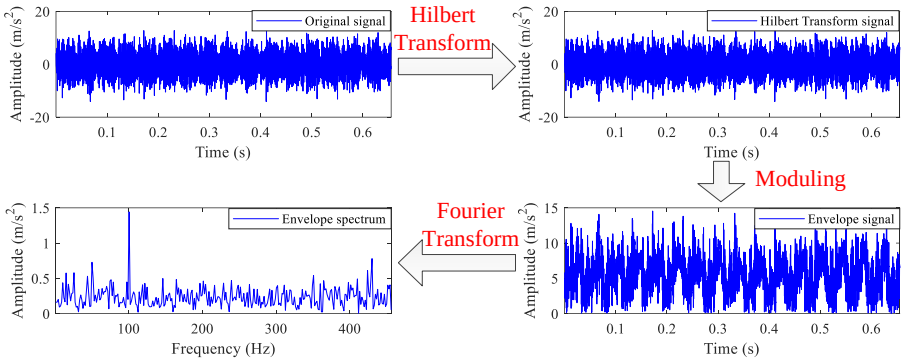

Fig. 7 The principle of envelope spectrum

2.4.4 Energy spectrum

Energy spectrum represent the distribution of signal energy at each frequency point, it is the square of the modulus of the signal amplitude spectrum. The energy of the signal can be obtained by integrating the energy spectrum in the frequency domain. The spectrum reflects the distribution of the amplitude and phase of the signal with frequency, which describes the frequency domain characteristics of the signal, and the energy spectrum can be used to describe the frequency domain characteristics of the signal.

2.4.5 1.5-dimensional spectrum

The 1.5-dimensional spectrum is developed from the high-order spectrum method. It can not only extract the quadratic non-linear coupling characteristics in the signal and effectively eliminate the influence of noise, but also overcome the disadvantages of large amount of calculation of high-order spectrum. The vibration signal will show strong non-linear characteristics and secondary phase coupling, but the power spectrum can't identify the coupling characteristics in the fault signal because it will suppress the phase information. The 1.5-dimensional spectrum makes up for the deficiency of the power spectrum, it retains the amplitude and phase information, and can effectively suppress the Gaussian white noise and strengthen the fundamental frequency component.

2.5 Problems with signal processing methods

High-pass, low-pass, and band-pass filtering have been well applied in engineering signal processing, however, researchers need to fully understand the fault characteristic frequency to accurately set the cutoff frequency for signal filtering. The spectral kurtosis filtering method can help select the best center frequency, but this approach cannot work efficiently when a higher impulse is present. Although the artificial intelligent filtering methods does not require extensive experience, this method is computationally expensive, difficulty in parameter adjustment, and can

easily fall into the local optima.

Signal decomposition methods decompose the signal into multiple IMFs and extract the best IMF with the largest fault characteristic. Although the noise can be filtered out, it also inevitably weakens the energy of useful signals, and finally the SNR is lower, which affects the fault diagnosis accuracy. Besides, the EMD uses cubic spline interpolation to fit the envelope, which has obvious shortcomings such as over-envelope, under-envelope, end effect and mode mixing; EEMD and its improved methods could alleviate the above deficiencies, they still introduce new problems, such as the white noise cannot be completely neutralized and resulting in false components, therefore, the fault feature extraction is still seriously affected under strong background noise; VMD has certain limitations, including breakpoint effects and modal aliasing; LMD have shortcomings that the moving averaging method may cause phase error of the functions after several iterations, which has an adverse effect on the accuracy of PF components; the definition of the baseline in the ITD method is based on the linear transformation of the signal itself, and there is an evident signal distortion starting from the second component.

TEO has the advantage of enhancing the signal impulse, it also has the disadvantages of low demodulation accuracy and substantial noise interference. FWEO as an improved TEO method, it can assess instantaneous energy, and improve the analytic performance, but it still imperfect when signals have strong noise.

Signal demodulation method can improve the energy of impact signal, but it still needs to be further improved for strong noise background and weak fault signal.

Chapter 3 Signal processing method based on weighted kurtosis VMD and improved FWEO

3.1 Introduction

Rotating machinery has complex structure and poor working environment, the vibration signal acquired by the acceleration sensors often contains strong background noise [110, 111]. These noises submerged the signal impulse generated by the fault so that it is difficult to extract the fault feature from the signal to realize fault diagnosis. Hence, this chapter proposed a fault signal processing method based on improved VMD and frequency weighted energy operator.

VMD can complete the adaptive division of the frequency band according to the frequency characteristics of the signal itself, and it is suitable for the separation of multi-component non-stationary signals. Therefore, this chapter employs the VMD to decompose fault signal, and based on the weighted kurtosis indictor to extract the decomposed component which carries abundant fault information to reconstruct the signal. The signal reconstructed by VMD could extract the impulse signal. However, the extracted signal impulse also has some noise, and the impulse signal should be enhanced, so it needs further processing methods.

TEO is an effective signal feature enhancement method, and it has the advantages of simple algorithms and response quickly. FWEO as an improved TEO method, it can assess instantaneous energy, and improve the analytic performance, but it still imperfect when signals have strong noise. According to the third-order cumulant mentioned in [112, 113] could effectively improve the SNR, this chapter introduced it into FWEO to improve the performance, the improved FEWO (IFWEO) method is presented to analyze VMD reconstructed signal for enhancing rotating machinery fault impulse.

To verify the effectiveness of the method presented in this chapter, a low-speed bearing inner race fault simulation analytical model is established, and engineering signals are acquired for experiments. The results prove that this method could effectively extract the signal impulse from the strong background noise and enhance the fault characteristic frequency value, realizing low speed bearing fault diagnosis.

3.2 Weighted kurtosis VMD

VMD completes the frequency band adaptive subdivision according to the frequency domain characteristics of the signal itself. By solving the constrained variational model in the variational framework, several bandpass signal components are obtained to realize the decomposition of the signal. VMD has perfect mathematical principles and better noise robustness, and it could effectively suppress mode mixing and end effect, and is suitable for the separation of multi-component non-stationary signals [114, 115].

3.2.1 Principle of VMD

For the one-dimensional non-stationary signal $x(t)$, define the VMD intrinsic mode function components are the amplitude modulation-frequency modulation signal $u_k(t)$:

$$u_k(t) = A_k(t)\cos(\omega_k(t)) \tag{1}$$

where $A_k(t)$ is the instantaneous amplitude and $\omega_k(t)$ is the instantaneous frequency.

Assuming that the signal $x(t)$ is decomposed into k IMF components, the constructed

constrained variational model equation is given by:

$$\begin{aligned} &\min_{\{u_k,\omega_k\}}\left\{\sum_k\left\|\partial t[(\sigma(t)+j/\pi t)*u_k(t)]e^{-j\omega t}\right\|_2^2\right\} \\ &s.t.\ \sum_{k=1}^{k}u_k=x(t) \end{aligned} \tag{2}$$

where $\{u_k\}=\{u_1,u_2,\cdots,u_k\}$ is VMD decomposed k IMFs; $\{\omega_k\}=\{\omega_1,\omega_2,\cdots,\omega_k\}$ is the frequency center of each IMFs; $(\sigma(t)+\frac{j}{\pi t})*u_k(t)$ is the one-sided spectrum obtained by the Hilbert transform of the signal $x(t)$.

Introducing the quadratic penalty factor α and Lagrange operator $\lambda(t)$, and transforming Eq. (2) into a non-constrained variational problem, the extended Lagrange operator is as shown in follows:

$$\begin{aligned} L(\{u_k\},\{\omega_k\},\lambda)=&\alpha\sum_k\left\|\partial t[(\sigma(t)+\frac{j}{\pi t})*u_k(t)]e^{-j\omega t}\right\|_2^2 \\ &+\left\|x(t)-\sum_k u_k(t)\right\|_2^2+\left\langle\lambda(t),x(t)-\sum_k u_k(t)\right\rangle \end{aligned} \tag{3}$$

Using the multiplication operator alternating direction method to find the optimal solution, and through Eq. (4), Eq. (5), and Eq. (6) to update u_k^{n+1}, ω_k^{n+1}, and λ^{n+1}.

$$\hat{u}_k^{n+1}(\omega)=\frac{\hat{x}(\omega)-\sum_{i=k}\hat{u}_i(\omega)+\frac{\hat{\lambda}(\omega)}{2}}{1+2\alpha(\omega-\omega_k)^2} \tag{4}$$

$$\omega_k^{n+1}=\frac{\int_0^\infty\omega\left|\hat{u}_k(\omega)\right|^2d\omega}{\int_0^\infty\left|\hat{u}_k(\omega)\right|^2d\omega} \tag{5}$$

$$\hat{\lambda}^{n+1}(\omega)=\hat{\lambda}^n(\omega)+\tau(\hat{x}(\omega)-\sum\hat{u}_k^{n+1}(\omega)) \tag{6}$$

According to the convergence conditions Eq. (7) to end the decomposition and complete the IMFs extraction.

$$\sum_k\left\|\hat{u}_k^{n+1}-\hat{u}_k^n\right\|_2^2\Big/\left\|\hat{u}_k^n\right\|_2^2<\varepsilon \tag{7}$$

3.2.2 Weighted kurtosis index

Ensuring to select the best signal component from the VMD IMFs, the weighted kurtosis is used to evaluate the IMFs. The weighted kurtosis (WK) combines kurtosis (Kur) and correlation functions ($Corr$), it is given by:

$$WK=Kur\cdot Corr \tag{8}$$

$$Kur=\frac{\frac{1}{N}\sum_{n=0}^{N-1}u_k^{\,4}(n)}{(\frac{1}{N}\sum_{n=0}^{N-1}u_k^{\,2}(n))^2} \tag{9}$$

$$Corr=\frac{E\left[(u_k-\overline{u}_k)(x-\overline{x})\right]}{E\left[(u_k-\overline{u}_k)^2\right]E\left[(x-\overline{x})^2\right]} \tag{10}$$

where Kur is Kurtosis of each component, $Corr$ is the correlation coefficient between each sub-mode and the original signal, and N is the signal length.

3.2.3 IMF selection

The weighted kurtosis could both characterize the correlation coefficient between each sub-

mode with the original signal and the impact of the original signal, Fig. 8 shows the method for selecting effective IMFs. In this method, the signal is decomposed into different layers, and the weighted kurtosis of each IMFs is calculated to find the best decomposition layer and the optimal IMF based on the biggest weighted kurtosis value.

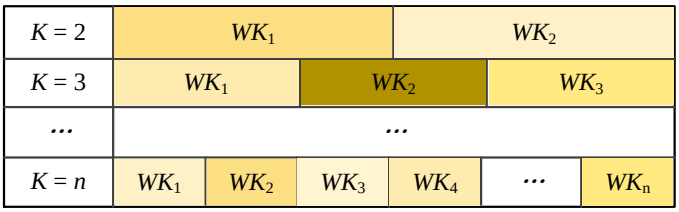

Fig. 8 Effective IMF selection based on weighted kurtosis

3.3 Improved FWEO

The FWEO takes the derivative function as a filtering and introduces the instantaneous frequency weight, by calculating the envelope of the signal derivative to calculate the modulated signal instant energy [116]. FWEO has stronger robustness under background noise and other frequency component interference. At the same time, the third-order cumulant method could effectively improve the SNR and better enhance the impulse signal feature.

3.3.1 TEO principle

TEO has good time-frequency resolution, it could express the signal instantaneous energy, and enhance the signal impulse. The TEO is as follows:

$$\psi\left[x(t)\right]=\dot{x}^2(t)-x(t)\ddot{x}(t) \tag{11}$$

where $\dot{x}(t)=dx(t)/dt$ and $\ddot{x}(t)=d^2x(t)/dt^2$.

3.3.2 IFWEO principle

For the selected signal $y(t)$ based on weighted kurtosis VMD, it contains periodic impulse $s(t)$ and Gaussian random noise $n(t)$, as shown in follows:

$$y(t)=s(t)+n(t) \tag{12}$$

According to the high-order cumulant definition, the third-order cumulant of the signal $y(t)$ can be given as:

$$\begin{aligned} c(\tau_1,\tau_2) &= cum\left\{y(t)y(t+\tau_1)y(t+\tau_2)\right\} \\ &= E\left\{s(t)s(t+\tau_1)s(t+\tau_2)\right\}+E\left\{n(t)n(t+\tau_1)n(t+\tau_2)\right\} \end{aligned} \tag{13}$$

where τ_1 and τ_2 are the delay parameter, and E is the expectation calculate method.

Because the high-order cumulant of $n(t)$ is always equal to 0, and at the same time, make $\tau_1=\tau_2$ to reduce the computational complexity, the 1.5-dimensional slice of the third-order cumulant is given by:

$$c(t)=R_{3y}(\tau,\tau)=E\left\{y(t)y(t+\tau)^2\right\} \tag{14}$$

Using the analytical signal form to define the demodulated signal $c(t)$ as follows:

$$C(t)=c(t)+jH\left[c(t)\right] \tag{15}$$

where $H\left[c(t)\right]$ is the Hilbert transform of $c(t)$. The signal energy is determined by the square of

the signal amplitude, and is given by:

$$S\left[c(t)\right]=\left|c(t)+jH\left[c(t)\right]\right|^2 \tag{16}$$

where $S[\cdot]$ is the envelope operator equation.

Therefore, introducing the TEO concept and define the frequency-weighted energy operator as:

$$\Gamma\left[c(t)\right]=\left|\dot{c}(t)+jH\left[\dot{c}(t)\right]\right|^2=\dot{c}^2(t)+H\left[\dot{c}(t)\right]^2 \tag{17}$$

To derive the discrete signal, the symmetric difference method used is as follows:

$$\dot{c}(n)=\frac{c(n+1)-c(n-1)}{2} \tag{18}$$

where IFWEO discrete equation is given by:

$$\begin{aligned}\Gamma\left[c(n)\right]&=\frac{1}{4}\left[c^2(n+1)+c^2(n-1)+h^2(n+1)+h^2(n-1)\right]\\&+\frac{1}{2}\left[c(n+1)+c(n-1)+h(n+1)+h(n-1)\right]\end{aligned} \tag{19}$$

3.4 Rotating machinery fault diagnosis process

For the problem that it is difficult to accurately extract the rotating machinery fault characteristics frequency under the complex background noise, this chapter proposes a method based on weighted kurtosis to select the effective VMD IMFs and using IFWEO to enhance feature to realize the fault diagnosis. Fig. 9 shows the detailed steps and flowchart of this method.

Step1 Acquiring the vibration signal of the rotating machinery under different faults states;

Step2 Applying VMD to adaptively decompose the vibration signal, and set the initial decomposition layer K=2, extract the IMFs. The K plus one each time, and calculate the corresponding IMFs;

Step3 Calculating the weighted kurtosis of each IMFs under different decomposition layers K, and select the sensitive IMF which containing the most fault information. Reconstruct the signal with the selected signal

Step4 Using IFWEO to demodulate the reconstructed signal to obtain the envelope spectrum;

Step5 Dominant frequency in envelope spectrum compared with the fault characteristic frequency to realize rotating machinery fault diagnosis.

Take bearing fault as an example, the fault characteristic frequency calculation equation is as follows:

$$f_o=\frac{Z}{2}f_{rm}\left(1-\frac{d}{D}\cos\alpha\right) \tag{20}$$

$$f_i=\frac{Z}{2}f_{rm}\left(1+\frac{d}{D}\cos\alpha\right) \tag{21}$$

$$f_b=\frac{D}{d}f_{rm}\left(1-\frac{d^2}{D^2}\cos^2\alpha\right) \tag{22}$$

where f_o is the bearing outer race fault characteristic frequency; f_i is the inner race fault characteristic frequency; f_b is the roller fault characteristic frequency; Z is the number of rolling elements; f_{rm} is rotating frequency; d is the rolling element diameter; D is the pitch diameter; α is the contact angle.

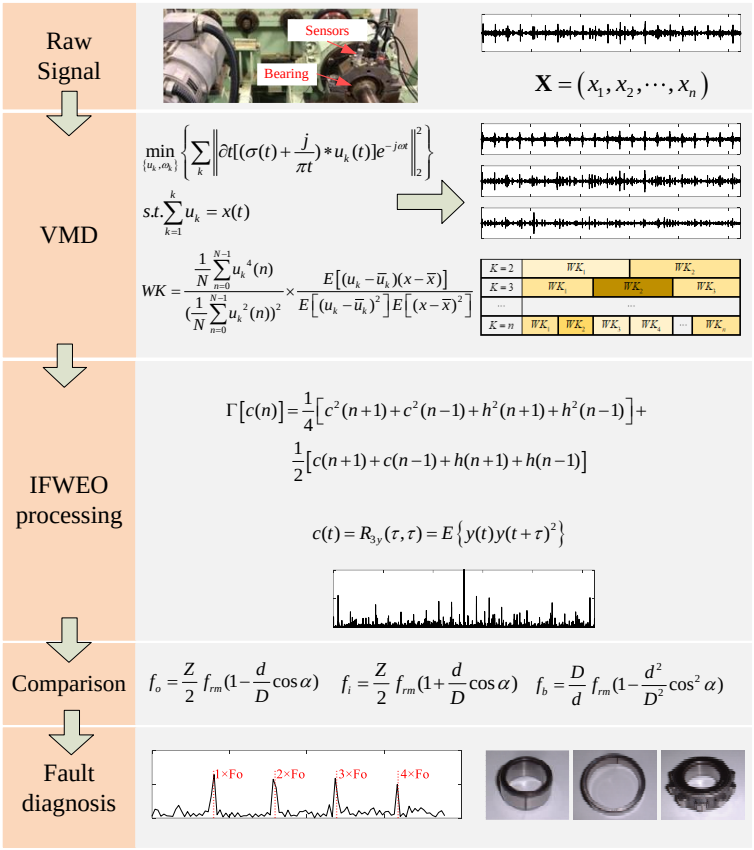

Fig. 9 Weighted kurtosis VMD and IFWEO fault diagnosis flow chart

3.5 Experimental verification

In order to verify the effect of the weighted kurtosis VMD and IFWEO methods proposed in this chapter in the removal of vibration signal background noise and the enhancement of fault feature information, this chapter uses low-speed bearing faults that are common in rotating machinery fault types for verification. The experimental verification is divided into two parts, simulation verification and engineering experimental verification.

3.5.1 Simulation analysis

To verify the effectiveness of weighted kurtosis VMD and IFWEO in low-speed bearing fault diagnosis under complex background noise, this chapter simulates an inner race fault signal analysis model, the sampling frequency is 12000 Hz, and the number of sampling points is 4096.

3.5.1.1 Simulation model establishment

The analytical model is as follows [26]:

$$f(t)=A(1-B\cos(2\pi f_{rm}t))\cdot\sum_{-\infty}^{\infty}U(t-KT-\tau_k)x(t)+n(t) \tag{23}$$

$$x(t)=e^{-c(t-KT-\tau_k)}\cos(2\pi f_n(t-KT-\tau_k)) \tag{24}$$

where f_{rm} is the rotating frequency, and the value is 10 Hz; T is the feature cycle and the value is 1/120; τ_k is the tiny fluctuation of the *k-th* shock and the value 0.000001; c is the signal damped exponent and the value is 1000; f_n is the resonance frequency and the value is 5000 Hz; $n(t)$ .is the noise signal.

The simulation signal result is shown in Fig. 10(a), and Fig.10(b) is the corresponding envelope spectrum. In Fig. 10(a) the time-domain signal, the periodic impulse of bearing inner race fault is

entirely submerged by noise. In Fig.10(b) there are more interference noises, and the effective information is covered. The fault characteristic frequency and its harmonics could not be extracted.

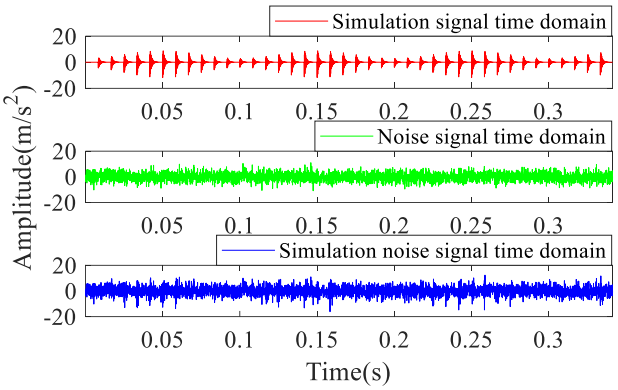

(a)

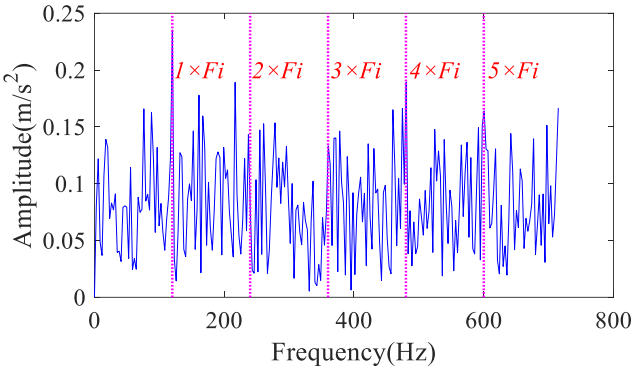

(b)

Fig. 10 Bearing inner race fault simulation time-domain signal and its spectrum: (a) time-domain signal; (b) spectrum

3.5.1.2 VMD verification

The VMD is used for signal decomposition, according to existing experience and references [117], set the initial center frequency (ICF) by uniform distribution and the quadratic penalty factor to 2000. And firstly, the initial decomposition layer is set to K=2, decomposing the IMFs and calculating the corresponding weighted kurtosis. Increase the value of K each time, and calculate the corresponding weighted kurtosis of IMFs, the result is shown in Fig. 11. It can be seen that when the decomposition layer is 3, the weighted kurtosis value of IMF3 is the largest, indicating that the IMF3 carries the best fault feature information. Fig. 12 shows the IMF3 time-domain signal and its spectrum. There are some fault impulses in the time-domain signal, and the noise is also partially suppressed. Although the fault characteristic frequency and harmonics have been improved in the original envelope spectrum, the fault characteristic frequency and 2nd harmonic are conspicuous. However, the 3rd harmonic and the higher harmonic can’t be found out, there is still noise interference.

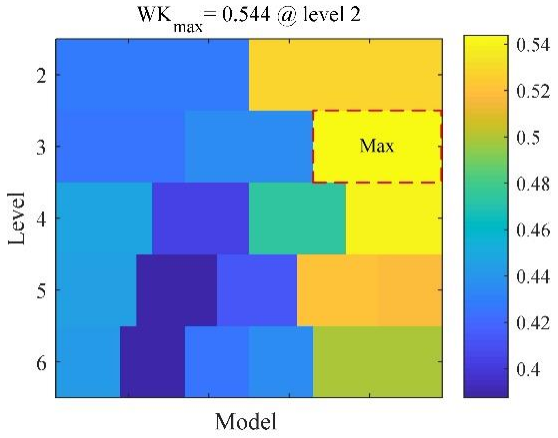

Fig. 11 The weighted kurtosis distribution

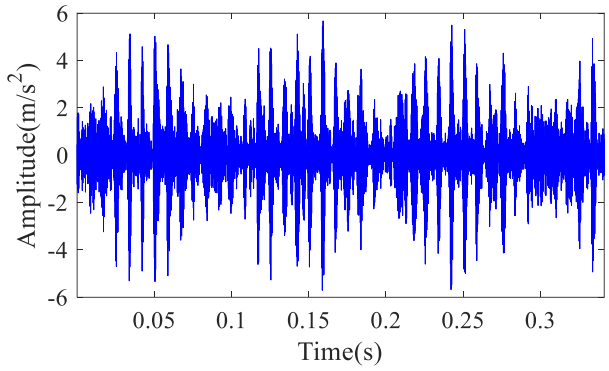

(a)

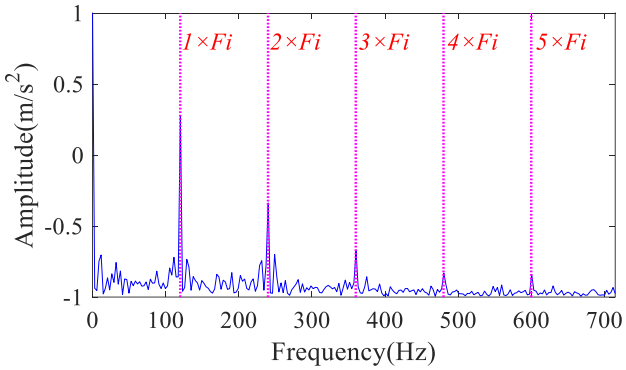

(b)

Fig. 12 Optimal IMF time-domain signal and its spectrum: (a) time-domain signal; (b) spectrum

3.5.1.3 IFWEO verification

For the optimal signal extracted by VMD decomposition, the third-order cumulant is calculated, and Fig.13 shows its frequency spectrum. In the calculation, the sample length of data is 4096, the estimated maximum delay is 2048, the data overlap percentage is 0, and fixed delay is 1. Fig.13 shows that the noise is significantly reduced after the third-order cumulant processed, and the fault characteristic frequency is improved. It proves that the third-order cumulant method can effectively remove the background noise, and the characteristic frequency can be better extracted.

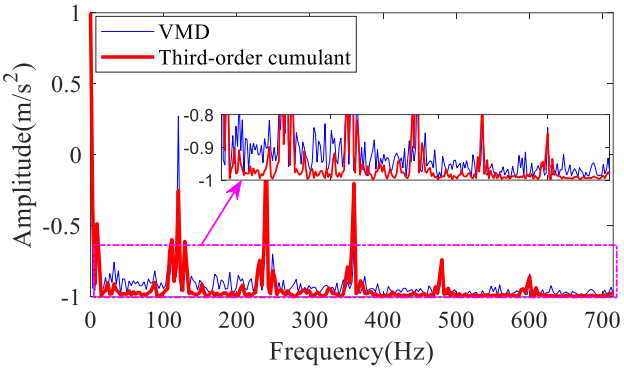

Fig.13 The third-order cumulant comparison

The IFWEO is applied to demodulate the reconstructed signal via weighted kurtosis VMD, and Fig. 14 shows the corresponding envelope spectrum. In the envelope spectrum, the fault characteristic frequency values and its harmonics have been significantly enhanced, and the noise is significantly reduced. Therefore, the simulation experiment results proved that the low-speed bearing fault diagnosis method presented in this study is effective; it could enhance the fault feature, suppress the background noise, and improve the signal SNR.

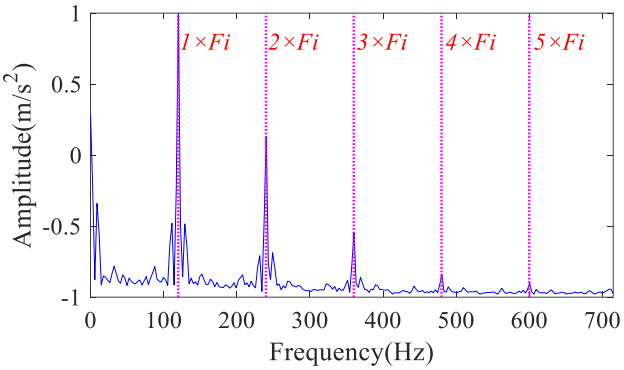

Fig. 14 The simulated signal IFWEO spectrum

3.5.2 Engineering experiment

This chapter carries out diagnosis research based on the bearing fault of rotating machinery low-speed rotating equipment, and verifies the accuracy of the method proposed in this chapter through the actual engineering signal.

3.5.2.1 Experiment platform

The low speed bearing fault experiment platform and the bearing fault types are shown in Fig. 15, and the bearing specific parameters are shown in Tab. 1. The bearing works at speed 100 RPM with load, and the load is setting to 0.5T. The vibration signal is acquired by the acceleration sensor, and the sampling frequency is 100000 Hz. On the bearing inner race, outer race, and rolling elements, a groove with a depth of 0.3 mm and a width of 5.0 mm is processed by wire cutting.

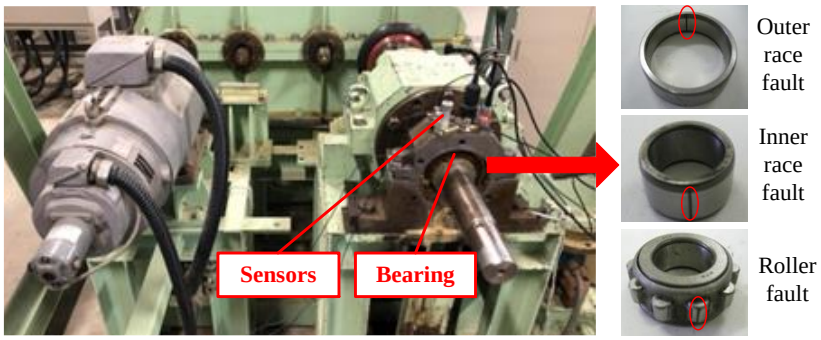

Fig. 15 Low speed bearing fault experiment platform and bearing fault types

Tab. 1 Bearing specific parameters

Parameter	Value
Rolling elements number	12
Rolling elements diameter	18 mm
Bearing pitch diameter	100.25 mm
Contact angle	0

According to Eq. (20), Eq. (21) and Eq. (22), the bearing fault characteristic frequency is shown in Tab. 2.

Tab. 2 Low speed bearing fault characteristic frequency

Type	Outer race	Inner race	Roller
Frequency	8.20 Hz	11.79 Hz	8.98 Hz

3.5.2.2 Outer race fault

Fig. 16 (a) shows the vibration signal of the normal bearing, and the outer race fault bearing. It can be seen that the normal bearing vibration signal is stable and the amplitude variation range is small. But in the outer race fault vibration signal, the amplitude fluctuates greatly, and the impulse occurs significantly. However, due to excessive background noise, the periodic impulse features caused by the outer race fault is submerged, the regular and complete periodic impulse cannot be found in the time domain signal. In the Fig. 16 (b) signal envelope spectrum, although the fault characteristic frequency could not be found conveniently, the value is too low, and it is greatly affected by background noise. Therefore, it is necessary to further processing the signal to reduce background noise, improve the SNR, and enhance the fault impulse feature.

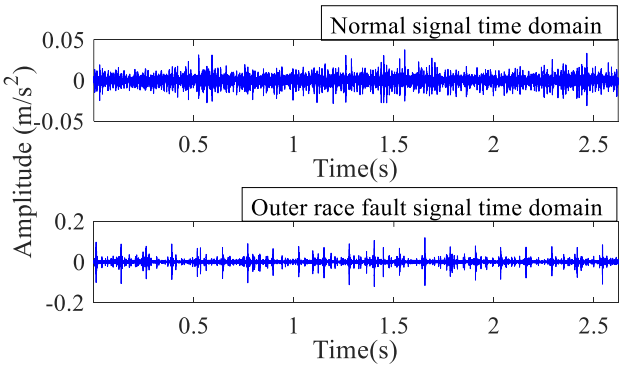

(a)

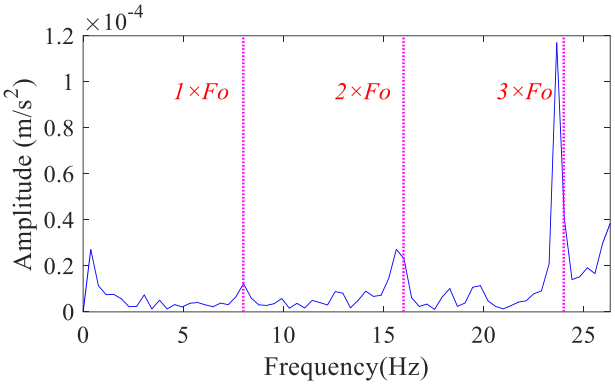

(b)

Fig. 16 Bearing outer race fault time-domain signal and its spectrum: (a) time-domain signal; (b) spectrum

The original signal is decomposed by VMD, and using the weighted kurtosis to select the best optimal IMF under different decomposition layers. In VMD algorithm, the initial center frequency (ICF) is set by uniform distribution and the quadratic penalty factor is set to 2000. The weighted kurtosis distribution is shown in Fig. 17. It can be seen that when the decomposition layer is 4, the IMF3's weighted kurtosis value is the largest, and the signal carry the fault information is the best. Fig. 18 shows the IMF3 time-domain signal and its envelope spectrum. In the Fig. 18(a), it can be seen that the signal background noise is obviously reduced and the regular and complete periodic impulse is strengthened, but in the Fig. 18(b) envelope spectrum, the fault characteristic frequency and harmonics value are weak, it still needs to be enhanced.

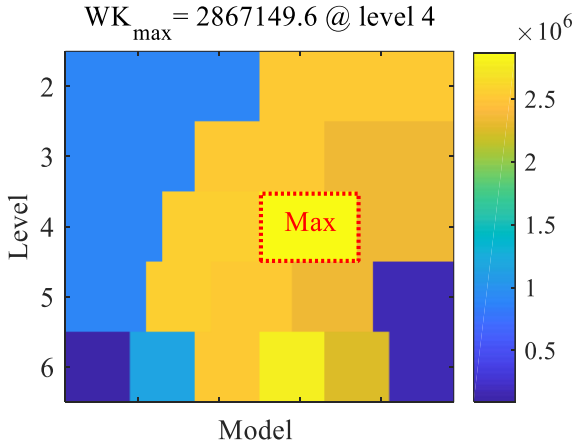

Fig.17 The weighted kurtosis distribution

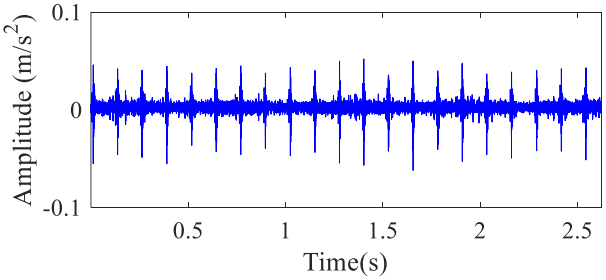

(a)

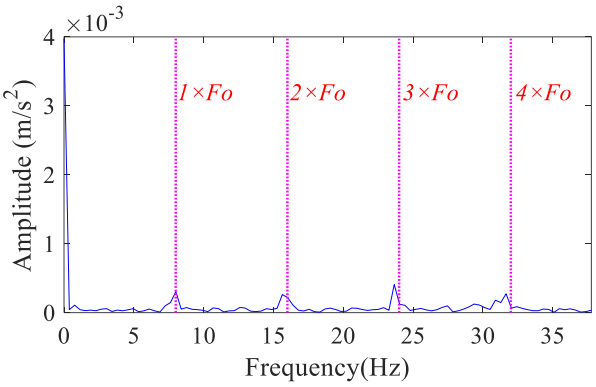

(b)

Fig.18 The IMF3 time-domain signal and its envelope spectrum: (a) time-domain signal; (b) spectrum

Using the IFWEO to process the optimal signal and Fig. 19 shows the corresponding envelope spectrum. In the calculation of third-order cumulant, the sample length of data is 262144, the estimated maximum delay is 131072, the data overlap percentage is 0, and fixed delay is 1. It can be seen that the impulse feature is obviously, the fault characteristic frequency value, and its 2nd, 3rd, 4th harmonics are much higher than other frequencies. The noise is effectively suppressed, and the SNR is significantly improved. The result proved that the method presented in this paper is effective.

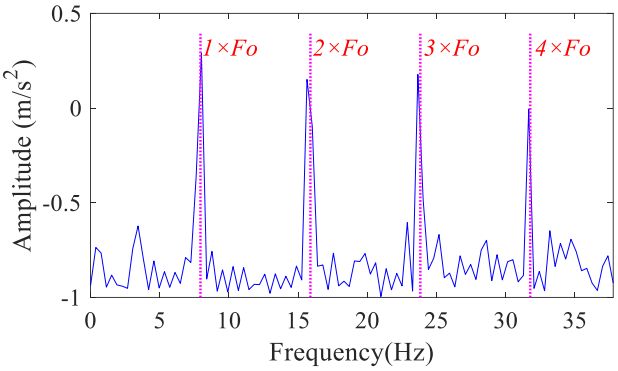

Fig.19 The IFWEO spectrum of outer race fault

3.5.2.3 Inner race fault

Verified the effectiveness of the method for the diagnosis of inner race faults, and the results are shown in Fig. 20. In Fig. 20 the inner race fault envelope spectrum, the fault characteristic frequency, and its harmonics are significantly higher than other frequencies, and the impulse is obvious.

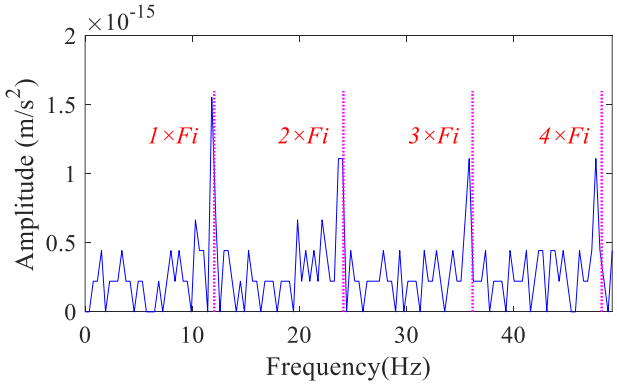

Fig. 20 The IFWEO spectrum of inner race fault

Therefore, this method also effective for inner race fault; it could enhance the fault feature so that to accurately extract the fault characteristic frequency and realize fault diagnosis.

3.5.2.4 Roller fault

Verified the effectiveness of the method for the diagnosis of inner race faults, and the results are shown in Fig. 21. In Fig. 21 roller fault envelope spectrum, shows that the fault characteristic frequencies are also effectively extracted.

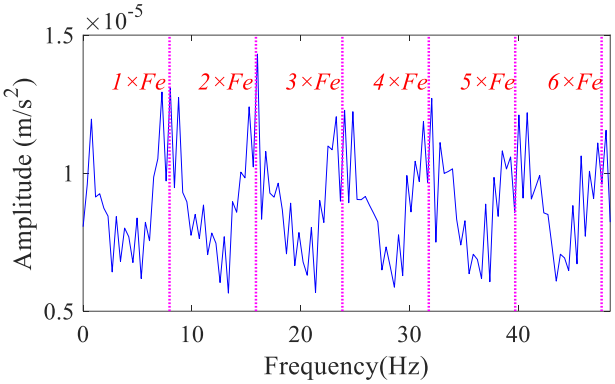

(b)

Fig. 21 The IFWEO spectrum of roller fault

Therefore, this method also effective for inner race fault and roller fault; it could enhance the fault feature so that to accurately extract the fault characteristic frequency and realize fault diagnosis.

3.5.3 Comparative experiment

To verify that this method has better diagnostic performance, the comparisons were carried out from three aspects that are decomposition method, weighted kurtosis methods and the IFWEO methods. In the comparison experiment, the type of fault is the outer race fault, and the speed is 100 RPM.

3.5.3.1 Decomposition method comparison

In bearing fault diagnosis, extracting the effective feature information from the vibration signal is the key to accurately identifying the fault. To verify the decomposition effect of VMD under strong noise background, the EMD, LMD, and ALIF are used as comparison method, Fig.22 shows the IFWEO spectrum corresponding to the optimal characteristic signals extracted by the four methods. It is clearly that the four methods can effectively extract the characteristic frequency of the outer race fault, however, compared with the EMD, LMD, and ALIF, the noise of the optimal signal extracted by VMD is the smallest. It proves that VMD has the best decomposition effect under strong noise background and is most suitable for bearing fault diagnosis.

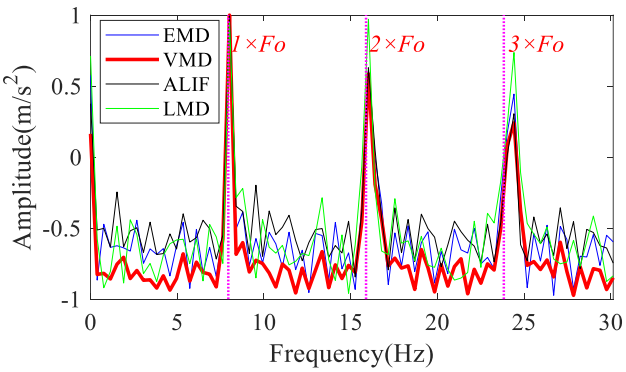

Fig. 22 IFWEO spectrum comparison of the four decomposition methods

3.5.3.2 Weighted kurtosis comparison

The kurtosis is sensitive to the impulse of the bearing fault vibration signal, but it only depends on the distribution density of the impact signal, and it may ignore the large amplitude and scattered components. Correlation coefficient could characterize the correlation between the reconstructed signal and the original signal, but it is susceptible to noise interference. Therefore, combines the advantages of the kurtosis and correlation coefficient, the weighted kurtosis could more accurately evaluate the signal. Hence, to verify the effectiveness of the weighted kurtosis, the kurtosis and correlation coefficient are selected as comparison indexes respectively. Set the VMD decomposition layer is 2, and sequentially increase decomposition layers, and calculate the values of the three indexes according to each IMFs. The results are shown in Fig. 23(a) and (b). In Fig. 23(a) the kurtosis distribution, the optimal decomposition layer is 6, the IMF3 has the largest value with 85.2, and in Fig.23(b) the correlation coefficient distribution, the optimal decomposition layer is 5, the IMF5 has the largest value with 54592.5.

Combine with Fig. 17, select the optimal IMFs under the three indexes, and extract the fault characteristic frequency, the envelope spectrum is shown in Fig. 23(c). Compare the fault characteristic frequency value, and it can be seen that the weighted kurtosis selected signal is the highest. At the same time, in the envelope spectrum, the weighted kurtosis selected signal has the most prominent impulse, and the background noise filtered is obviously better than the kurtosis and correlation coefficient. Therefore, the weighted kurtosis is best for the signal selected.

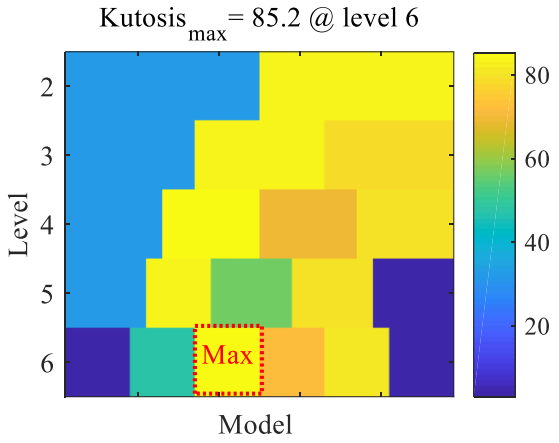

(a)

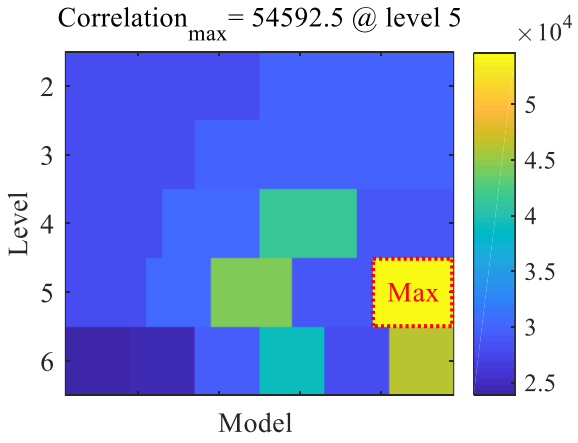

(b)

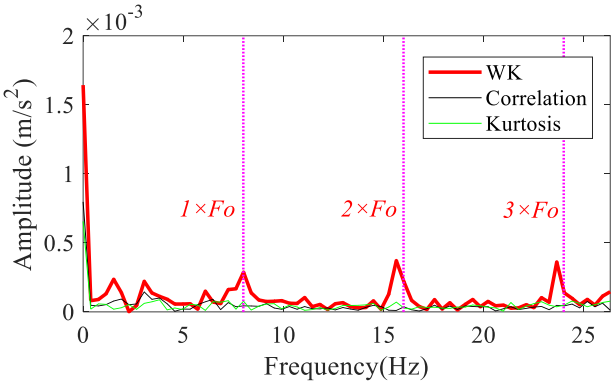

(c)

Fig. 23 Kurtosis, correlation coefficient and weighted kurtosis comparison: (a) Kurtosis distribution; (b) correlation coefficient distribution; (c) the spectrum of optimal IMF selected by three methods

3.5.3.3 Energy operator comparison

For comparing the effectiveness of TEO, FWEO, and IFWEO, to extract the fault characteristic frequency of the optimal signal, and the comparison result is shown in Fig.24. It can be seen that all three methods could effectively extract the fault characteristic frequency, and it further proves that the weighted kurtosis presented in this paper could effectively extract the optimal IMF. At the same time, combined with the fault characteristic frequency values shown in Fig. 25 (to better compare the results, the values are normalized to [-1,1]), the IFWEO has the highest value and the smallest background noise. Therefore, the IFWEO proposed in this paper has the best performance on the enhancement of the fault features.

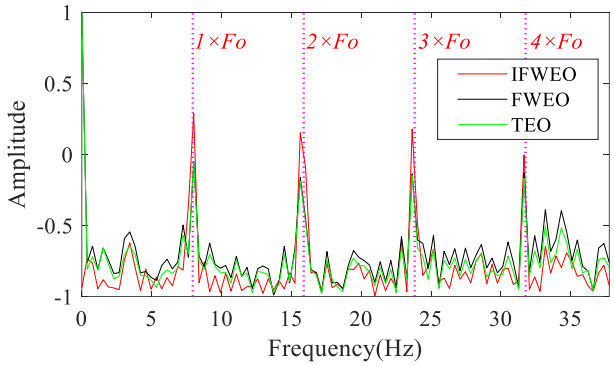

Fig. 24 Energy operator comparison

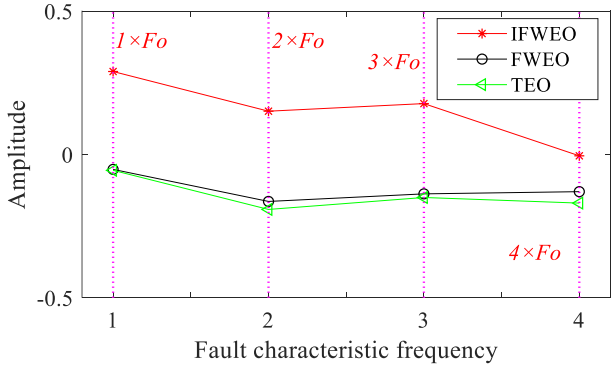

Fig. 25 Fault characteristic frequency values of IFWEO, FWEO and TEO

Combining all the above experiments, it is verified that the weighted kurtosis VMD and the IFWEO presented in this study could not only accurately extract the characteristic frequencies of the low speed bearing faults, but also the best compare with the similar methods. All of the results

show that the proposed method can effectively extract and accurately diagnose the low speed rolling bearing.

3.6 Conclusion

This chapter is for the problems of rotating machinery fault signal with strong background noise and difficult to diagnosis faults, presented a method based on weighted kurtosis VMD and IFWEO to filtered noise and enhance fault feature. The VMD is employed to decompose signal, and the weighted kurtosis is applied to select the optimal IMFs which carry abundant fault information. The third-order cumulant is introduced into the FWEO to improve the analysis performance, and then the IFWEO is used to further improve the signal SNR and enhance the signal impulse. The simulation analysis and engineering experiment results verified that this method could effectively realize the low speed bearing fault diagnosis. Through the method presented in this study, the low speed bearing fault feature is improved obviously, the fault characteristic frequency is easily extracted from the envelope spectrum, and the low bearing fault could be effectively diagnosed.

Chapter 4 Signal processing method based on Rad-SSF and 1.5-dimensional third-order energy spectrum

4.1 Introduction

Raw vibration signals poorly perform in industrial rotating machinery fault diagnosis because the impulse features are damped and masked by disturbances and noises. The fact that the fault features are weak makes the fault diagnosis more challenging. This work presents a signal filtering and fault characteristic enhancement method based on reconstruction adaptive determinate stationary subspace filtering (Rad-SSF) and 1.5-dimensional third-order energy spectrum to address the above-mentioned problems.

However, the impulse is often weakened compared with the fault source due to other vibration interferences caused by the complex structure of the equipment. Worse, an excitation exists among other components, and the fault impact characteristic often suppressed when coupled with the industrial working noise [118]. Previous studies have shown that the background noise must be filtered, and the impact characteristic of the vibration signal must be enhanced to effectively realize rotating machinery fault diagnosis. Stationary subspace analysis (SSA) [119] is an effective blind source separation method, and it could effectively decompose the high-dimensional signal into stationary and non-stationary ones.

In this chapter, Rad-SSF reconstructs an adaptive self-determined and decomposed vibration signal trajectory matrix to obtain the non-stationary signals. Thereafter, the filtered signal with the best fault characteristics is extracted according to the kurtosis. Meanwhile, a 1.5-dimensional third-order energy spectrum is performed to enhance the fault characteristics by strengthening the fundamental frequency and eliminating non-coupling harmonics. Finally, the dominant frequency in the spectrum is contrasted to recognize fault diagnosis, referring to the theoretical fault characteristic frequency.

To verify the effectiveness of the method presented in this chapter, a bearing outer race fault simulation analytical model is established, and engineering signals are acquired for experiments. The results prove that this method could effectively extract the signal impulse from the strong background noise and enhance the fault characteristic frequency value, realizing bearing fault diagnosis.

4.2 Rad-SSF principle

In rotating machinery fault diagnosis, the vibration signal is divided into fault impulse and background noise. If the fault impulse can be extracted using the signal separation method, then the signal will be effectively filtered, and the SNR will be improved [120]. The Rad-SSF method can adaptively expand the vibration signal to a high-dimensional one and decompose it into stationary and non-stationary signals to realize the extraction of the best fault characteristic signal. This mechanism is an effective signal filtering method.

4.2.1 Phase space matrix

The vibration signal $\mathbf{X}=\{x_1,x_2,\cdots x_N\}$ is dimensionally expanded to reconstruct a *d*-dimensional trajectory matrix:

$$\mathbf{X}=\begin{bmatrix}\mathbf{X_1}\\ \mathbf{X_2}\\ \vdots\\ \mathbf{X_d}\end{bmatrix}=\begin{bmatrix}x_1 & x_2 & \cdots & x_{N-(d-1)}\\ x_2 & x_3 & \cdots & x_{N-(d-2)}\\ \vdots & \vdots & \ddots & \vdots\\ x_d & x_{d+1} & \cdots & x_N\end{bmatrix} \tag{25}$$

where $\mathbf{X}_i=\{x_i,x_{i+1},\cdots x_{N-(d-i)}\}$ is the *i*th phase point, and it represents a vector in the trajectory matrix.

4.2.2 False nearest point

In each vector $\mathbf{X}_i$, a nearest neighbor $\mathbf{X}_i^{NN}$ is within a certain distance, and the distance is:

$$R_d=\left\|\mathbf{X}_i-\mathbf{X}_i^{NN}\right\| \tag{26}$$

When the dimensionality of the trajectory matrix increases from *d* to *d*+1, the distance between $\mathbf{X}_i$ and $\mathbf{X}_i^{NN}$ changes:

$$R_{d+1}^2=R_d^2+\left\|\mathbf{X}_{i+\tau d}-\mathbf{X}_{i+\tau d}^{NN}\right\| \tag{27}$$

If R_{d+1} is much larger than R_d because two non-adjacent points in the high-dimensional become adjacent when projected onto the low-dimensional, then $\mathbf{X}_i^{NN}$ is the false nearest neighbor of $\mathbf{X}_i$ [121]. Definition:

$$a(i,d)=\left\|\mathbf{X}_{i+\tau d}-\mathbf{X}_{i+\tau d}^{NN}\right\|/R_d \tag{28}$$

$$\begin{cases}E(d)=\dfrac{1}{N-\tau d}\displaystyle\sum_{i=1}^{N-\tau d}a(i,d)\\ E1(d)=E(d+1)/E(d)\end{cases} \tag{29}$$

In the vibration signals, $E1(d)$ gradually increases. The best embedding dimension is when $E1(d)$ slowly changes because the reconstructed trajectory matrix has completely recovered from the time sequence.

4.2.3 Improved stationary subspace analysis

SSA is used for trajectory matrix decomposition, as in Fig. 26.

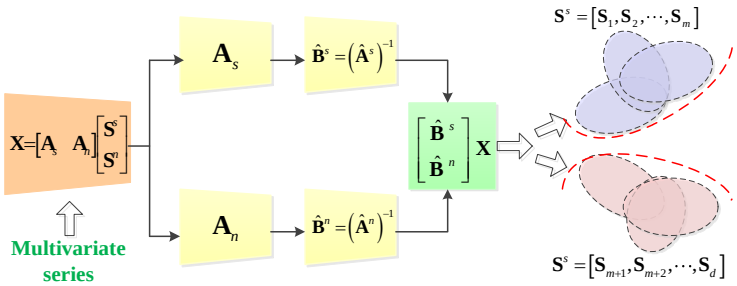

Fig. 26 SSA main idea

The *d*-dimensional trajectory matrix $\mathbf{X}$ can be decomposed into *m*-dimensional stationary $\mathbf{S}^s$ and *n*-dimensional (*n*=*d*-*m*) non-stationary $\mathbf{S}^n$ [122, 123]:

$$\mathbf{S}^s=\left[\mathbf{S}_1,\mathbf{S}_2,\cdots,\mathbf{S}_m\right] \tag{30}$$

$$\mathbf{S}^n = \left[\mathbf{S}_{m+1}, \mathbf{S}_{m+2}, \cdots, \mathbf{S}_d\right] \tag{31}$$

Invertible matrix $\mathbf{A}$ is satisfies the following transformation:

$$\mathbf{X} = \left[\mathbf{A}_s \quad \mathbf{A}_n\right]\begin{bmatrix}\mathbf{S}^s \\ \mathbf{S}^n\end{bmatrix} \tag{32}$$

where $\mathbf{A}_s$'s column vector is called stationary space ($s-$), $\mathbf{A}_n$'s column vector is called non-stationary space ($n-$).

The core of the SSA is to find a linear transformation matrix $\hat{\mathbf{B}} = \hat{\mathbf{A}}^{-1}$, which is used to distinguish between stationary and non-stationary, as follows:

$$\begin{bmatrix}\hat{\mathbf{S}}^s \\ \hat{\mathbf{S}}^n\end{bmatrix} = \hat{\mathbf{B}}\mathbf{X} = \begin{bmatrix}\hat{\mathbf{B}}^s \\ \hat{\mathbf{B}}^n\end{bmatrix}\mathbf{X} \tag{33}$$

where $\hat{\mathbf{S}}^s$ is an estimated stationary, $\hat{\mathbf{S}}^n$ is an estimated non-stationary, $\hat{\mathbf{B}}^s$ is an estimated stationary space projection, $\hat{\mathbf{B}}^n$ is an estimated non-stationary space projection, and $\hat{\mathbf{A}}^{-1}$ is an inverse matrix of the estimated invertible matrix $\hat{\mathbf{A}} = \left[\hat{\mathbf{A}}_s \quad \hat{\mathbf{A}}_n\right]$.

Kurtosis can well represent the impulse feature of the vibration signal in bearing fault diagnosis. The kurtosis of each non-stationary signal is calculated, and the $\hat{\mathbf{S}}^{n_i}$ with the largest kurtosis as the filtered signal is selected.

$$\begin{aligned}&\arg\max\left(g\left(\hat{\mathbf{S}}^{n_i}\right)\right) \\ &g\left(x\right) = \frac{1}{N}\sum_{i=1}^{N}\left(x_i - \overline{x}/\sigma\right)^4\end{aligned} \tag{34}$$

4.2.4 Mechanism of Rad-SSF

Tab.3 shows the Rad-SSF algorithm steps, which mainly include three parts: trajectory matrix adaptive determinate reconstruction; stationary subspace analysis extracts the non-stationary signal to filter out background noise; and the best filtered signal containing bearing fault characteristic is selected according to the maximum kurtosis.

Tab. 3 Rad-SSF algorithm

Algorithm 1 Reconstruction adaptive determinate stationary subspace filtering method (Rad-SSF)
Input: The acquired one dimensional vibration signal $\mathbf{x} = \{x_1, x_2, \cdots x_N\}$ and $L(\hat{\mathbf{B}}^s)$, $L(\hat{\mathbf{B}}^n)$
Output: The Rad-SSF filtered signal $\tilde{\mathbf{X}} = \{\tilde{x}_1, \tilde{x}_2, \cdots \tilde{x}_N\}$

For i from 1 to d **do**
Reconstruct trajectory matrix $\mathbf{X}_i$ and calculate $R_{d+1}^2 = R_d^2 + \left\|\mathbf{X}_{i+\tau d} - \mathbf{X}_{i+\tau d}{}^{NN}\right\|$, according to the Criteria to decide the embedding dimension d.
End for

Reconstruct the matrix $\mathbf{X}_d$ and calculate the mean $\hat{\mu}_i$ and standard deviation $\hat{\Sigma}_i$
While $i < i_{\max}$ and $f(\hat{\mathbf{B}}^s) > L(\hat{\mathbf{B}}^s)$ **do**

For a random initial $\hat{\mathbf{B}}^s$, Calculate each time period stationary source estimation signal mean value $\hat{\mu}_{s,i}=\hat{\mathbf{B}}^s\hat{\mu}_i$, covariance matrix $\hat{\Sigma}_{s,i}=\hat{\mathbf{B}}^s\hat{\Sigma}_i$, distribution $Norm(\hat{\mu}_{s,i},\hat{\Sigma}_{s,i})$ and the sum of Kullback Leibler (KL) divergence to construct the objective function $f(\hat{\mathbf{B}}^s)=\sum_i^L D_{KL}\left[Norm(\hat{\mu}_{s,i},\hat{\Sigma}_{s,i})\middle\| Norm(0,I)\right]$

End while

According to the minimum $f(\hat{\mathbf{B}}^s)$, the optimal stationary space projection $\hat{\mathbf{B}}^s$ is obtained, and then the stationary source estimation signal $\hat{\mathbf{S}}^s$ is obtained.

While $i<i_{\max}$ and $f(\hat{\mathbf{B}}^n)<L(\hat{\mathbf{B}}^n)$ **do**

For a random initial $\hat{\mathbf{B}}^n$, Calculate each time period stationary source estimation signal mean value $\hat{\mu}_{s,i}=\hat{\mathbf{B}}^n\hat{\mu}_i$, covariance matrix $\hat{\Sigma}_{s,i}=\hat{\mathbf{B}}^n\hat{\Sigma}_i$, distribution $Norm(\hat{\mu}_{s,i},\hat{\Sigma}_{s,i})$ and the sum of Kullback Leibler (KL) divergence to construct the objective function

$f(\hat{\mathbf{B}}^n)=\sum_i^L D_{KL}\left[Norm(\hat{\mu}_{n,i},\hat{\Sigma}_{n,i})\middle\| Norm(0,I)\right]$

According to the minimum $f(\hat{\mathbf{B}}^n)$, the optimal stationary space projection $\hat{\mathbf{B}}^n$ is obtained, and then the stationary source estimation signal $\hat{\mathbf{S}}^n$ is obtained.

End while

Accord to the Eq. (10) to choose the best $\hat{\mathbf{S}}^{n_i}$ as the filtered signal for fault diagnosis

Fig. 27 shows the illustrations of the calculation steps for the Rad-SSF. The fault impulse in the filtered signal is more obvious compared with the raw vibration signal, demonstrating that this Rad-SSF can effectively filter out background noise.

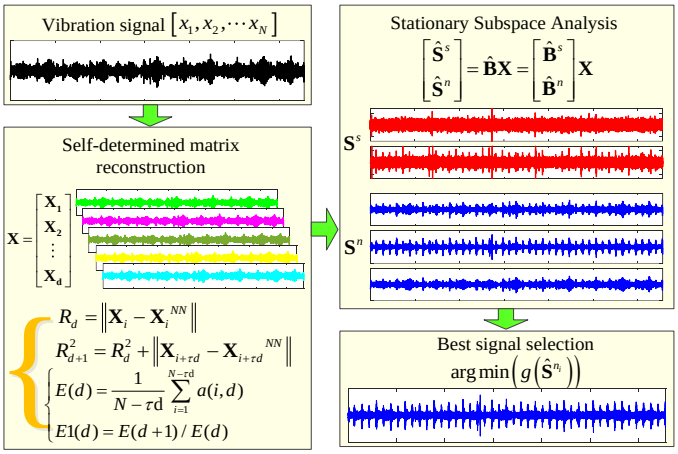

Fig. 27 Illustrations of the calculation steps for the Rad-SSF

4.3 1.5-dimensional third-order energy spectrum

The improved demodulation method of 1.5D third-order energy spectrum is applied to enhance the impact signal feature caused by bearing fault for its advantages of strengthening the fundamental frequency, and eliminating the non-coupling harmonic components.

4.3.1 Third-order TEO

The TEO is defined as follows for continuous time signals [124, 125]:

$$\psi\left[x(t)\right]=\dot{x}^2(t)-x(t)\ddot{x}(t) \tag{35}$$

where $\dot{x}(t)$ and $\ddot{x}(t)$ are the first and second derivatives, respectively.

The expression for discrete sampling signals is as follows:

$$\psi\left[x(n)\right]=x^2(n)-x(n-1)x(n+1) \tag{36}$$

The traditional TEO only performs the second derivative on the fault vibration signal with strong background noise, causing the result to be seriously disturbed by noise. In the third derivative [126], the number of symmetric sample data used is 5, which can better distinguish the instantaneous changes in terms of time resolution. Therefore, the TEO is extended to the third-order TEO to ensure the mathematical symmetry, and the discrete form is as follows:

$$\begin{aligned}\varphi\left[x(n)\right]=&\left[x(n)\right]^3+\left[x(n+1)\right]^2x(n-1)-\\&x(n+1)\left[x(n-1)\right]^2-x(n)x(n-2)x(n+2)\end{aligned} \tag{37}$$

Fig. 28 shows a schematic of the third-order TEO. In comparison with the original signal and TEO, the impact is greatly improved because of the third derivative.

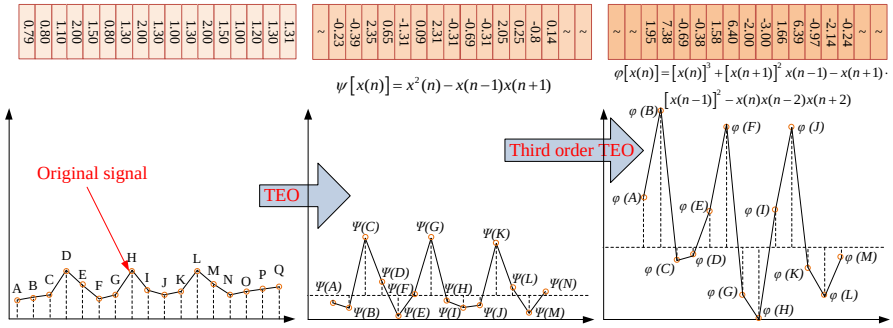

Fig. 28 Schematic diagram of the third-order TEO

4.3.2 1.5-dimensional spectrum

The third-order cumulant diagonal tangent has the advantages of suppressing the Gaussian white noise, strengthening the fundamental frequency, and eliminating the non-coupling harmonic components [127]. The third-order cumulant diagonal tangent for $\varphi\left[x(n)\right]$ is calculated as follows:

$$C(\tau)=E\left[\varphi\left[x(n)\right]\varphi\left[x(n+\tau)\right]\varphi\left[x(n+\tau)\right]\right] \tag{38}$$

where τ is the delay parameter, and E is the expectation.

Fourier transform is performed on $C(\tau)$, and the 1.5-dimensional third-order energy spectrum is as follows:

$$C(\omega)=\int_{-\infty}^{\infty}C(\tau)e^{-j\omega n}d\tau \tag{39}$$

4.4 Method flow chart

A rotating machinery signal processing method based on Rad-SSF and 1.5-dimensional third-order energy spectrum is illustrated in this work. This method can effectively filter the background noise of industrial vibration signal and enhance fault impulse characteristics. The implementation steps are as follows:

Step 1: Place the acceleration sensor to acquire the vibration signal.

Step 2: Adaptively reconstruct the trajectory matrix based on the Rad-SSF method to decompose it into non-stationary, and the best filtered signal is selected on the basis of kurtosis;

Step 3: Calculate the 1.5-dimensional third-order energy spectrum of the filtered signal.

Step 4 Extract the dominant frequency from the 1.5-dimensional third-order energy spectrum, and compare it with the theoretical fault characteristic frequency to realize fault diagnosis.

The specific framework is shown in Fig. 29, and it is takes bearing fault as an example.

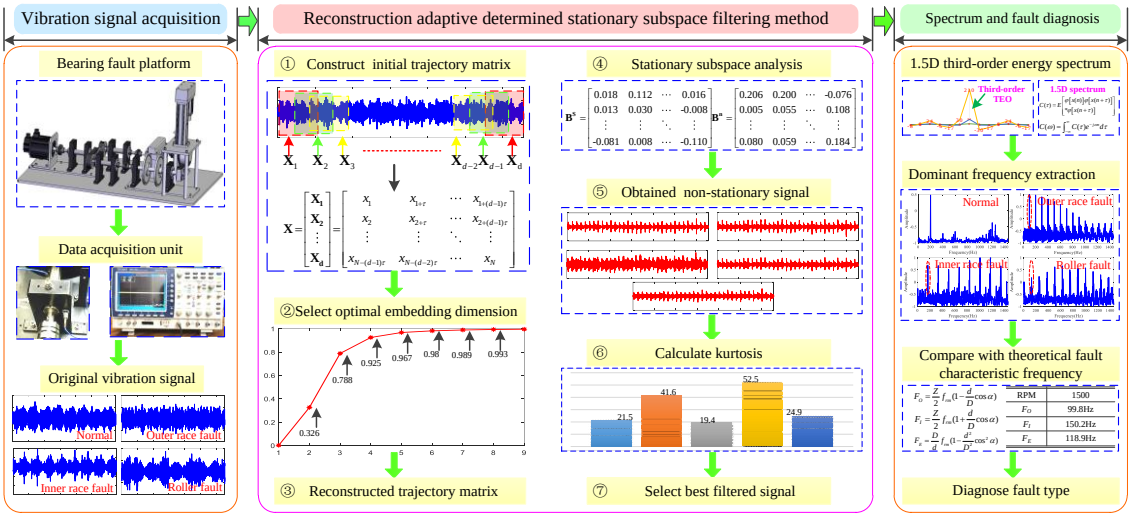

Fig. 29 Bearing fault diagnosis framework based on Rad-SSF and 1.5D third-order energy spectrum

4.5 Experimental verification

In order to verify the effect of Rad-SSF and 1.5-dimensional third-order energy spectrum method proposed in this chapter on non-stationary extraction of vibration signal and enhancement of fault characteristic, this chapter uses medium and high-speed bearing faults common in rotating machinery fault types for verification. The experimental verification is divided into two parts, simulation verification and engineering experimental verification.

4.5.1 Simulation analysis

This work establishes a bearing outer race fault simulation model according to Eq. (40) to verify the practicability of the proposed method in terms of signal filtering and fault feature enhancement.

4.5.1.1 Simulation model establishment

The model includes two parts: the specific fault impulse and the noise. The random noise is in the range of (0, 1). Tab. 4 shows the main parameters of the model, where $n(t)$ is the simulated background noise, which is a random number that follows the normal distribution, N_0 is RPM.

$$f(t)=\sum_{i=1}^{N_0}\left[\begin{array}{l}\sin 2\pi(t-i/f_0)\sqrt{1-\xi_0^2}\cdot \\ (f_{01}e^{-\xi_0 2\pi f_{01}(t-i/f_0)}+f_{02}e^{-\xi_0 2\pi f_{02}(t-i/f_0)})\end{array}\right]+n(t) \tag{40}$$

Tab. 4 Specific parameters of simulation model

Parameter	Value
Period	N_O=41
carrier centers frequencies	f_{01}=2000 Hz
	f_{02}=5200 Hz
damping ratio	ζ_0=0.02
characteristic frequency	F_O=50 Hz

Fig. 30(a) shows the fault impulse signal without noise, and the signal is regular and periodic. Fig. 30(b) shows the spectrum without noise signal, and the dominant frequency is 50 Hz, which is consistent with the setting in the model. Fig. 30(c) shows the signal with random noise, and the fault impulse is submerged. In the spectrum shown in Fig. 30(d), no dominant frequency is found at 50 Hz; thus, the fault characteristic frequency could not be extracted.

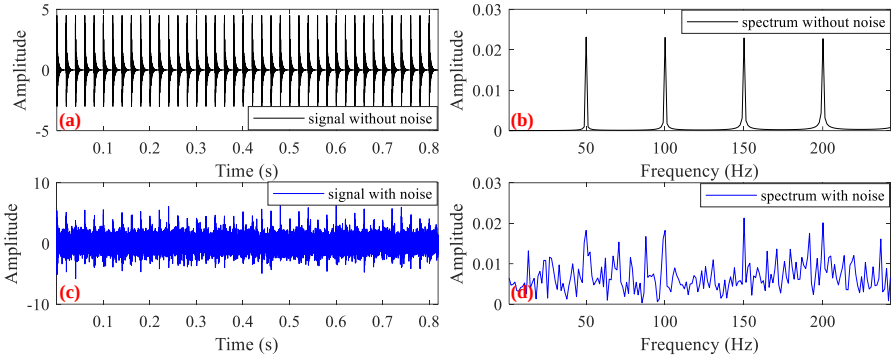

Fig. 30 Simulated signal and its spectrum under noisy and noise-free

4.5.1.2 Rad-SSF verification

The trajectory matrix of the simulation signal is adaptively reconstructed on the basis of the Rad-SSF method. Fig. 31(a) shows the *E1(d)* value with the increase in the embedding dimension. If the embedding dimension is small, then the false adjacent points will be large in the trajectory matrix; if it is large, then the calculation will be complex. When the embedding dimension is greater than six, *E1(d)* slowly increases. Fig. 31(b) shows the 6D signal of the trajectory matrix.

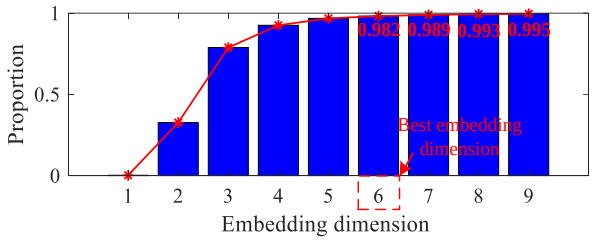

(a)

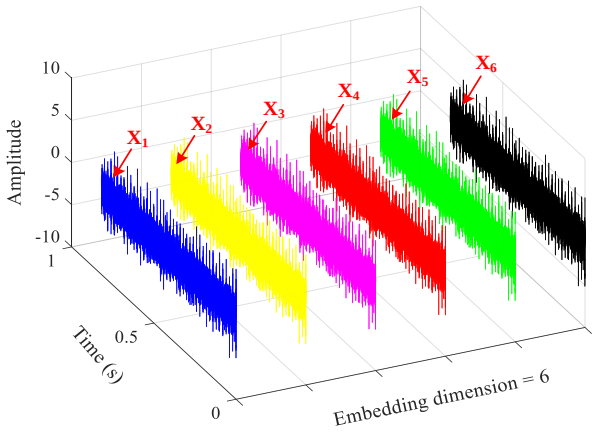

(b)

Fig. 31 *E1(d)* value changes and reconstructed trajectory matrix signal: (a) The E1(d) value at different embedding dimension; (b) 6D signal of the trajectory matrix

Fig. 32 shows that the trajectory matrix signal is divided into stationary and non-stationary, and a part of the signal is analyzed for probability distribution. In Figs. 32(a), 32(b), and 32(c) (stationary signal), the signal probability distributions are basically in line with the normal

distribution. Meanwhile, Figs. 32(d), 32(e), and 32(f) (non-stationary signal) show a different distribution. The bearing fault impulse has a non-stationary characteristic.

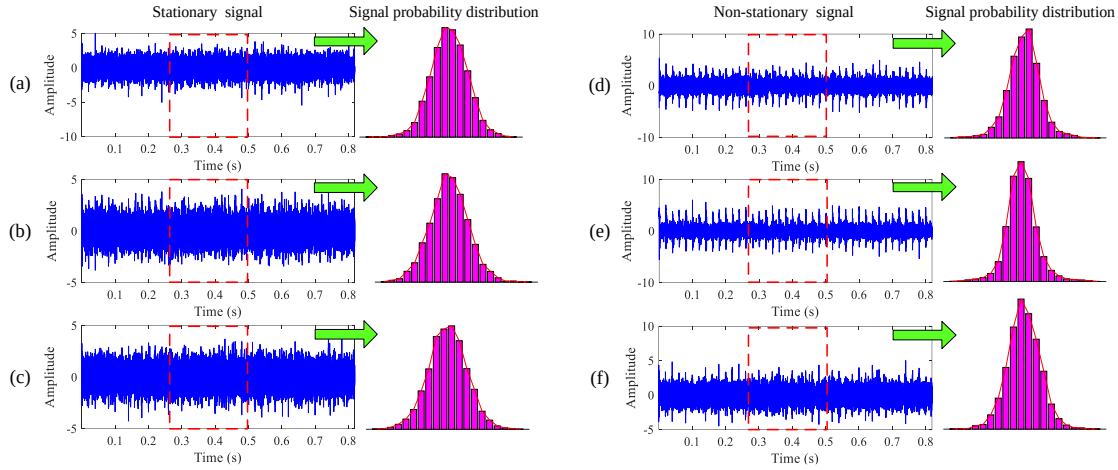

Fig. 32 Stationary subspace analysis and its signal probability distribution

Tab. 5 illustrates the kurtosis of the signals in Fig. 32(a) - (f). The maximum kurtosis (5.582) corresponds to the second non-stationary signal. Therefore, Fig. 32(e) is the best filtered signal that contains the optimal fault characteristic.

Tab. 5 Kurtosis of stationary and non-stationary signal

stationary signal	kurtosis	non-stationary signal	kurtosis
1	3.351	1	4.607
2	3.249	***2***	***5.582***
3	3.186	3	3.660

4.5.1.3 1.5-dimensional third-order energy spectrum verification

The 1.5-dimensional third-order energy spectrum of the filtered signal to enhance the fault impulse characteristics is shown in Fig. 33. In the energy spectrum, the dominant frequency is consistent with the fault characteristic frequency set in the simulation model. In comparison with Fig. 30(d), the dominant frequency and its harmonics are prominent, and the noise is significantly filtered.

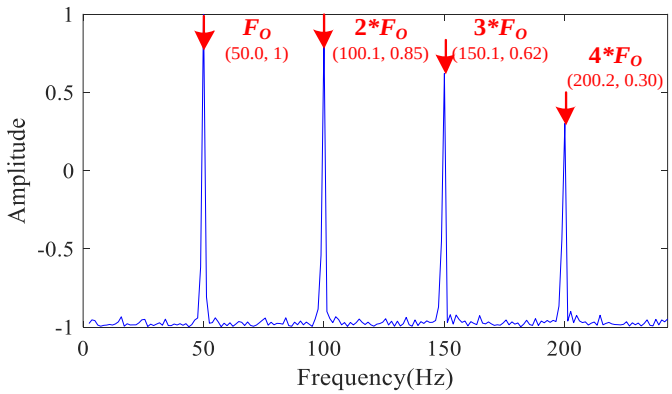

Fig. 33 1.5D third-order energy spectrum of the filtered signal

4.5.2 Engineering experiment

This chapter carries out diagnosis research based on the bearing fault of high-speed rotating machinery, and verifies the accuracy of the method proposed in this chapter through actual engineering signal.

4.5.2.1 Experiment platform

Fig. 34 shows the bearing fault signal acquisition platform used in this experiment, and it is designed according to the industrial environments. This platform consisted of a servo motor, a control system, an intermediate shaft, and removable bearing base. The system can realize uniform operation and RPM regulation, and had a maximum speed of 1800 RPM. The acceleration sensor is placed above the bearing base to acquire vibration signals. The bearing used in this platform is a rolling bearing from NTN Bearing Co., Ltd with a type of NU204 ET2X. Using wire cutting technology to cut square notches on the bearing, it can carry out bearing inner race fault experiment, outer fault experiment, and rolling fault experiment. The bearing is located in the detachable base, and the acceleration sensor is used to acquire vibration signals.

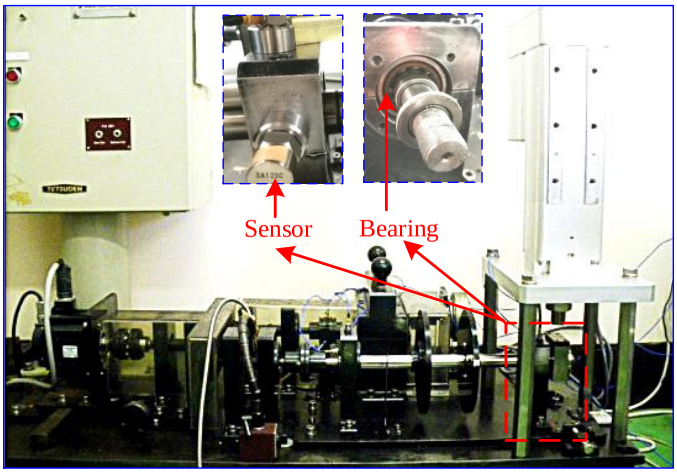

Fig. 34 Bearing fault signal acquired platform

To manufacture the single point faults of the test bearings, square notches were cut on the outer race, inner race, and rolling elements respectively through wire cutting, as shown in Fig. 35.

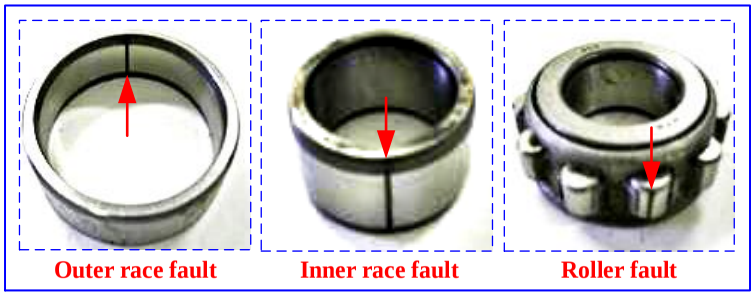

Fig. 35 The manifestation of bearing faults (fault degree: big)

The bearing fault degrees are divided into small, middle, and big according to the depth and width of the square notch. Tab. 6 shows the specific parameters of the bearings. The bearing used in outer race fault experiment has 10 rolling elements, and 11 rolling elements in the inner race and rolling fault experiments.

Tab. 6 Specific parameters of the bearings

	Parameter	Value
Bearing parameters	number of rollers (Z_n)	10 (or 11)
	roller diameter (d)	6.5 mm
	pitch diameter (D)	32.25 mm
	contact angle (α)	0
Fault degree (depth*width)	Small	0.05 mm*0.3 mm
	Middle	0.15 mm*0.5 mm
	Big	0.25 mm*0.7 mm

The bearing fault characteristic frequency refers to the specific inherent component in the spectrum, which corresponds to the bearing fault types. It is only related to bearing parameters and rotating frequency. Equations. 20 - 22 are used to calculate the bearing fault characteristic frequency, and Tab. 7 shows the specific characteristic frequency in this experiment.

Tab. 7 Bearing fault characteristic frequency

RPM	Fault characteristic frequency		
	F_O	F_I	F_E
500	33.2 Hz	55.7 Hz	39.6 Hz
1000	66.5 Hz	110.1 Hz	79.3 Hz
1500	99.8 Hz	165.2 Hz	118.9 Hz

4.5.2.2 Outer race fault experiment

In this experiment, the vibration signals are acquired at 500, 1000, and 1500 RPM, the sampling frequency is 100 kHz, and the signal length is 65,536. Fig. 36 shows the vibration signal and its envelope spectrum. The fault impulse is submerged by strong background noise. In the envelope spectrum, the fault characteristic frequency (F_O) cannot be extracted.

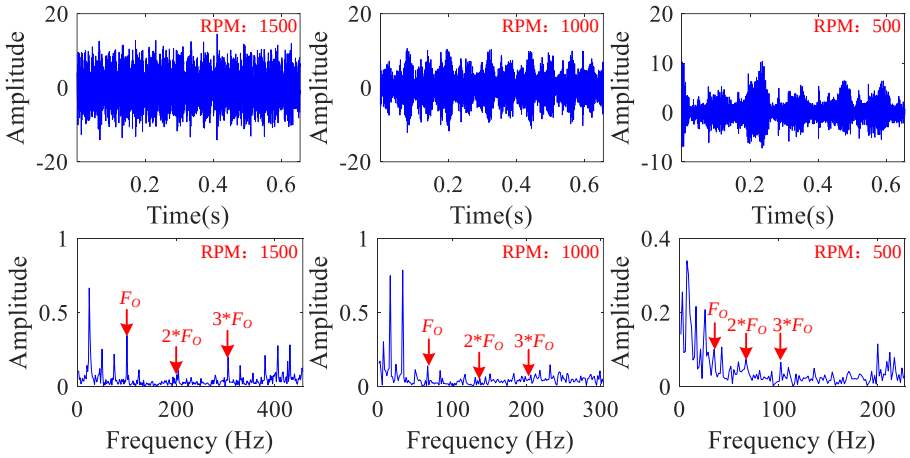

Fig. 36 Vibration signal and its envelope spectrum

Fig. 37 shows that the *E1(d)* value as the embedding dimension expands during trajectory matrix reconstruction when using the Rad-SSF method to filter the signal. In Fig. 37, the *E1(d)*

distribution in all three states is similar. When the embedding dimension is 5, the *E1(d)* increase gradually slows down, and the value at 8 is close to the value at 9. Therefore, embedding dimension 8 is the best for the trajectory matrix.

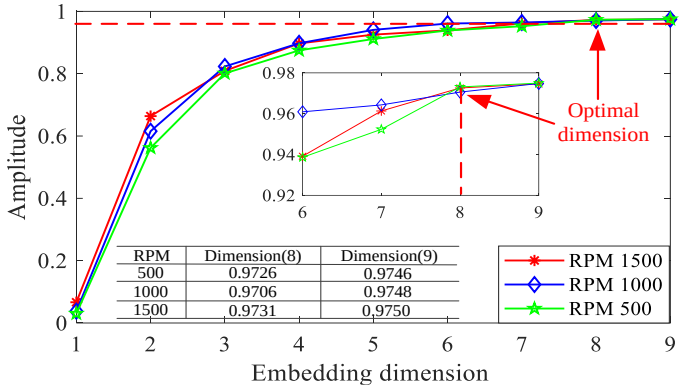

Fig. 37 *E1(d)* distribution as embedding dimension increase

The natural vibration generated by machinery operation and the background noise have stability properties for industrial bearing fault signal, and the fault impulse is non-stationary. Fig. 38 shows the SSA result of the vibration signal, and the regular impulse caused by the outer race fault can be seen in the non-stationary signals. The scatter plot with signals is drawn (x-axis: non-stationary signal; y-axis: stationary signal), with the distribution of the scatter points on the x-axis being more dispersed, and that on the y-axis being more concentrated. Those rules are the same as the probability distribution; the stationary signals follow the Gaussian normal distribution, and the non-stationary signals are different. This study has proven that the method in this work can effectively extract the non-stationary fault impulse from the background noise.

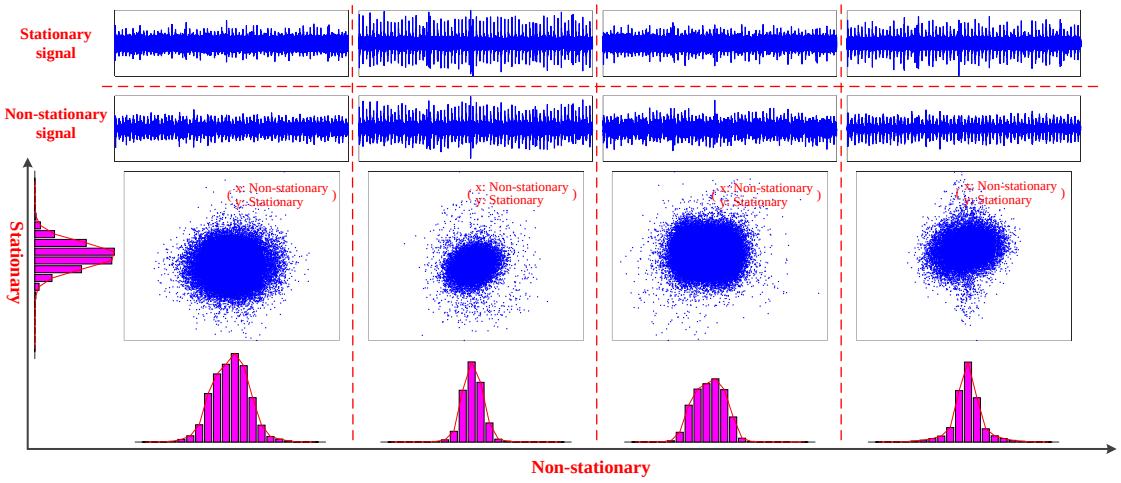

Fig. 38 SSA result of vibration signal, scatter plot figure and signal probability distribution

Fig. 39 shows the kurtosis of stationary and non-stationary signals at 500, 1000, and 1500 RPM; numbers 1- 4 correspond to the stationary signals, and 5 - 8 denote the non-stationary signals. The *6th* kurtosis is much higher in the 500 RPM state than those in the other components. Meanwhile, the *5th* kurtosis is maximum in the 1000 and 1500 RPM. Hence, the best filtered signal is selected as the fault characteristic signal according to the maximum kurtosis.

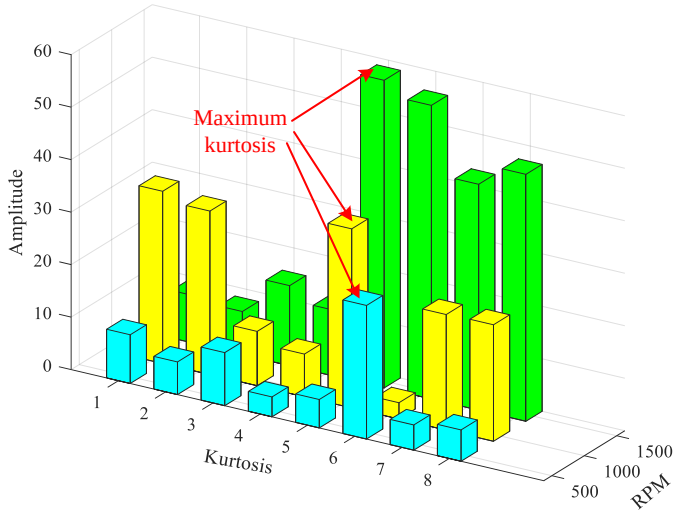

Fig. 39 Kurtosis of stationary signals and non-stationary signals

A 1.5-dimensional third-order energy spectrum is used to enhance the fault impulse characteristics of the Rad-SSF filtered signal, and the result is shown in Fig. 40. The spectrum is normalized to between [−1,1]. In the comparison of the fault characteristic frequencies in Table 7, the difference between the dominant frequency extracted from the energy spectrum and the theoretical value is small (within the allowable range of error) at all three speeds. The above results proved that the proposed method can effectively filter out background noise, enhance the fault impulse characteristics, and realize bearing outer race fault diagnosis.

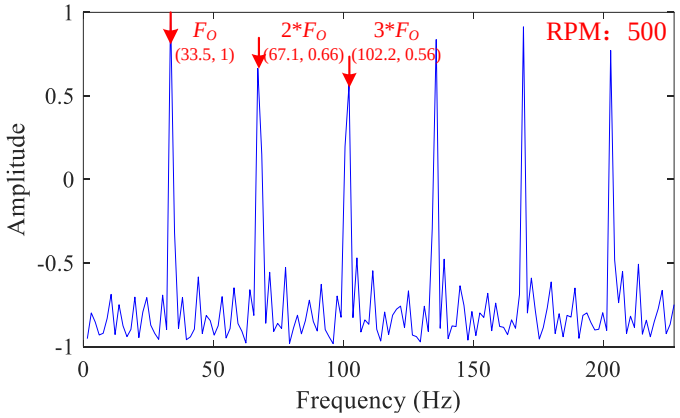

(a)

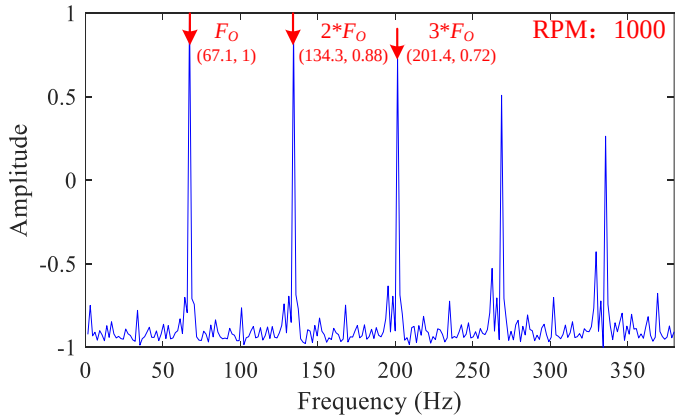

(b)

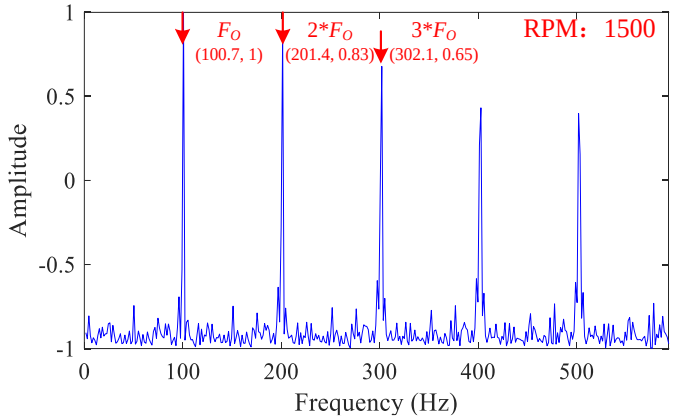

(c)

Fig. 40 1.5-dimensional third-order energy spectrum: (a) Outer race fault at 500 RPM; (b) Outer race fault at 1000 RPM; (a) Outer race fault at 1500 RPM

Experiments were carried out with bearing small, middle, and big faults at 1500 RPM to verify the diagnostic effect of this method for weak faults. Fig. 41(a) shows the corresponding vibration signal and its FFT spectrum. It described that the weaker the fault and the smaller the impact in vibration signal, the more difficult to extract the fault characteristic frequency in spectrum. The Rad-SSF 1.5D third-order energy spectrum are shown in Fig. 41(b), and the dominant frequencies extracted from each spectrum are 100.7, 102.2, and 100.7 Hz, and they are consistent with the theoretical fault characteristic frequency (99.8 Hz). It proves that the spectrum distribution is only related to the bearing fault type, and the fault characteristic frequency under different fault degree is consistent. Meanwhile, the dominant frequency and its harmonic are prominent, and the noise is small, verifying that the method can effectively realize the bearing fault diagnosis under different fault degrees.

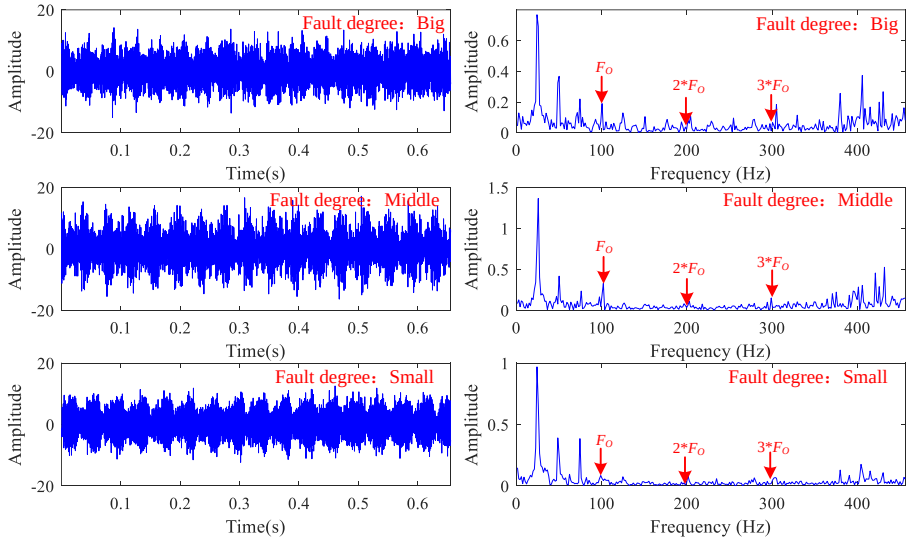

(a)

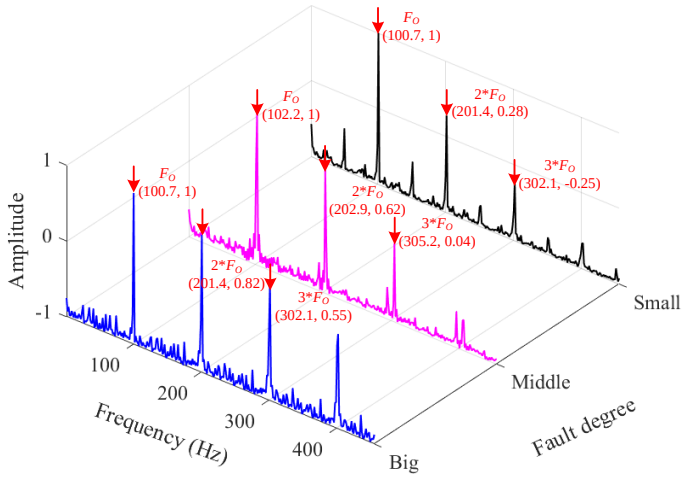

(b)

Fig. 41 Outer race fault diagnosis results under different fault degree: (a) Original signal and its spectrum; (b) Rad-SSF 1.5D third-order energy spectrum

4.5.2.3 Inner race fault experiment

The experiments were carried at three RPMs to verify the effectiveness of this method in the diagnosis of inner race faults. Tab. 8 shows the optimal embedding dimension and maximum kurtosis in the Rad-SSF method.

Tab. 8 Experiments parameters and Rad-SSF results

Parameters		Value
Sampling frequency		100 kHz
Data length		65536
Embedding dimension		6
Number of non-stationary states		3
Kurtosis (Maximum)	RPM: 500	22.1
	RPM: 1000	95.9
	RPM: 1500	225.8

Fig. 42(a) is the vibration signal and its FFT spectrum corresponding to the inner race fault. It shows that the impact caused by the bearing fault is submerged by background noise, and the fault characteristic frequency cannot be accurately extracted from the spectrum. Fig. 42(b) shows the corresponding Rad-SSF 1.5-dimensional third-order energy spectra. In comparison with Tab. 7, the deviation of the dominant frequency extracted from each energy spectrum and the theoretical is within the allowable range. Thus, the method given in this work can accurately diagnose the bearing inner race and roller faults.

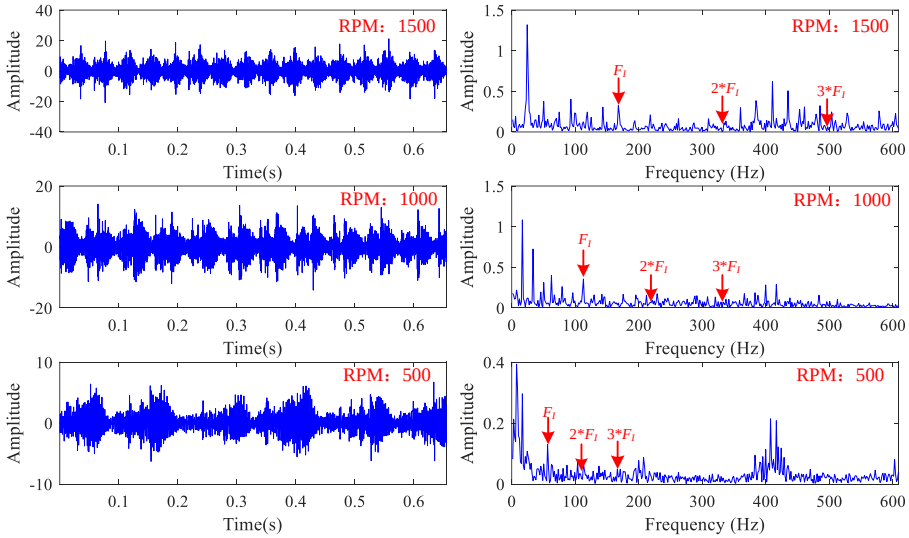

(a)

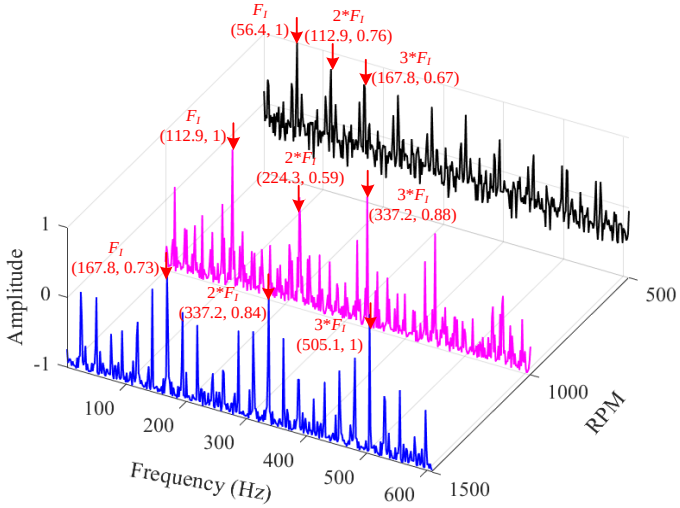

(b)

Fig. 42 Diagnosis result of inner race fault: (a) Original signal and its spectrum; (b) Rad-SSF 1.5D third-order energy spectrum

4.5.2.4 Roller fault experiment

The experiments were carried at three RPMs to verify the effectiveness of this method in the diagnosis of roller faults. Tab. 9 shows the optimal embedding dimension and maximum kurtosis in the Rad-SSF method.

Tab. 9 Experiments parameters and Rad-SSF results

Parameter		Value
Sampling frequency		100 kHz
Data length		65536
Embedding dimension		6
Number of non-stationary states		3
Kurtosis (Maximum)	RPM: 500	7.43
	RPM: 1000	12.48
	RPM: 1500	23.26

Fig. 43(a) is the vibration signal and its FFT spectrum corresponding to the roller fault. It shows that the impact caused by the bearing fault is submerged by background noise, and the fault characteristic frequency cannot be accurately extracted from the spectrum. Fig. 43(b) shows the corresponding Rad-SSF 1.5-dimensional third-order energy spectra. In comparison with Tab. 7, the deviation of the dominant frequency extracted from each energy spectrum and the theoretical is within the allowable range. Thus, the method given in this work can accurately diagnose the bearing inner race and roller faults.

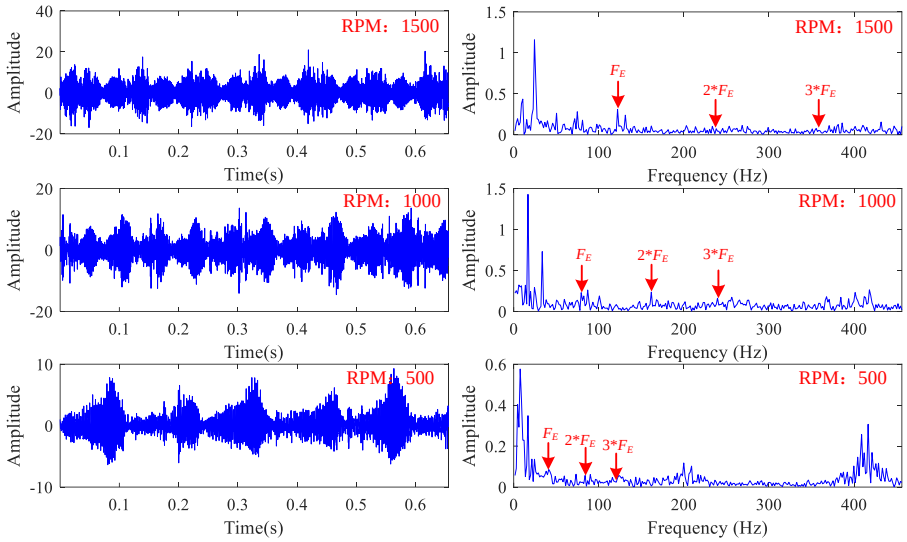

(a)

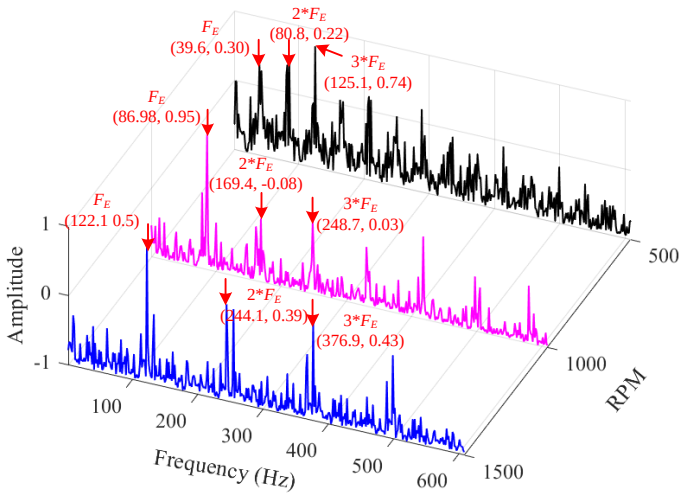

(b)

Fig. 43 Diagnosis result of roller fault: (a) Original signal and its spectrum; (b) Rad-SSF 1.5D third-order energy spectrum

4.5.3 Comparing experiments

In this section, the outer race fault signal is acquired at 1500 RPM. The comparative experiments were carried out from three aspects, namely, embedding dimension, filtering algorithm, and envelope spectrum.

4.5.3.1 Embedding dimension comparing

Experiments carried out at embedding dimensions 4 - 8 to verify the influence of the embedding dimension on the background noise filtering. Fig. 44(a) shows the kurtosis of stationary and non-stationary signals at different embedding dimensions, while Fig. 44(b) depicts the 1.5-

dimensional third-order energy spectrum of each best filtered signal. In Fig. 44(a), the maximum kurtosis gradually increases with the increase in the embedding dimension. In Fig. 44(b), the noise in the spectral energy is the smallest when the embedding dimension is 8. Therefore, the adaptive determinate trajectory matrix reconstruction in Rad-SSF is effective.

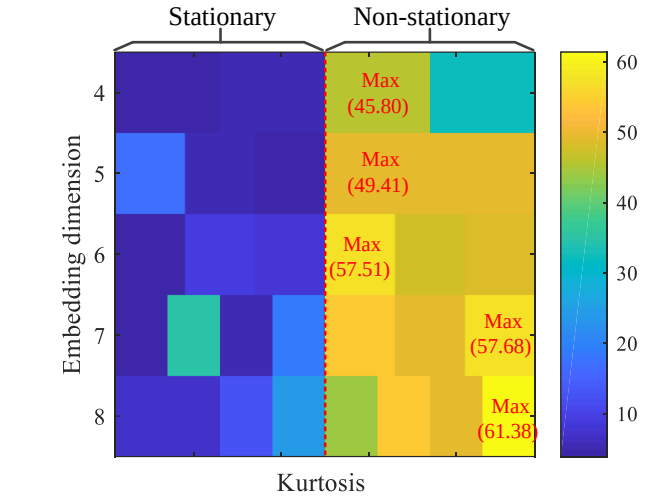

(a)

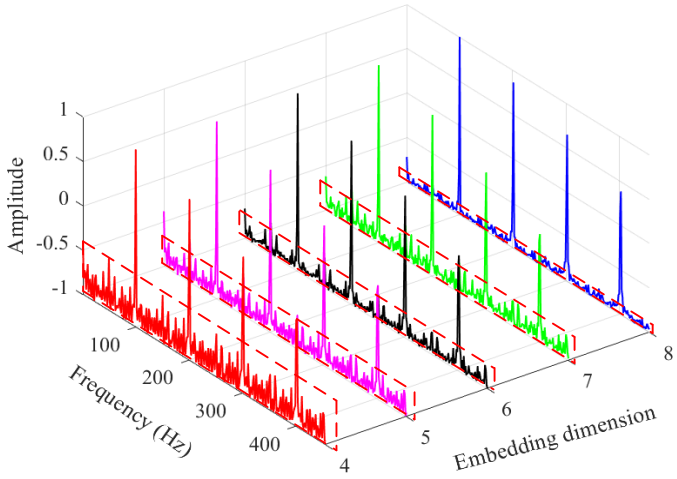

(b)

Fig. 44 Compare result of embedding dimension: (a) Kurtosis of stationary and non-stationary signals at different embedding dimensions; (b) Best filtered 1.5D third-order energy spectrum at different embedding dimensions

4.5.3.2 Filtering method comparing

High-pass filtering, WT, EMD, VMD, and LMD are used in this comparative experiment to verify the superiority of the Rad-SSF. Fig. 45 shows the envelope spectrum of the six algorithms. Although these six methods extracted the fault characteristic frequency, the Rad-SSF method has the smallest noise, and the dominant frequency and its harmonics have the strongest impact, affirming that the method has the best filtering effect on background noise.

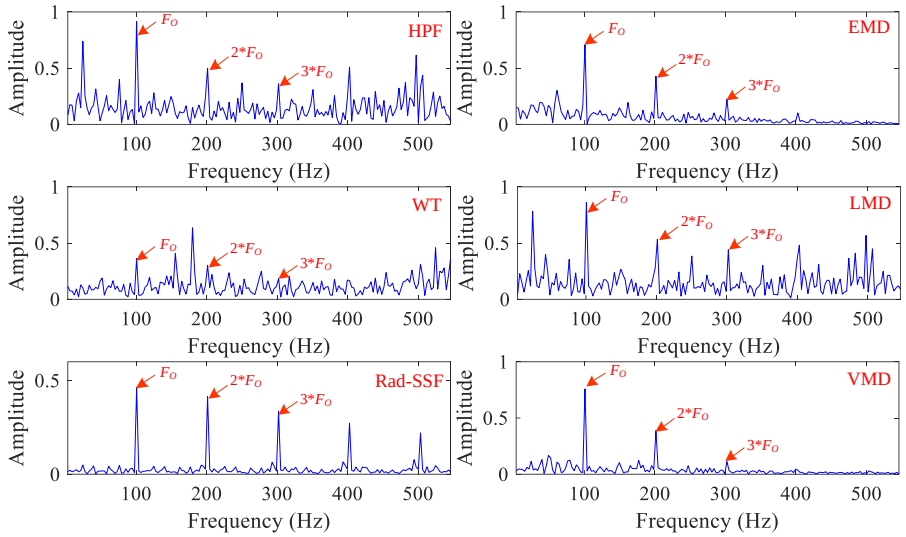

Fig. 45 Compare results of different filtering

The spectrum impairment (SII) and spectral variation (SVI) indices [56] are quoted to evaluate the effects of the RAD-SSF, and the computational time are counted, the results are shown in Tab. 10. The SII and SVI larger, the fault characteristic frequency and its harmonic components on the envelope spectrum more obvious, and the better the filtering effect. Although the calculation time of RAD-SSF is slightly higher, it is within the acceptable range for engineering applications.

Tab. 10 Evaluate results of different methods

Method	SII	SVI	Time (s)
Rad-SSF	40.68	2.93	78.52
HPF	11.29	1.48	1.58
WT	5.88	1.21	4.36
EMD	15.13	1.58	17.78
LMD	23.28	1.80	45.56
VMD	36.98	2.23	167.75

4.5.3.3 Spectrum method comparing

Comparative methods, such as the envelope spectrum, TEO, and third-order TEO, are used to verify the advantages of a 1.5-dimensional third-order energy spectrum in enhancing fault impulse characteristics. The dominant frequency and its harmonics have the largest amplitude in the 1.5-dimensional third-order energy spectrum, proving that the method is more effective in feature enhancement, as illustrated in Fig. 46.

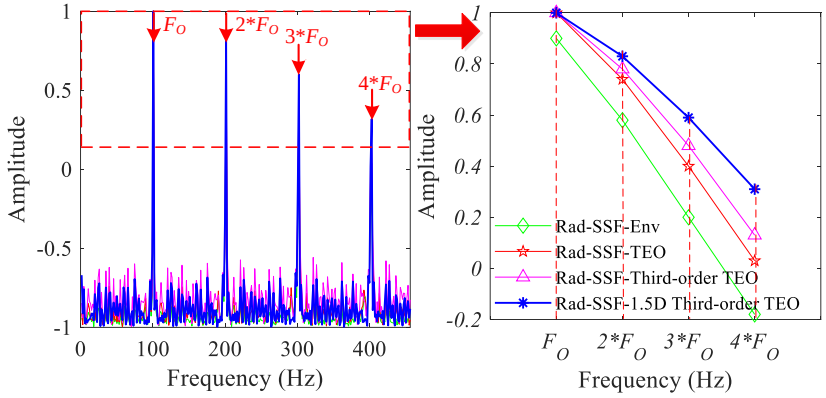

Fig. 46 Compare results of different spectrum

4.5.3.4 Low-speed bearing fault diagnosis comparing

Vibration signals of low-speed rotating machine are acquired to verify the bearing fault diagnosis effect of the method in this study, in terms of background noise filtering and fault feature enhancement. As shown in Fig. 15 (**3.5.2 Engineering Experiment**), the bearing has an outer race fault, and the acceleration sensor is placed directly above it.

The original signal as shown in Fig. 47(a) was acquired at 50 RPM with a sampling frequency of 96 kHz, and the fault characteristic frequency in the FFT spectrum is submerged by background noise. In Fig. 47(b), the comparison results of FIR, WT, and other filtering, the Rad-SSF and 1.5-dimensional third-order energy spectrum has the best performance because of the highest fault characteristic frequency value, smallest background noise, and most evident harmonic component.

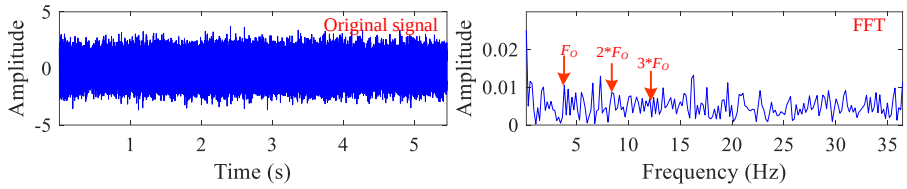

(a)

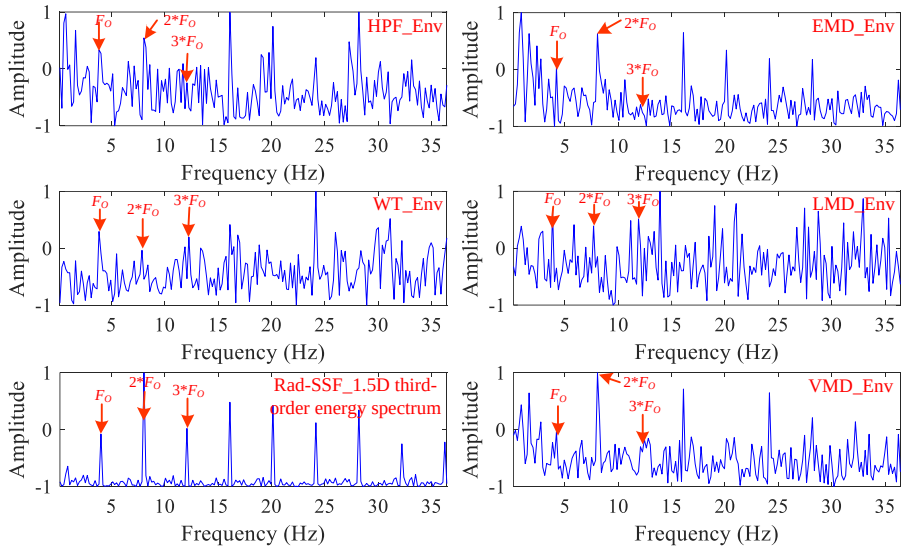

(b)

Fig. 47 Low-speed outer race fault diagnosis: (a) Original signal and its spectrum; (b) Compare results of different filtering

4.6 Conclusion

A signal processing method based on Rad-SSF and 1.5-dimensional third-order energy spectrum is proposed in this chapter. The method employs the Rad-SSF to extract the best bearing fault signal and 1.5-dimensional third-order energy spectrum to enhance the fault characteristics. The dominant frequency is compared with the theoretical fault characteristic frequency to detect fault diagnosis. The feasibility and effectiveness of the proposed method are demonstrated by different experiments. The results show that the proposed method can effectively filter noise and enhance the fault characteristic to bearing fault diagnosis.

Chapter 5 Signal processing method based on adaptive multi-band filtering

5.1 Introduction

The key to precisely diagnosing rotating machinery structural faults is to accurately extract the rotating frequency and its harmonics in the vibration signal. However, given that engineering vibration signals contain a large amount of background noise, improving the SNR of the raw signal is a prerequisite for accurate diagnosis.

The multi-band filtering [128] is specifically designed for filtering the vibration signal of rotating machinery structure faults and only retains the rotating frequency and its harmonics. However, the traditional multi-band filtering takes the theoretical rotating frequency as the cutoff frequency and is usually unable to extract the actual rotating frequency and its harmonics in engineering applications because of deviations.

To solve the problem where the actual rotating frequency and its harmonics cannot be accurately extracted in engineering applications, an improved adaptive multi-band filtering method is designed. This method takes the theoretical rotating frequency as the search center, extracts the maximum within the positive and negative deviation as the actual rotating frequency, and sets a threshold according to the actual value to realize multi-band filtering. This method can effectively remove background noise and accurately extract the actual rotating frequency and its harmonics.

In this chapter, rotating machinery structural faults, such as pedestal looseness, angular misalignment, and static imbalance, were carried out to verify the effectiveness and superiority of this method.

5.2 Principle of adaptive multi-band filtering

The traditional multi-band filtering sets the cutoff frequency based on the theoretical rotating frequency, which usually cannot work well in engineering applications. Therefore, an adaptive multi-band filtering is designed to extract the actual rotating frequency and its harmonic based on a reasonable setting deviation coefficient.

For the vibration signal $\boldsymbol{V}(v_1, v_2, v_3 \cdots v_n) \sim f(v)$, the following Fourier transform is initially applied:

$$F(f) = \sum_{i=0}^{n-1} f(v) e^{-j\frac{2\pi}{n}ki}, k = 0,1,2,\cdots n-1 \tag{41}$$

Afterward, the actual rotating frequency $F_r^{'}$ is computed as

$$F_r^{'} = \max(F_r \pm \beta) \tag{42}$$

where β is the search threshold that is set according to the engineering signal, and F_r is the theoretical rotating frequency calculated by the RPM as shown in Eq. (43):

$$F_r = \frac{RPM}{60} \tag{43}$$

The deviation Δf_r between $F_r^{'}$ and F_r can then be calculated as

$$\Delta f_r = \left| F_r^{'} - F_r \right| \tag{44}$$

Afterward, the multi-band parameters are set as follows:

$$F^{'}(f) = F(k(F_r \pm \Delta f_r) \pm \delta) \tag{45}$$

where δ is the deflection coefficient that is designed to effectively extract the harmonics components. This coefficient usually ranges from 0 Hz to 3 Hz.

The inverse Fourier transform (IFFT) is eventually used for the extracted signal, and the adaptive multi-band filtering is completed.

$$f^{'}(v) = \frac{1}{n}\sum_{i=0}^{n-1} F(f) e^{j\frac{2\pi}{n}ki}, k = 0,1,2,\cdots n-1 \tag{46}$$

Fig. 48 shows the framework of the traditional multi-band filtering and adaptive multi-band filtering. In the raw spectrum, there have a deviation Δf_r between the actual rotating frequency $F_r^{'}$ and the theoretical rotating frequency F_r. The traditional multi-band filtering cannot effectively extract harmonic components (after $2F_r^{'}$) when the deviation reaches a certain value. However, the adaptive multi-band filtering can accurately extract the rotating frequency and its harmonics.

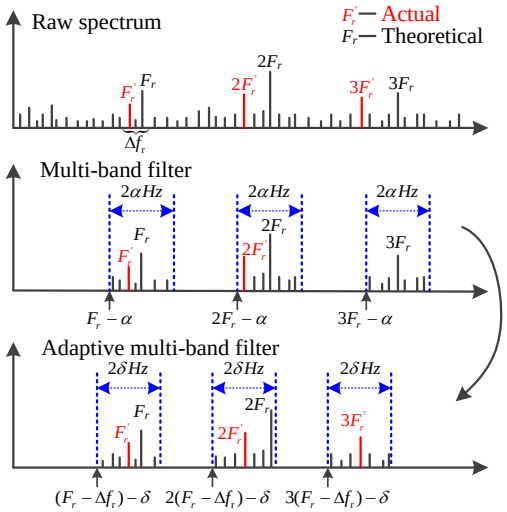

Fig. 48 The framework of the adaptive multi-band filtering and traditional multi-band filtering

5.3 Structural faults background

Couplings, connecting shafts, bolts, and support bases are critical mechanical parts of a rotating machinery. When faults appear in these mechanical structures, especially in high-precision equipment, the machinery will be damaged in serious cases. In rotating machinery structure faults, an obvious impulse is detected at the rotating frequency and its harmonic [129]. Fig. 49(a) shows a simplified model of a rotating machinery, whose common structural faults include coupling looseness, angular misalignment (Fig. 49(b)), dynamic load imbalance (Fig. 49(c)), static load imbalance (Fig. 49(d)), and pedestal looseness.

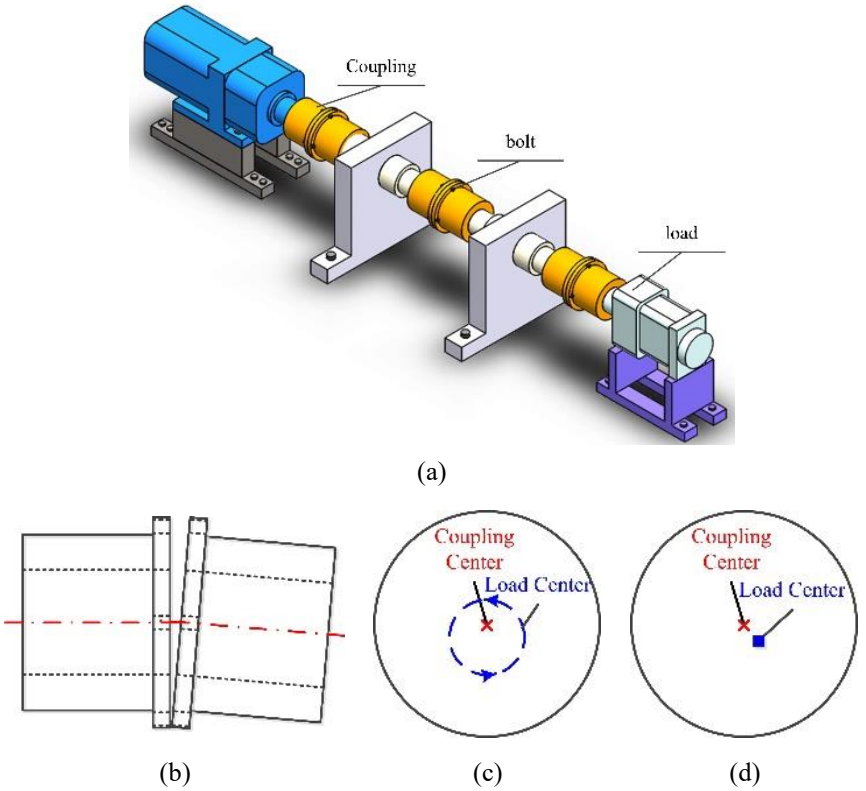

Fig. 49 Simplified model of rotating machinery and its typical structural faults: (a) simplified model; (b) angular misalignment fault; (c) load dynamic imbalance fault; (d) load static imbalance fault

In the vibration spectrum, those characteristics that represent rotating machinery structure faults are obviously detected in the low frequency (less than 1 kHz). Less than 20 times of the rotating frequency are usually extracted in structural fault diagnosis. Fig. 50 shows the spectrum of angular misalignment and pedestal looseness faults. In the structural fault spectrum, shocks occur at the rotating frequency and its harmonics, and the captured impulse obviously differs from that captured for other fault types.

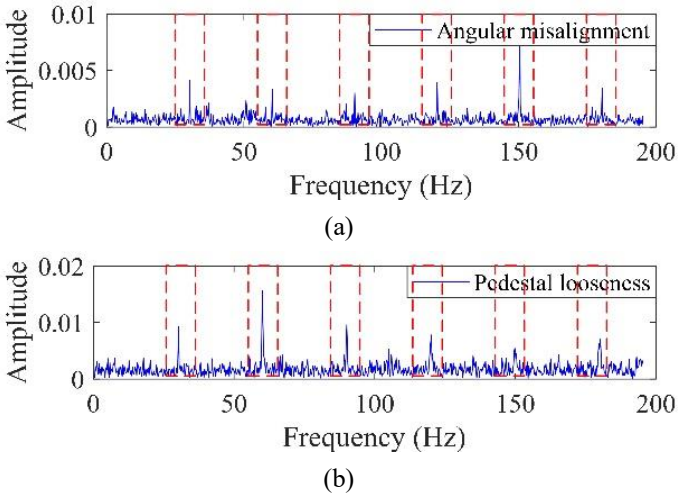

Fig. 50 Vibration spectrum of rotating machinery structure faults: (a) angle misalignment fault; (b) pedestal looseness fault

5.4 Method flow chart

This chapter proposes an adaptive multi-band filtering and verified by rotating machinery structural faults intelligent diagnosis. Meanwhile, the stacked autoencoder (SAE) is used as the classifier to identify fault types.

5.4.1 SAE classification model

SAE is an unsupervised neural network based on deep learning that usually comprises multiple autoencoders stacked in series. The feedback of the output data is realized via back-propagation algorithm [130, 131]. SAE can automatically extract the in-depth characteristics of the input signal in order for the output to achieve a better signal reproduction. Fig. 51 shows the typical autoencoder (AE) structure, which contains an encoder represented by $\mathbf{h} = f(\mathbf{x})$ and a reconstructed decoder represented by $\mathbf{y} = g(\mathbf{h})$. The input signal $\mathbf{x}=(x_1, x_2, x_3 \cdots x_n)$ is mapped to the output $\mathbf{y} = (y_1, y_2, y_3, \cdots y_n)$ through the hidden layer $\mathbf{h} = (h_1, h_2, h_3 \cdots h_m)$, where $m < n$.

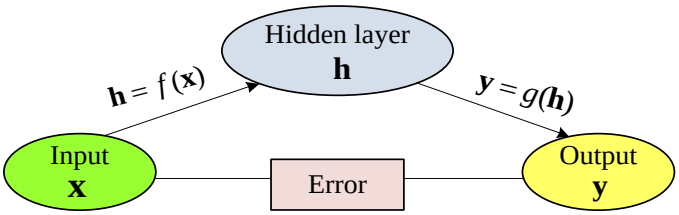

Fig. 51 Principle of autoencoder

The AE specific principle is defined as follows.

First, the signal $\mathbf{x}=(x_1, x_2, x_3 \cdots x_n)$ is inputted into the AE model, and the hidden layer $\mathbf{h} = (h_1, h_2, h_3 \cdots h_m)$ can be expressed as

$$\mathbf{h} = f(\boldsymbol{\omega}_h \mathbf{x} + \mathbf{b}_h) \tag{47}$$

Second, the hidden layer $\mathbf{h}$ is mapped to the original high-dimensional space, and the reconstructed output data $\mathbf{y} = (y_1, y_2, y_3, \cdots y_n)$ are obtained as

$$\mathbf{y} = g(\boldsymbol{\omega}_y \mathbf{h} + \mathbf{b}_y) \tag{48}$$

where $\boldsymbol{\omega}_h$ and $\boldsymbol{\omega}_y$ are the weight matrices, and $\mathbf{b}_h$ and $\mathbf{b}_y$ are the bias terms. $\boldsymbol{\omega}_h$ and $\mathbf{b}_h$ work for the input and hidden layers, respectively, whereas $\boldsymbol{\omega}_y$ and $\mathbf{b}_y$ work for the hidden and output layers, respectively. Both $f(\mathbf{x})$ and $g(\mathbf{h})$ are activation functions called Sigmoid that can be computed as

$$f(\mathbf{x}) = \frac{1}{1+e^{-\mathbf{x}}} \tag{49}$$

The parameters are updated constantly until the reconstruction error $e(\mathbf{x}, \mathbf{y})$ reaches the minimum value.

The SAE classification model is stacked by multiple autoencoders in series [132], which means that the hidden layer of the previous autoencoder is used as the input layer of the next autoencoder as shown in Fig. 52. The adaptive multi-band filtered spectrum is used as the input data of the first encoder, and $h(N)$ represents the N_{th} hidden layer information.

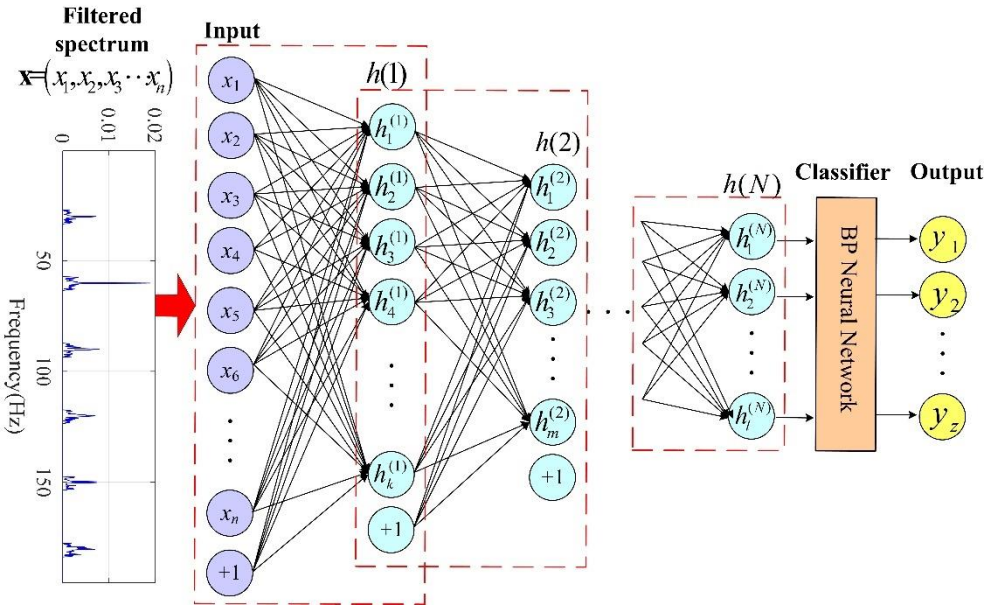

Fig. 52 The principle of SAE classification model

5.4.2 Diagnostic method architecture

The detailed diagnosis process is shown in Fig. 53, and the specific diagnosis steps are described as follows:

Step 1: Acquire the vibration signal by using the accelerometer under the normal state of the rotating machinery.

Step 2: Acquire the vibration signals under different structural faults, and the sampling frequency and sampling time are the same as those under the normal state.

Step 3: Filter the vibration signals using the adaptive multi-band filtering and extract the rotating frequency and its harmonic components (less than 20 times of the rotating frequency).

Step 4: Divide the samples into training and testing samples.

Step 5: Build and train a SAE classification model based on training samples.

Step 6: Input the test samples to diagnose the rotating machinery structural fault types.

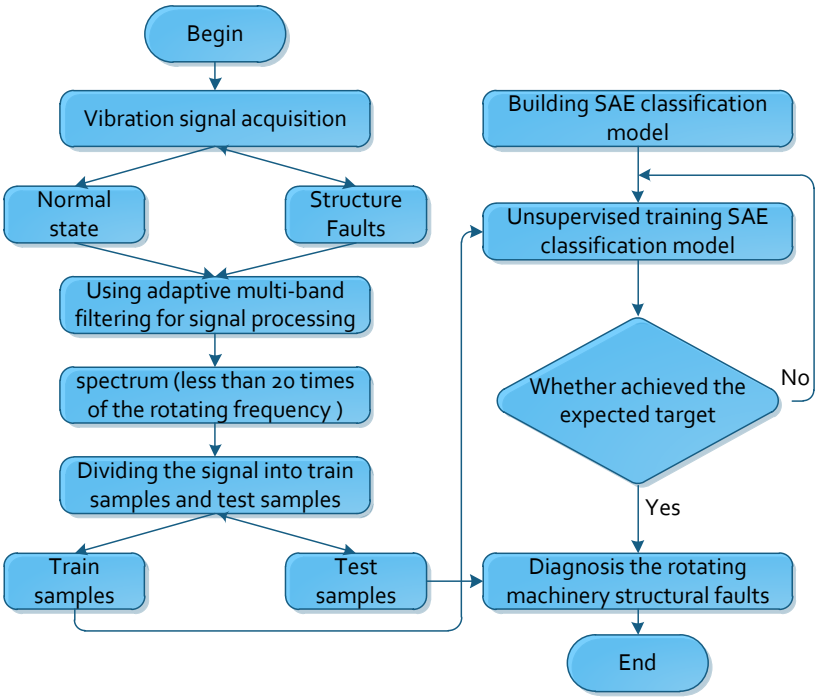

Fig. 53 The automatic diagnosis process of rotating machinery structural faults

Tab. 11 shows the detailed algorithm steps of the rotating machinery structural faults automatic diagnosis.

Tab. 11 Rotating machinery automatic diagnosis algorithm

Adaptive multi-band filtering and SAE automatic diagnosis algorithm:

Input: Original signal of different fault $\boldsymbol{V}=\{v_1, v_2, \cdots, v_N\}$.

1. Adaptive multi-band filtering:

For: *i=1: N*

(1) $\boldsymbol{V}_i(t)$ $\underline{FFT}$ $\boldsymbol{V}_i(f)$

(2) $F_r^{'}=\max(F_r \pm \beta)$, $F_r = RPM/60$

(3) $\Delta f_r = \left|F_r^{'} - F_r\right|$

(4) $\boldsymbol{V}_i^{'}(f)=\boldsymbol{V}_i(k(F_r \pm \Delta f_r) \pm \delta)$

End

2. SAE diagnosis model

(1) $\mathbf{X}_i^{'}(f)=\boldsymbol{V}_i^{'}(f)=(x_1, x_2, x_3 \cdots x_n)$,

$Y \in \{[1,0,\cdots,0],[0,1,\cdots,0],\cdots,[0,0,\cdots,1]\}$

(2) $\mathbf{X}^{'}(f) \rightarrow \left(\mathbf{X}_{train}^{'}(f),\ \mathbf{X}_{test}^{'}(f)\right)$, $Y \rightarrow \left(Y_{train}(f),\ Y_{test}(f)\right)$

(3) For i =1: epochs

$\left(\mathbf{X}_{train}^{'}(f),\ \mathrm{Y}_{train}\right)$ $\underline{SAE\ Training}$ SAE_{diag}

End

(4) $\left(\mathbf{X}_{test}^{'}(f),\ \mathrm{Y}_{test}\right)$ $\underline{SAE_{diag}}$ Y_{diag}

Output: Accuracy rate of test samples.

5.5 Experimental verification

In order to verify the effect of the adaptive multi-band filtering method proposed in this chapter in extracting the frequency conversion and adaptive filtering of vibration signals, this chapter uses the common structural abnormal faults of rotating machinery for verification. The experimental verification is divided into two parts: engineering experimental verification and comparative experimental verification.

5.5.1 Engineering experiment

5.5.1.1 Experiment platform

To verify the effectiveness of the proposed method, the experimental platform shown in Fig. 54 is used for acquiring vibration signals. This experimental platform mainly includes shafts, support elements, couplings, counterweight plates, attachment bolts, bearings, and bearing bases.

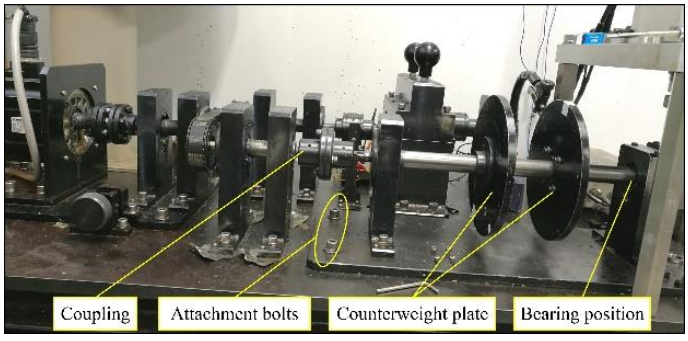

Fig. 54 Rotating machinery experimental platform

Fig. 55 shows the rotating machinery structural faults, including angle misalignment (AM), coupling looseness (CL), dynamic imbalance (DI), pedestal looseness (PL), and static imbalance (SI), for the experiment. The laser alignment instrument is used in the angular misalignment experiment to set the coupling misalignment angle. Meanwhile, weights are added in one of the counterweight plates in the dynamic imbalance experiment and in both two counterweight plates in the static imbalanced experiment. For the coupling and pedestal looseness experiments, the bolts are all loose.

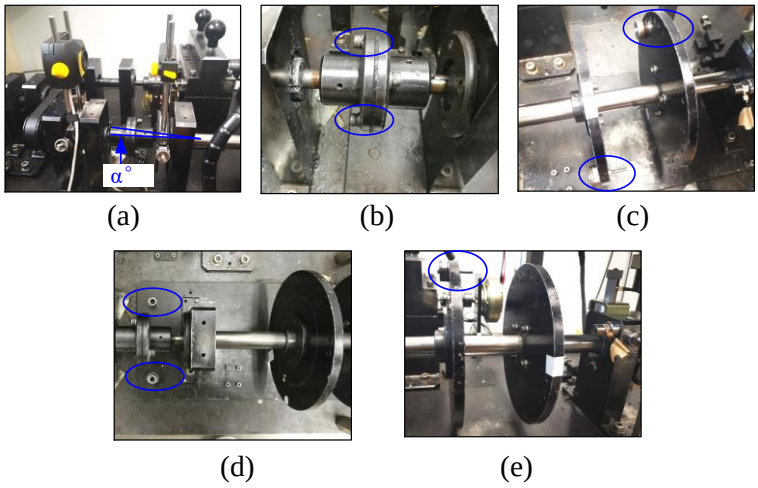

Fig. 55 Rotating machinery structural faults experiments: (a) angular misalignment; (b) coupling looseness; (c) dynamic imbalance; (d) pedestal looseness; (e) static imbalance

5.5.1.2 Performance evaluations

To evaluate the effect of the proposed automatic diagnosis method, a rotating machinery structure faults experiment is carried out under 1800 RPM. The accelerometer is used to acquire the vibration signals, and Tab. 12 presents specific information.

Tab. 12 Experimental conditions and parameters

Parameter	Values
RPM	1800
Rotation frequency	30 Hz
Sampling frequency	5000 Hz
Sampling points	25600

Fig. 56 shows the raw vibration signals (in red) and their spectrums (in blue) under normal states and the five fault states. In the vibration signal, given that the background noise floods the impact of the structural fault, distinguishing the rotating machinery status is impossible. In the spectra, although the characteristics at the rotating frequency and its harmonics differ across six states, the background noise still affects the fault diagnosis.

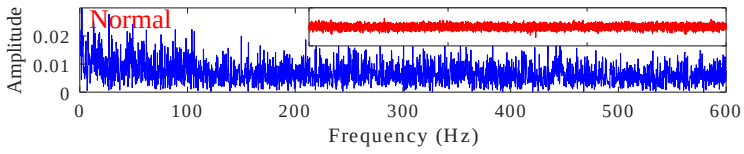

(a)

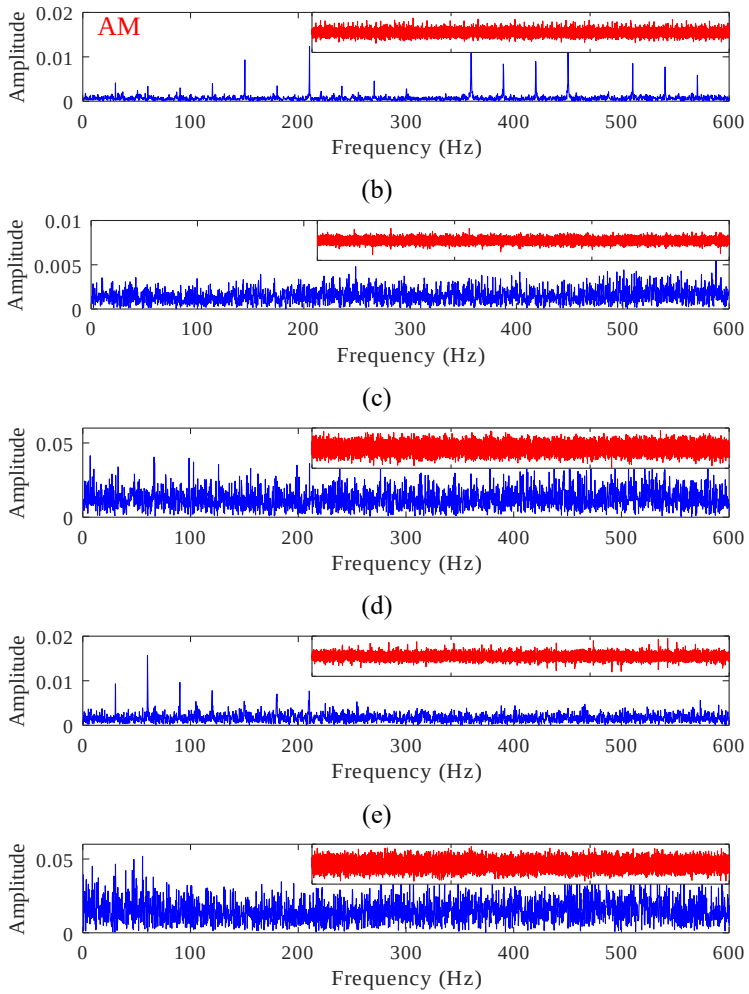

Fig. 56 The vibration signal (in red) and spectrum (in blue)

The diagnosis accuracy rates of the raw vibration signal and its original spectrum are compared based on the SAE classification model. Tab. 13 shows 3 hidden layers (Layer1 to Layer3) in the SAE model. The other specific parameters are described as follows.

Tab. 13 SAE classification model parameters

Types	Parameters		
	Values	Activation function	Learning rate
Hidden layer 1	100	Sigmoid	0.9
Hidden layer 2	50	Sigmoid	0.8
Hidden layer 3	20	Sigmoid	0.8

The diagnosis results are presented in Fig. 57. The diagnosis accuracy rate is recorded 10 times to avoid contingency. Fig. 57 shows that the diagnosis accuracy rate of the raw signal is low and that the average accuracy rate is only 15.83%. Although the accuracy rate of the spectrum increased significantly with an average value of 91.83%, this rate cannot meet the ideal requirements in engineering applications.

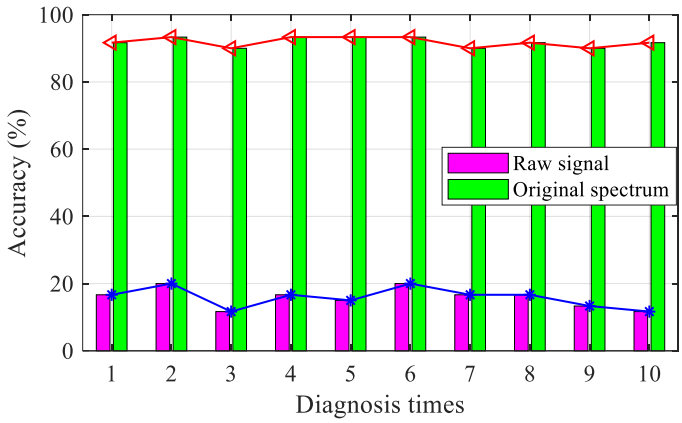

Fig. 57 SAE diagnosis results of raw vibration signal and its spectrum

Therefore, to improve fault diagnosis accuracy, the signal should be filtered before inputting into the SAE classification model. Fig. 58 shows the spectrum filtered by the adaptive multi-band filtering. Compared with the original spectrum shown in Fig. 56, the background noise was removed effectively, and the rotating frequency and its harmonic components were accurately extracted.

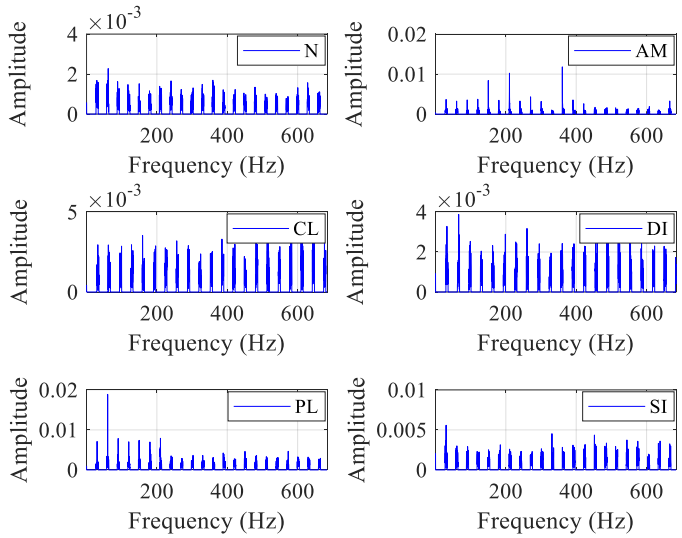

Fig. 58 The filtered spectrum by adaptive multi-band filtering

As shown in Tab. 14, the spectrums under the normal and structural faults states were divided into train and test samples. Fig. 59 shows that the SAE diagnosis accuracy rate is 100%, thereby confirming that the proposed method can accurately diagnose faults.

Tab. 14 SAE automatic diagnosis parameters

Types	Train samples	Test samples	Sample label
N	40	10	1
AM	40	10	2
CL	40	10	3
DI	40	10	4
PL	40	10	5
SI	40	10	6

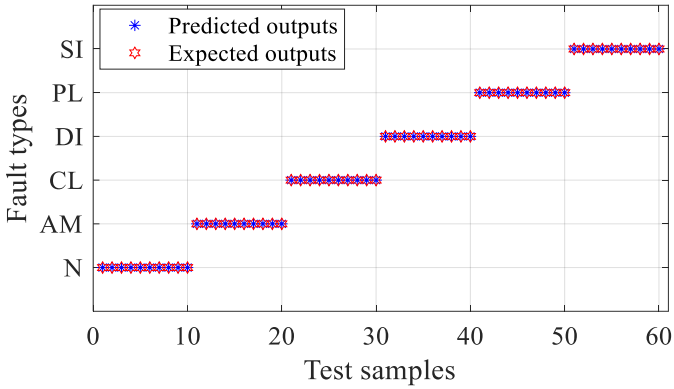

Fig. 59 SAE diagnosis results

5.5.1.3 Diagnosis result under different RPMs

To verify the accuracy of the proposed method at different RPMs, experiments were performed under 700, 900, and 1100 RPM. Fig. 60 shows the original spectrum and adaptive multi-band filtered spectrum. Compared with the original spectrum, the background noise in the filtered spectrum was removed, and the actual rotating frequency and its harmonics were accurately extracted.

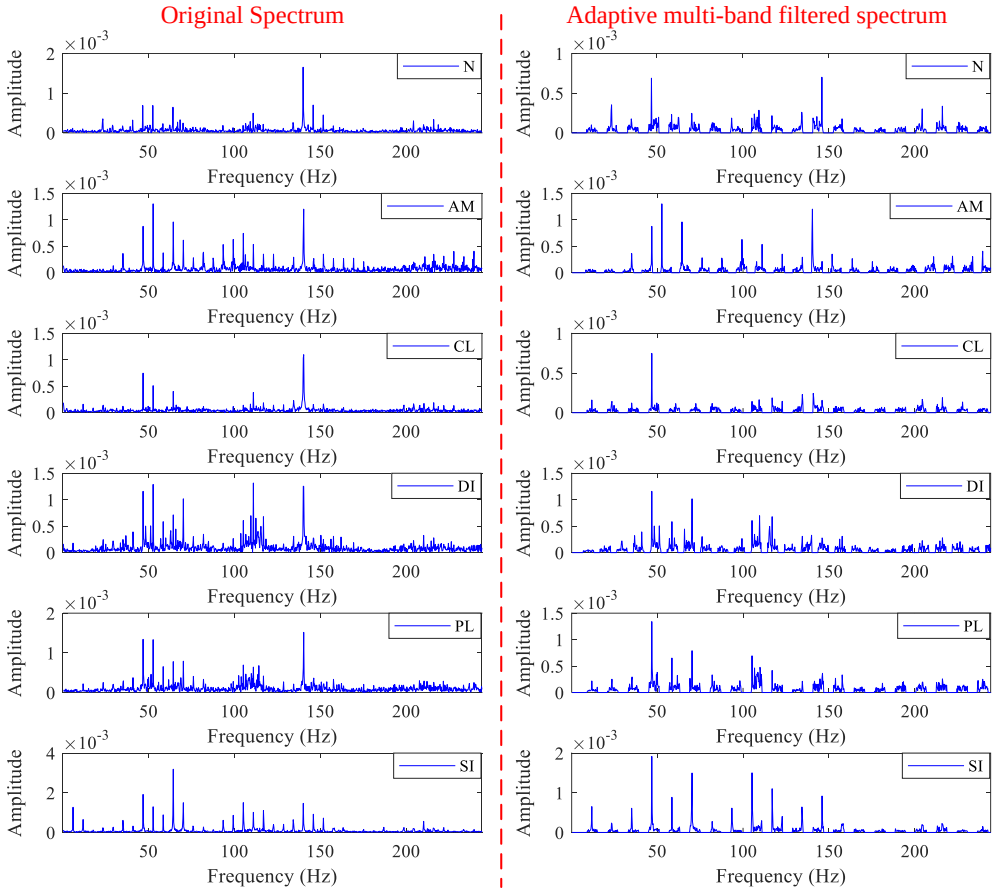

(a)

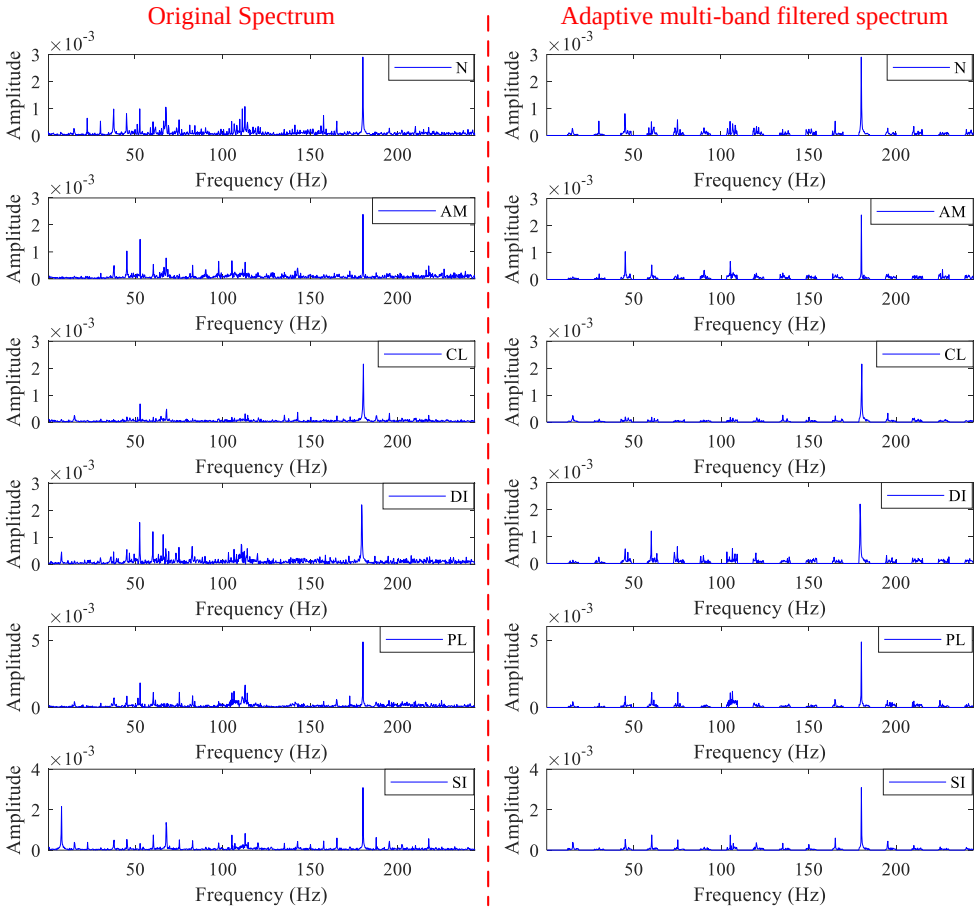

(b)

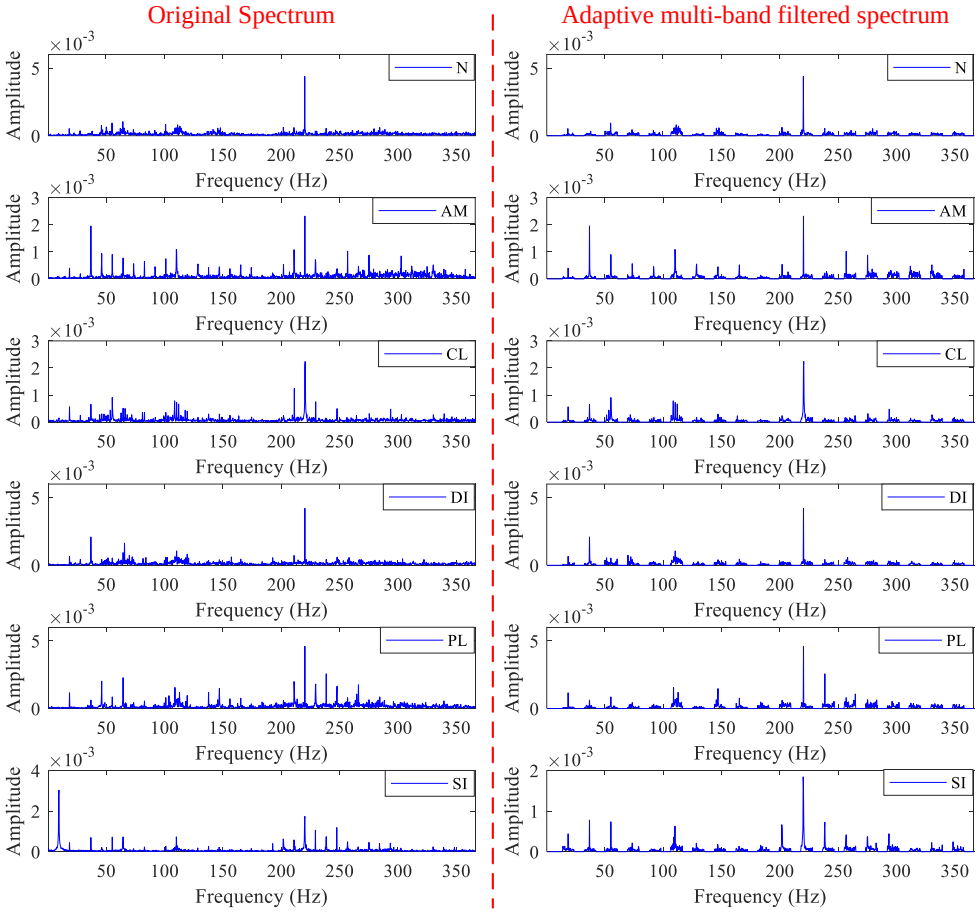

(c)

Fig. 60 The original and adaptive multi-band filtered spectrum: (a) 700 RPM; (b) 900 RPM; (c) 1100 RPM

Fig. 61 shows the diagnostic accuracy rate of the adaptive multi-band filtered spectrum and original spectrum under different RPMs. In these experiments, to avoid contingency of identification, the final diagnosis accuracy rates were computed as the average of 10 measurements. For the adaptive multi-band filtered diagnosis, the accuracy rates recorded under 700 RPM and 900 RPM were 98.49% and 99.16%, respectively, whereas those recorded under 1100 RPM and 1800 RPM were both 100%. The variance among the measurements were relatively smaller than those captured in the original spectrum, thereby further confirming the effectiveness of the proposed automatic diagnosis method.

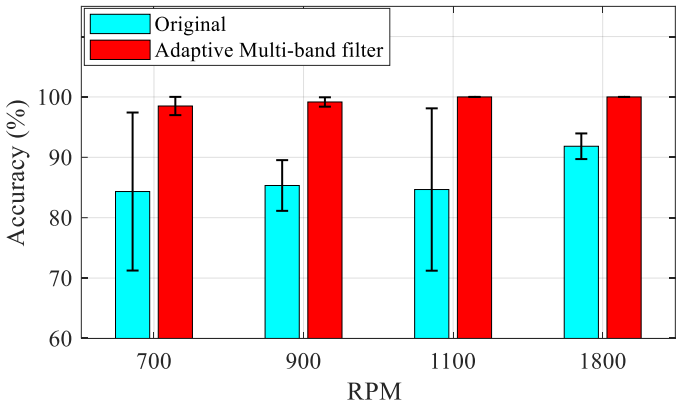

Fig. 61 Diagnosis results at different RPMs

5.5.2 Comparative experiment

5.5.2.1 Comparison of different filtering methods

To verify the effectiveness of adaptive multi-band filtering methods, the raw vibration signal was filtered by low-pass and multi-band filtering for comparation. Tab. 15 shows the parameter settings of the three filtering.

Tab. 15 Filtering related parameter

Filtering	Parameters
Low-pass	Cut-off frequency: 1000 Hz
Multi-band	Deflection coefficient: 3 Hz
Adaptive multi-band	Deflection coefficient: 3 Hz

Fig. 62 shows the original spectrum and the three filtered spectra. In the original spectrum, the actual rotating frequency was 32.26 Hz, which deviates from the theoretical rotating frequency (30 Hz) by 2.26 Hz. Meanwhile, in the low-pass filtered srectrum, the noise is still obvious, which affects the rotating frequency and its harmonic extraction; In the traditional multi-band filtered spectrum, the harmonic components cannot be accurately extracted after the second harmonic. The adaptive multi-band filtering can accurately extract the rotating frequency and its harmonic components.

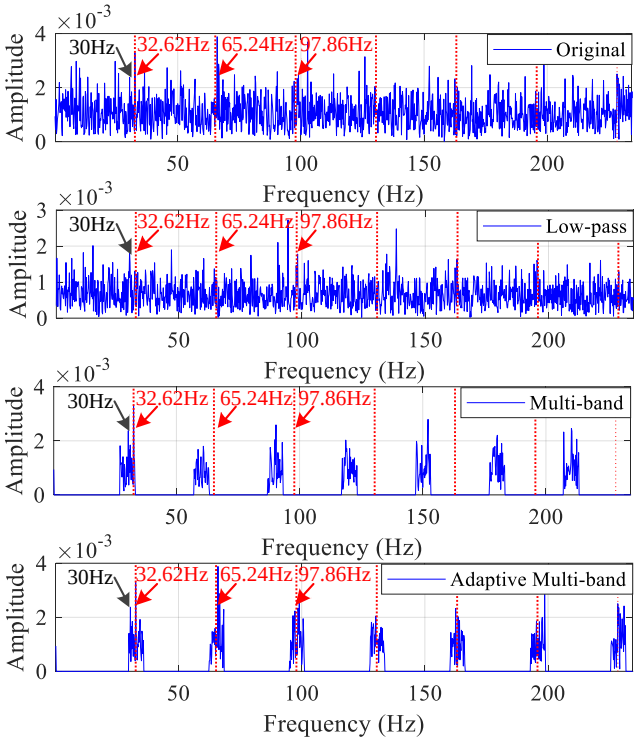

Fig. 62 Comparison of multi-band filtering and adaptive multi-band filtering

Fig. 63 shows the 10 SAE multi-classification model diagnosis results captured for the original spectrum and the three filtered spectra. The average accuracy rates of the low-pass and multi-band filtering were 86% and 89.67%, respectively, both below 90%, thereby proving that the adaptive multi-band filtering can effectively remove background noise, accurately extract the rotating frequency and its harmonics characteristic components, and greatly improve the rotating machinery structural fault automatic diagnosis accuracy rate.

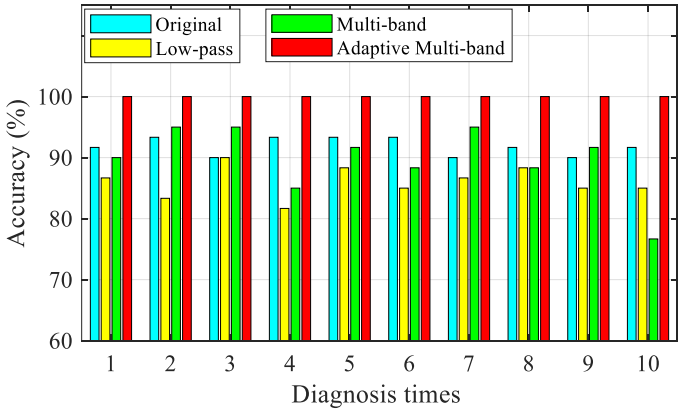

Fig. 63 Comparison of different filtering

5.5.2.2 Comparison of different classification models

In the classification model comparison, the BP neural network, radial basis function (RBF) neural network, and extreme learning machine (ELM) neural network were used to establish automatic diagnosis models. Fig. 64 presents the results. Among the three classification models, SAE obtained the highest diagnostic accuracy rate and the smallest variance for the of 10 measurements, thereby indicating that the SAE multi-classification model has the best stability among all compared models. Meanwhile, among the four classification models, the accuracy rate of adaptive multi-band filtered spectrum was significantly improved compared with that of the original spectrum, and all of these models obtained accuracy rates of greater than 98.5%. Therefore, the proposed automatic diagnosis method is further proven to be effective.

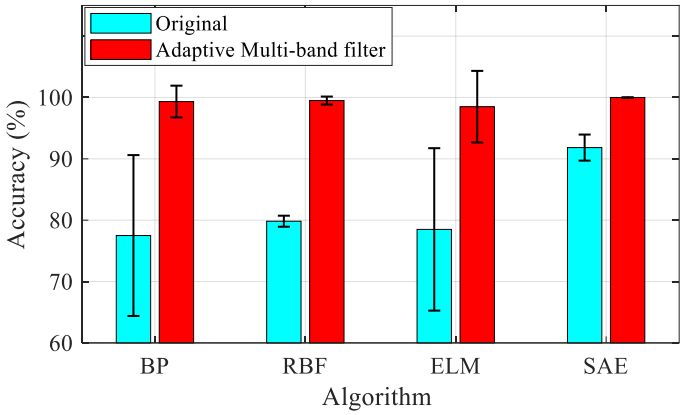

Fig. 64 Comparison of the corresponding diagnosis results of different classification models

5.6 Conclusion

This chapter proposed an adaptive multi-band filtering specially for the problem of inconsistency between the engineering actual rotating frequency and the theoretical value. The engineering experiments and comparisons prove that comparing with traditional multi-band filtering, the proposed filtering method, which was improved by setting reasonable search thresholds and deviations, can accurately extract the actual rotating frequency and its harmonic in engineering experiments. At the same time, the comparison with different filtering methods further validated the effectiveness of the proposed adaptive multi-band filtering.

Chapter 6 Signal processing method based on incremental accumulation holographic SDP

6.1 Introduction

Aiming at the problem that the image discrimination is not obvious when one-dimensional vibration signal is transformed into two-dimensional image in the process of visual fault diagnosis of rotating machinery, this chapter proposes a method based on incremental accumulation of vibration signal characteristics and holographic symmetrical dot pattern (SDP) fusion. In this study, the time- and frequency-domain characteristics are simultaneously extracted by the incremental accumulation method to avoid inconspicuous difference and small discrimination generated by a single signal. Subsequently, the extracted characteristics are merged into a 2D graph based on the SDP method to amplify the differences between the signals.

SDP can reflect the difference between the signals because it can observe the fault characteristics more. In combination with the incremental accumulation method, the vibration signal time- and frequency-domain characteristics are extracted simultaneously. Based on the SDP method, the characteristics are merged into a graph to enlarge the difference between fault types.

In order to verify the effectiveness of the methods in this chapter, the bearing fault is used for verification. Simulations and engineering experiments are proved that the method can effectively fuse the characteristics and realize the division enhancement.

6.2 SDP principle

The SDP is a signal conversion method that transforms 1D signal into a 2D polar coordinate image, where the difference between the signals is reflected by the shape distribution. The 1D vibration signal can be expressed as:

$$\mathbf{X}=[x_1, x_2 \cdots x_i, x_{i+1} \cdots x_N] \tag{50}$$

Hence, it can be converted to a polar coordinate system by Equations (51) - (53):

$$r(i)=\frac{x_i - x_{\min}}{x_{\max} - x_{\min}} \tag{51}$$

$$\theta(i)=\beta+\frac{x_{i+\tau} - x_{\min}}{x_{\max} - x_{\min}}\xi \tag{52}$$

$$\phi(i)=\beta-\frac{x_{i+\tau} - x_{\min}}{x_{\max} - x_{\min}}\xi \tag{53}$$

where $r(i)$ is the polar diameter, β is the rotation angle of the mirror symmetry plane, which controls the number of shapes in the SDP image, $\theta(i)$ is a clockwise rotation angle along the initial line β, $\phi(i)$ is a counterclockwise rotation angle, ξ is the angle magnification factor, which controls the distribution angle of the shape, and τ is the delay parameter, which controls the degree of shape distribution.

Fig. 65 shows the SDP diagram. The signal $\mathbf{X}$ is converted by polar coordinates to form a petal-shaped pattern ($r(i)$, $\theta(i)$). Then, according to Eq. 53, ($r(i)$, $\phi(i)$) is formed by the mirror symmetry of ($r(i)$, $\theta(i)$). Therefore, SDP image can be formed according to the rotation angle β.

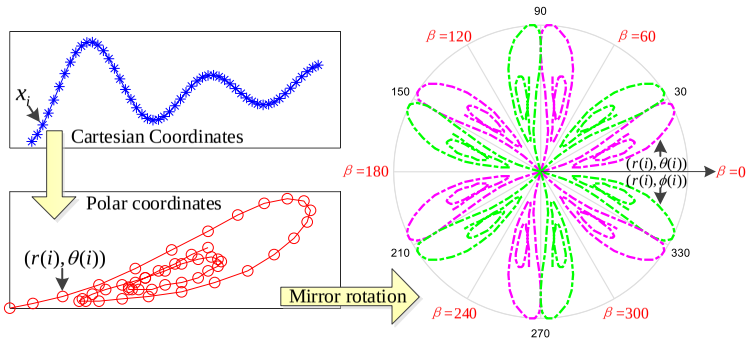

Fig. 65 SDP schematic diagram converted from signals

6.3 Incremental cumulative characteristic parameter extraction method

The vibration signal time-domain characteristics are often used as basis for the rotating machinery fault threshold, which reflects the signal fluctuation, dispersion degree, and impact strength. The frequency-domain characteristic can analyze the frequency change range and reflect the dominant components distribution in the spectrum.

6.3.1 Incremental cumulative method

The accurate extraction of fault characteristic can reflect the signal change promptly, and the incremental cumulative method can reflect the change of the signal in real time. For a vibration signal $\mathbf{X}=[x_1,x_2\cdots x_i,x_{i+1}\cdots x_N]$ with a data length of N, it can be divided into several segments, the characteristic parameter c_d of each segment can be described as:

$$c_d=c(x_{(d-1)*n+1}:x_{d*n}) \tag{54}$$

where n is the segment length incremented each time, which can be calculated according to the sampling frequency and RPM, that is, $n>\frac{60f_s}{RPM}$. d is the rounding of the total data length N and n, thus $d=[\frac{N}{n}]$.

Then, the characteristic parameters of vibration signal $\mathbf{X}$ obtained by the incremental accumulation method is:

$$C=[c_1,c_2,\cdots c_d] \tag{55}$$

Fig. 66 shows the diagram of incremental accumulation methods.

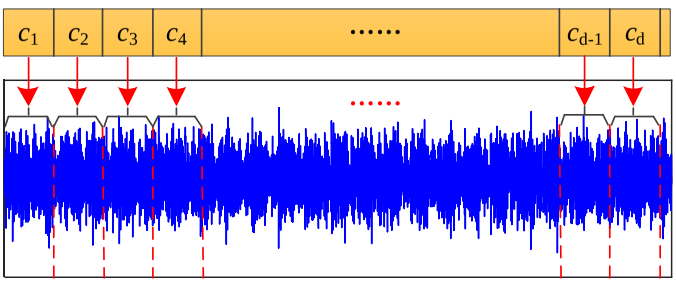

Fig. 66 The schematic diagram of incremental accumulation methods.

6.3.2 Time-domain characteristic parameters

For a vibration signal $\mathbf{X}=[x_1,x_2\cdots x_i,x_{i+1}\cdots x_N]$, the mean value ($\overline{x}$) and standard deviation (σ) are given as follow:

$$\bar{x} = \frac{1}{N}\sum_{i=1}^{N} x_i \tag{56}$$

$$\sigma = \sqrt{\frac{1}{N-1}\sum_{i=1}^{N}(x_i - \bar{x})^2} \tag{57}$$

According to the bearing fault vibration signal distribution changes, the following time-domain characteristic parameters are selected:

(1) Kurtosis: A characteristic index for detecting the breadth of vibration signals, highly sensitive to changes in amplitude, and suitable for surface damage fault detection.

$$P_1 = \frac{\sum_{i=1}^{N}(x_i - \bar{x})^4}{N\sigma^4} \tag{58}$$

(2) Skewness: The asymmetry of positive and negative amplitudes, which is equivalent to zero, thus vibration signal is symmetrically distributed. The larger the skewness value, the stronger the asymmetry.

$$P_2 = \frac{\sum_{i=1}^{N}(x_i - \bar{x})^3}{N\sigma^3} \tag{59}$$

(3) Root mean square (RMS): The degree of data dispersion. The greater the RMS value, the higher the degree of dispersion.

$$P_3 = \sqrt{\frac{1}{N}\sum_{i=1}^{N} x_i^2} \tag{60}$$

(4) Peak-to-peak value: The fluctuation range of the vibration signal. The larger the peak-to-peak value, the larger the signal fluctuation range, the more severe the fluctuation, and the more unstable signal.

$$P_4 = \max(x_i) - \min(x_i) \tag{61}$$

6.3.3 Frequency-domain characteristic parameters

Using Fourier transform, the signal $\mathbf{X}$ is converted to the spectrum, and the $F(f_i), i = 1, 2 \cdots I$ is the spectral component at frequency f_i. The following frequency-domain characteristic parameters are selected:

(5) Average frequency: The magnitude of vibration energy in the spectrum. The larger the average frequency value, the greater the energy of the spectrum.

$$P_5 = \sqrt{\frac{\sum_{i=1}^{I} F(f_i)}{I}} \tag{62}$$

(6) Center frequency: The change of the main energy peak position of the power spectrum.

$$P_6 = \frac{2}{f_s} \cdot \frac{\sum_{i=1}^{I} f_i \cdot F(f_i)}{\sum_{i=1}^{I} F(f_i)} \tag{63}$$

where f_s is the sampling frequency.

(7) Ricean frequency: The distribution of dominant components in the spectrum.

$$P_7 = \frac{2}{f_s}\sqrt{\frac{\sum_{i=1}^{I} f_i^2 \cdot F(f_i)}{\sum_{i=1}^{I} F(f_i)}} \tag{64}$$

(8) Frequency standard deviation: The degree of dispersion of the spectrum.

$$P_8 = \sqrt{\frac{\sum_{i=1}^{I}(f_i - P_6)^2 \cdot F(f_i)}{I-1}} \tag{65}$$

Fig. 67 shows the SDP images corresponding to the eight characteristic parameters. The said SDP images differ in shape distribution and distinctions.

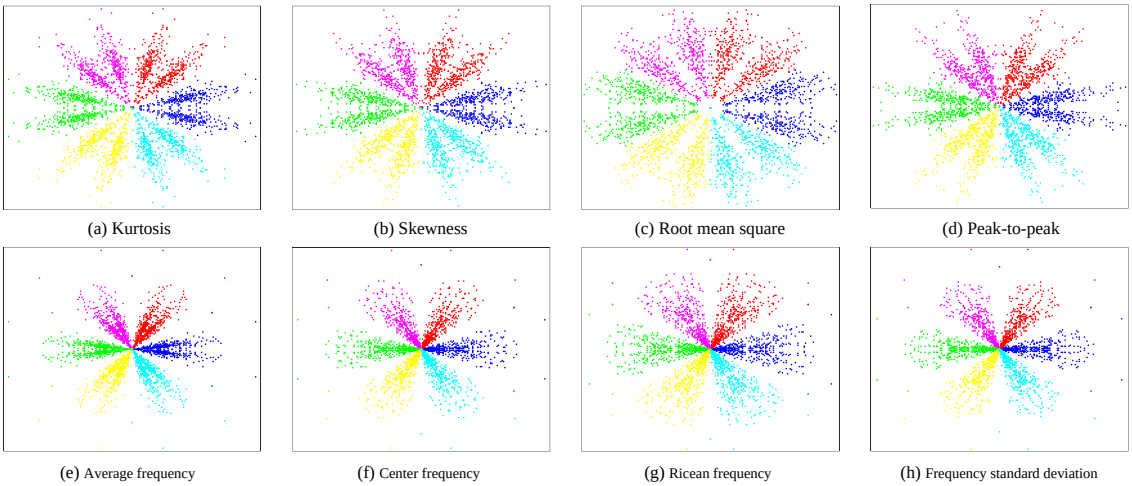

(a) Kurtosis (b) Skewness (c) Root mean square (d) Peak-to-peak

(e) Average frequency (f) Center frequency (g) Ricean frequency (h) Frequency standard deviation

Fig. 67 The SDP images corresponding to the 8 characteristic parameters

6.4 Holographic SDP fusion method architecture

To address the problem on rotating machinery faults visual diagnosis, the difference between the SDP images converted by vibration signal is not obvious. Thus, this chapter proposes an incremental cumulative holographic SDP characteristic fusion method. Fig. 68 shows the specific flow chart of this method and are stated below:

1) Acceleration sensor is used to collect the vibration signals under normal and faulty states.

2) The optimal signal segment length n is calculated according to RPM and sampling frequency. The incremental accumulation method is used to extract the time- and frequency-domain characteristics.

3) SDP parameters, mirror symmetry rotation angle, angle amplification factor, time delay parameters, etc. are set. Information fusion is performed on eight characteristic parameters based on SDP.

4) Taking rotating machinery bearing fault as an example, its fault diagnosis is realized upon the combination of SDP image similarity.

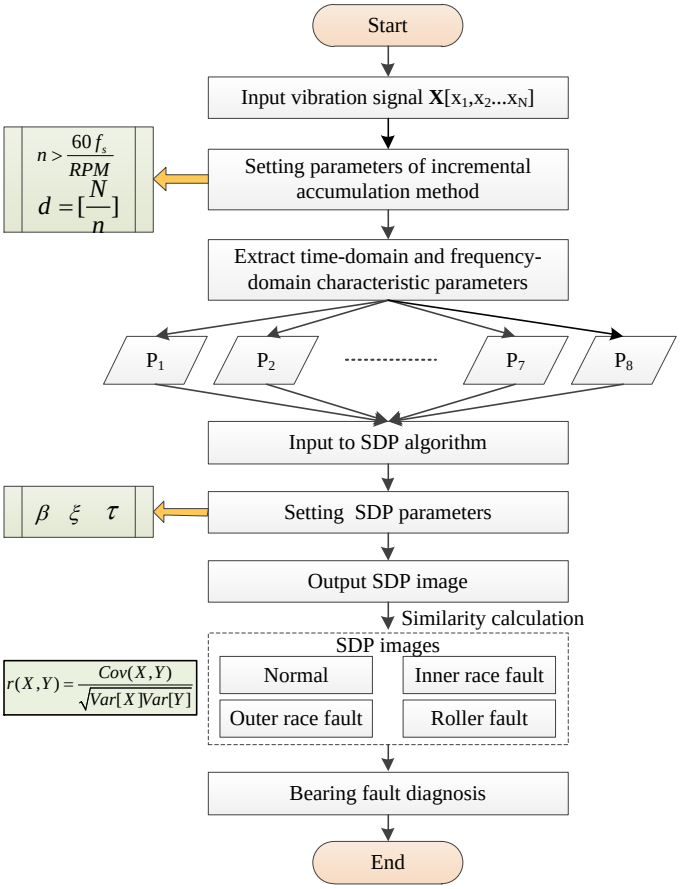

Fig. 68 Flowchart of the incremental accumulation holographic SDP

To reduce the complexity of fault identification, the polar coordinates are divided into 8 regions based on the rotation angle β, and the characteristic parameters are fused into an SDP image. Fig. 69 shows that SDP image is the fusion result of eight characteristic parameters, thus differences between each parameter are obvious.

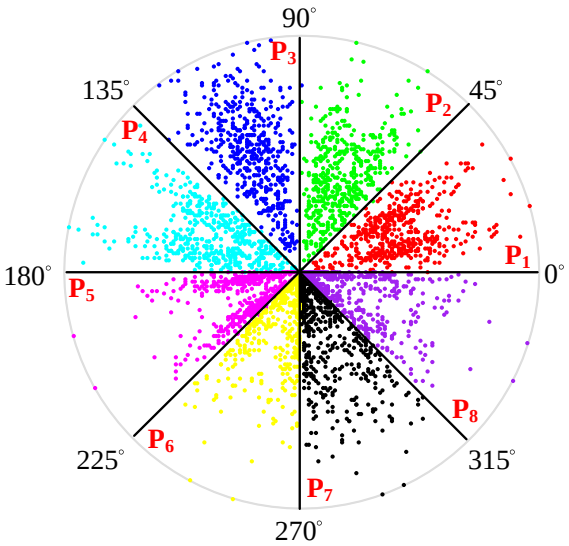

Fig. 69 The holographic SDP image

6.5 Experimental verification

In order to verify the effect of the incremental cumulative holographic SDP characteristic fusion method proposed in this chapter on increasing the discrimination after the vibration signal is transformed into two-dimensional image, this chapter uses the common bearing faults of rotating

machinery for verification. The experimental verification is divided into two parts: simulation verification and engineering experimental verification.

6.5.1 Simulation analysis

To verify the effect of this method in characteristic parameters visual display, a bearing outer race fault simulation model was established. The simulation model is the same as Eq. (40). (**4.5.1.1 Simulation model establishment**).

6.5.1.1 SDP images

Fig. 70 shows the simulation signal and SDP images. Fig. 70(b) corresponds to noise-free signal SDP image, Fig. 70(c) corresponds to random noise SDP image, and Fig. 70(d) corresponds to with-noise signal SDP image. Fig. 70(a) shows that the regular impact caused by the bearing outer race fault is relatively strong, but the impact characteristics are submerged after the background noise is added. Fig. 70(b) illustrates that the points are relatively concentrated, while relatively scattered in Fig.70(c). Fig. 70(d) also shows that the bearing fault impact is submerged by the noise, and the distribution of $f(t)$ and $n(t)$ in the SDP is similar.

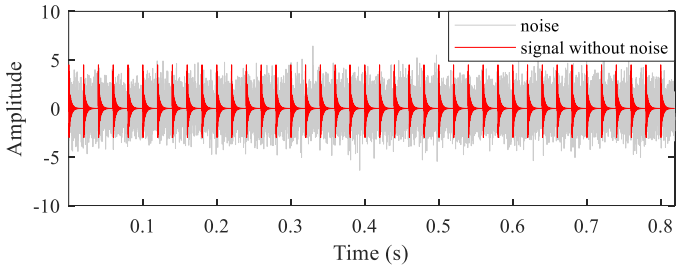

(a)

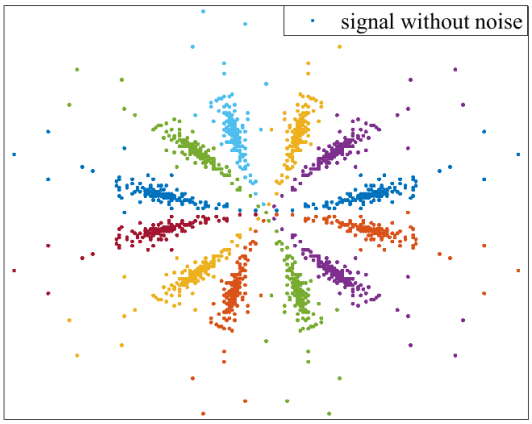

(b)

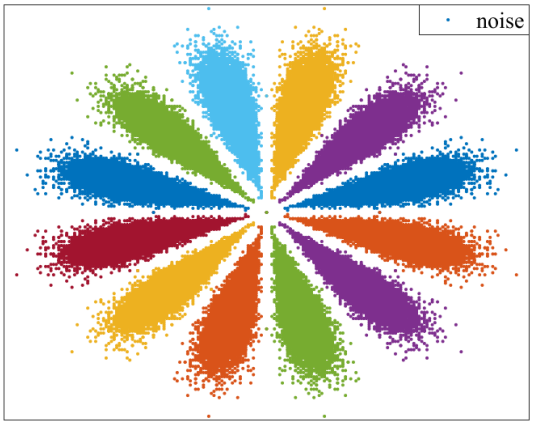

(c)

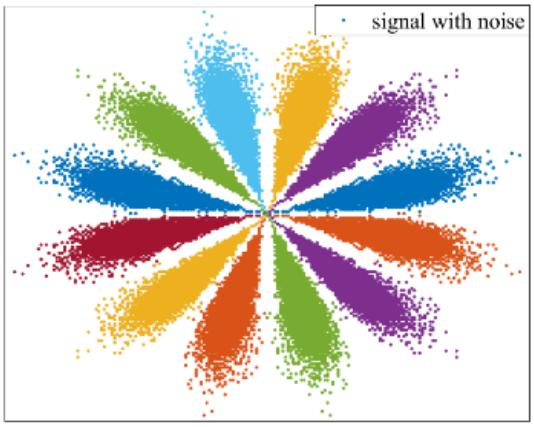

(d)

Fig. 70 Simulation signal and its SDP images: (a) Simulation signal; (b) Noise-free signal corresponding SDP image; (c) Random noise corresponding SDP image; (d) with-noise signal corresponding SDP image

6.5.1.2 Holographic SDP images

Fig. 71 shows the results from the extracted characteristics of simulation signal, where the incremental accumulation extracted parameters can better represent the volatility of data changes. However, the difference between each characteristic parameter is not obvious.

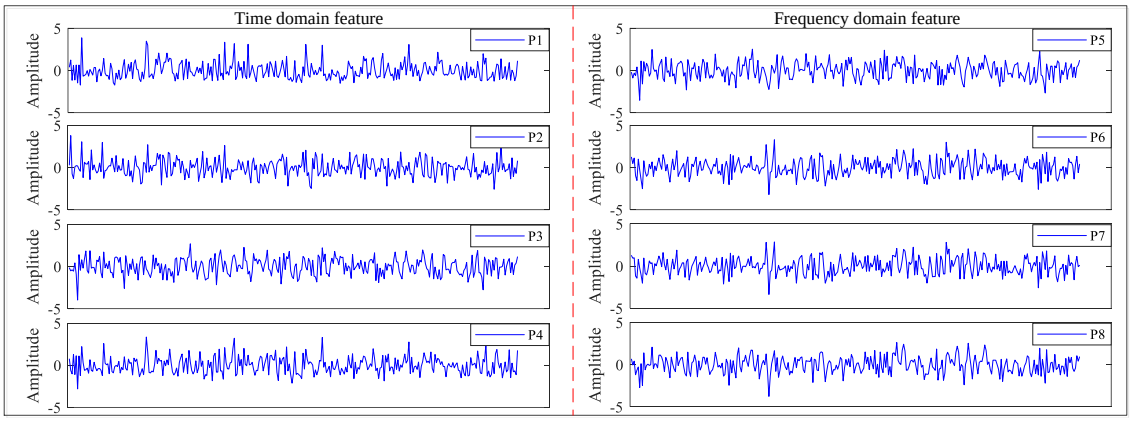

Fig. 71 Characteristic parameters based on incremental cumulative extraction method

Fig. 72 shows the holographic characteristic fusion of SDP image, thus difference between each parameter significantly increased.

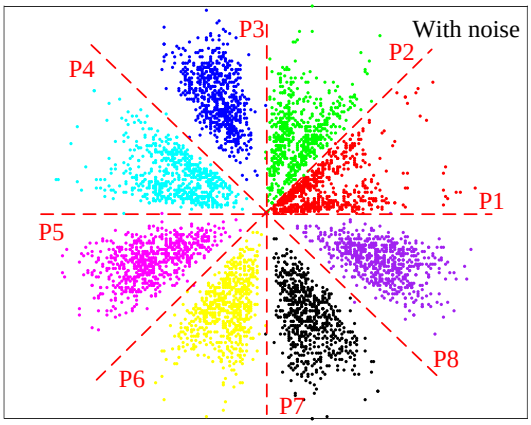

Fig. 72 Holographic characteristic fusion SDP

6.5.1.3 Similarity recognition

According to Eq. 66, the similarity between the noise-free and the with-noise signals is calculated.

$$r(X,Y)=\frac{Cov(X,Y)}{\sqrt{Var[X]Var[Y]}} \tag{66}$$

where *Cov* represents the covariance of X (noise-free signal) and Y (with-noise signal) and *Var* represents the variance.

Tab.16 shows that the similarity between the original signals is low, and improved between the holographic SDP images. Because the characteristic parameter tends to be stable and are relatively less affected by noise, the holographic SDP fusion can amplify the difference between the signals.

Tab. 16 Comparison of similarities

	$r(X_1,Y_1)$	$r(X_2,Y_2)$	$r(X_3,Y_3)$	$r(X_4,Y_4)$
Raw signal	0.1394	0.1417	0.1423	0.1402
Holographic SDP	0.5033	0.5080	0.5451	0.5404

6.5.2 Engineering experiment

This chapter carries out diagnosis research based on the bearing fault of high-speed rotating machinery, and verifies the accuracy of the method proposed in this chapter through actual engineering signal.

6.5.2.1 Experiment platform

To verify the effectiveness of the proposed bearing fault diagnosis method, experiments were carried out with the bearing fault simulation experiment platform, as shown in Fig. 31 (**4.5.2.1 Experiment Platform**) and the bearing as shown in Fig. 32.

6.5.2.2 Applications

The vibration signal is acquired by the acceleration sensor with a sampling frequency of 100 kHz at 1,500 RPM, as shown in Fig. 73. Fig. 73(a) - (d) correspond to the bearing normal state (N), outer race fault (O), inner race fault (I), and roller fault (R). Fig. 73 also illustrates that the impact caused by the bearing fault is submerged due to the background noise.

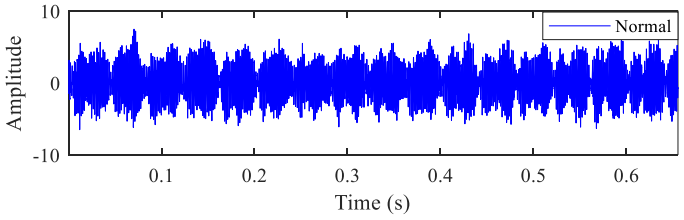

(a)

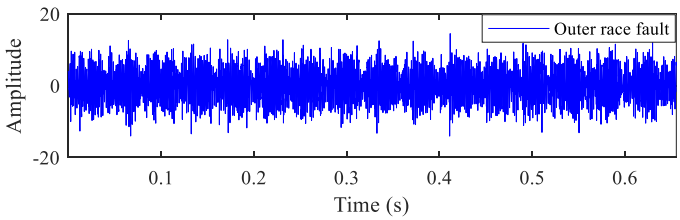

(b)

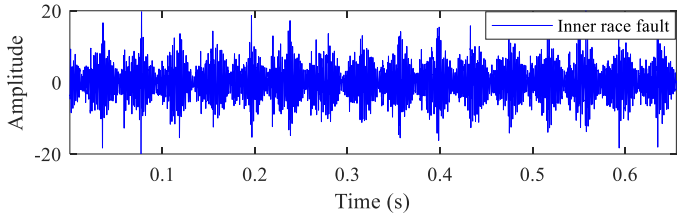

(c)

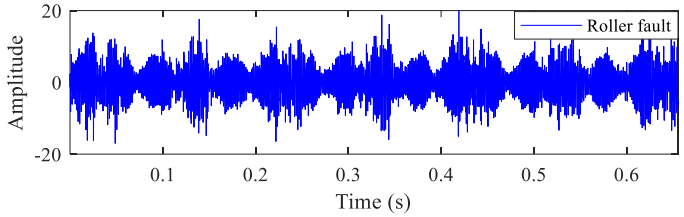

(d)

Fig. 73 Bearing vibration signal under normal and fault states: (a) Normal state; (b) Outer race fault state; (c) Inner race fault state; (d) Roller fault state

Fig. 74 shows the SDP images corresponding to the vibration signal. Tab. 17 shows the results from the extraction of the axis length (R), saturation (D), center space (d), and the deflection (θ) of the SDP image, thus SDP images have relatively small difference.

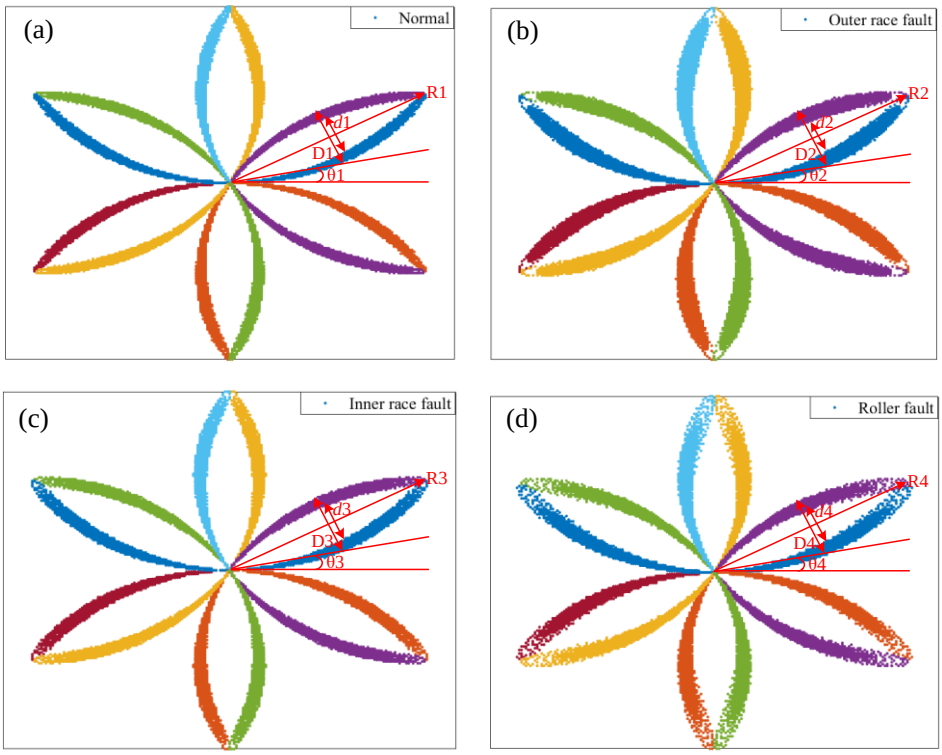

Fig. 74 SDP images under bearing normal and fault state: (a) Normal state; (b) Outer race fault state; (c) Inner race fault state; (d) Roller fault state

Tab. 17 Parameters extracted from SDP images

Bearing state	Parameters			
	R (cm)	D (cm)	D (cm)	Θ (°)
N	7.1	1.9	1.25	8.9
O	7.1	2.1	1.1	8.1
I	7.1	2.0	1.25	8.5
R	7.1	2.05	1.15	8.5

According to Eq. 66, calculating the similarity between the vibration signal corresponded with SDP images. Tab. 18 shows that the roller fault (R) was misidentified, and the noise in the vibration signal has an impact on the bearing diagnosis.

Tab. 18 Comparison of similarity

	N_2	O _2	I _2	R _2
N_1	***1.0000***	0.8836	0.9728	0.8815
O _1	0.8993	***1.0000***	0.9471	0.9545
I _1	0.9746	0.9345	***1.0000***	0.9233
R _1	0.8972	***1.0000***	0.9442	0.9661

Fig. 75 shows the result of incrementally and cumulatively extracting of the vibration signal time- and frequency-domain characteristic parameters.

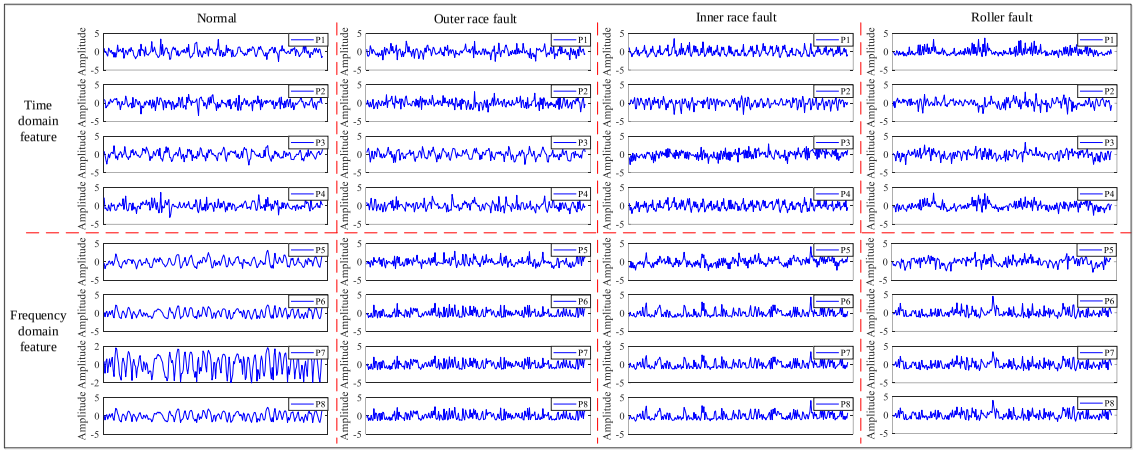

Fig. 75 The incremental accumulation extracted characteristic parameters under bearing normal and fault states

Tab. 19 shows the parameters extracted by part of vibration signal in the four states. Under the same parameter, the values of four states are different, and the differences are obvious. Thus, eight parameters are reasonable and can effectively distinguish the types of bearing faults.

Tab. 19 Characteristic parameters extracted from a section of vibration signal

Bearing state	Features parameters							
	P_1	P_2	P_3	P_4	P_5	P_6	P_7	P_8
N	2.139	0.084	2.595	14.348	8.067	0.044	0.115	46236.899
O	2.340	-0.010	4.534	29.481	12.628	0.061	0.135	85537.994
I	3.596	0.027	4.617	45.375	12.537	0.060	0.135	84665.293
R	2.793	0.058	4.601	37.954	13.314	0.054	0.116	77136.560

Fig. 76 shows that the that the differences in holographic characteristic fusion SDP images are obvious.

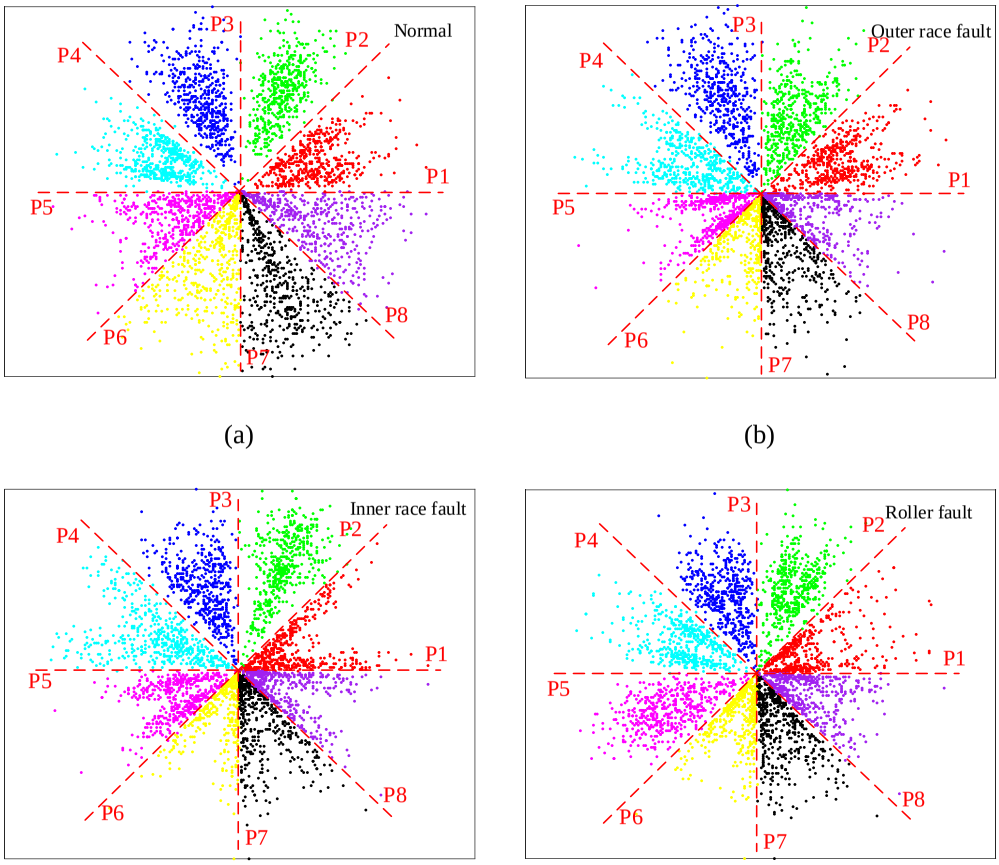

Fig. 76 holographic SDP images: (a) normal; (b) outer race fault; (c) inner race fault; (d) roller fault

Based on the holographic SDP, bearing faults are identified based on similarity. Therefore, Tab. 20 shows that the four states can achieve one-to-one correspondence and identify bearing faults accurately. The proposed method can effectively enhance the difference between signals and realize bearing fault diagnosis.

Tab. 20 Comparison of similarity based on holographic SDP

	N_2	O_2	I _2	R _2
N_1	***1.0000***	0.9030	0.9132	0.8743
O _1	0.8439	***1.0000***	0.9401	0.9521
I _1	0.6933	0.8209	***1.0000***	0.9571
R _1	0.7366	0.8552	0.9327	***1.0000***

6.5.3 Comparative experiment

In order to verify the effectiveness of this method, comparative experiments based on Case Western Reserve University data and image conversion methods are carried out respectively.

6.5.3.1 Case Western Reserve University data comparison

Based on the bearing data of Case Western Reserve University, the effectiveness of this method is verified. The similarity recognition results are shown in Tab. 21. It proves that the incrementally accumulated holographic SDP method in this study can accurately identify bearing faults.

Tab. 21 Similarity recognition results of Case Western Reserve signal

	N_2	O_2	I _2	R _2
N_1	***1.0000***	0.9108	0.9456	0.9725
O _1	0.9029	***1.0000***	0.9577	0.9778
I _1	0.9366	0.9340	***1.0000***	0.9659
R _1	0.9035	0.9344	0.9044	***1.0000***

6.5.3.2 Comparison of image visualization methods

At present, short-time Fourier transform (STFT), continuous wavelet decomposition (CWT), and Wigner-ville distribution (WVD) are the three common time-frequency feature imaging methods in the field of bearing visual diagnosis research. The definitions, advantages, and disadvantages are shown in Tab. 22.

Tab. 22 Time-frequency feature imaging methods

Methods	Literature	Formula	Characteristic
Short-time Fourier transform	[133], [134]	$STFT(\tau, f)=\int[f(\tau)\cdot\omega(\tau-t^*)]\cdot e^{-2\pi ik\tau}d\tau$	High-frequency signals are better reflected in the time-domain, while low-frequency signals in the frequency-domain.
Continuous wavelet decomposition	[135], [136]	$W(a,b;\psi)=\int_{-\infty}^{\infty}x(t)\psi_{a,b}(t)dt$	The selection of wavelet basis is difficult, and different wavelet basis has different results
Wigner-ville distribution	[137], [138]	$W(t, f)=\int_{-\infty}^{\infty}x(t+\frac{\tau}{2})x^*(t-\frac{\tau}{2})e^{-j2\pi f\tau}d\tau$	It will be interfered by the cross term when analyzing multi-component signals

Fig.77 shows the bearing vibration signal time-frequency images under normal and fault states using three methods. Images generated by the STFT and the CWT show that the difference between the four states is very minimal and difficult to distinguish. To verify the effects of these three methods in bearing fault diagnosis, the results based on similarity are shown in Tab. 23(1), (2), and (3).

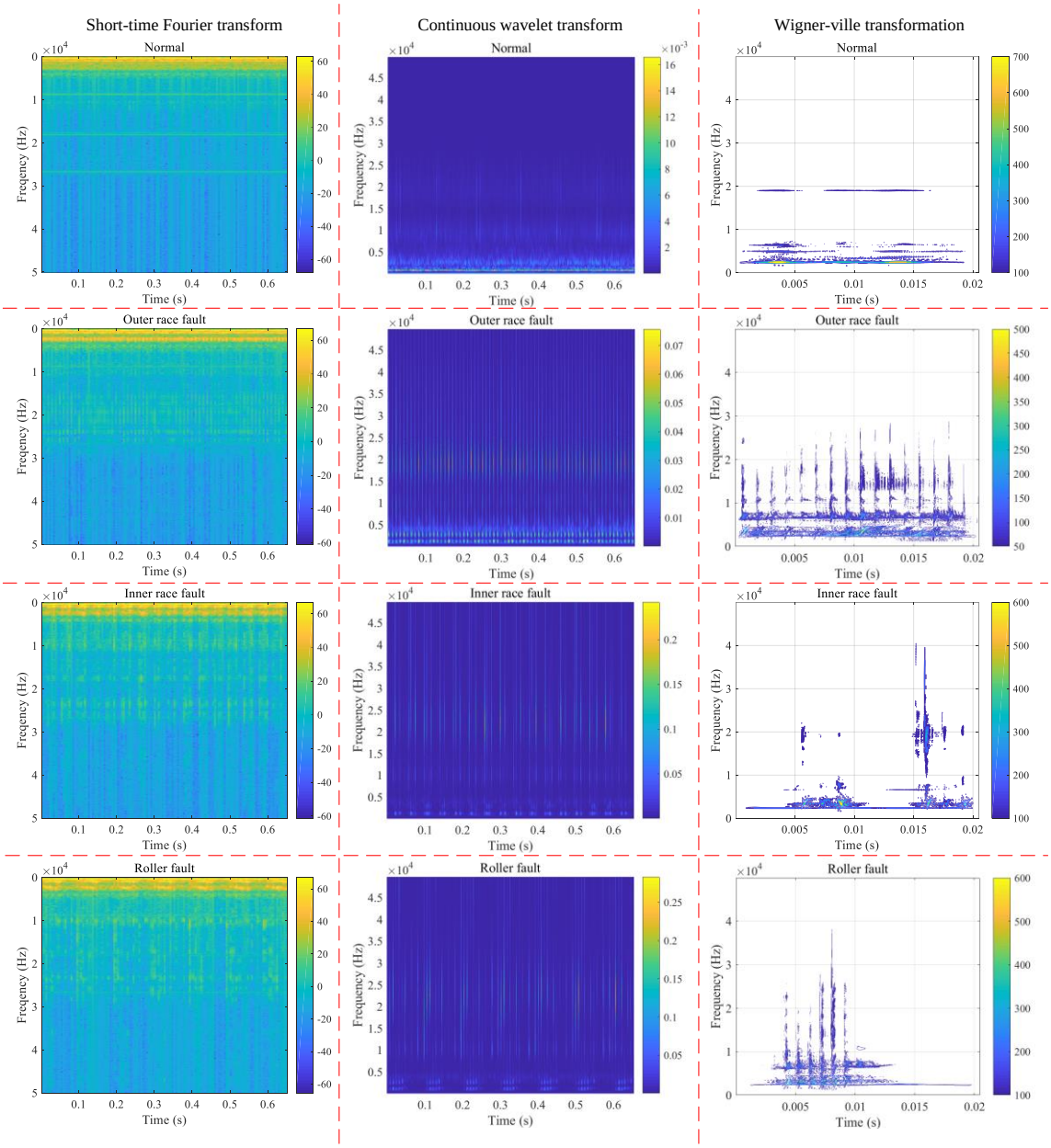

Fig. 77 Bearing vibration signal time-frequency images under normal and fault states by three methods

In Tab. 23(1) and 23(2), both the inner race (I) and roller (R) faults have been misdiagnosed, indicating that the STFT and CWT cannot effectively distinguish the changes in the time-frequency image. In Tab. 23(3), the roller fault (R) was misidentified. Although in Fig. 77, the WVD images are quite different, the similarity results cannot meet the diagnosis requirements.

Tab. 23(1) Similarity comparison based on STFT

	N_2	O _2	I _2	R _2
N_1	***1.0000***	0.9981	0.9984	0.9985
O _1	0.9988	***1.0000***	0.9983	0.9980
I _1	***1.0000***	0.9998	0.9989	0.9995
R _1	***1.0000***	0.9998	0.9998	0.9991

Tab. 23(2) Similarity comparison based on CWT

	N_2	O _2	I _2	R _2
N_1	***1.0000***	0.9997	0.9995	0.9998
O _1	0.9995	***1.0000***	0.9994	0.9997
I _1	***1.0000***	0.9996	0.9998	0.9994
R _1	***1.0000***	0.9998	0.9997	0.9999

Tab. 23(3) Similarity comparison based on WVD

	N_2	O _2	I _2	R _2
N_1	***1.0000***	0.6789	0.5735	0.5821
O_1	0.7636	***1.0000***	0.6471	0.6363
I _1	0.9168	0.8793	***1.0000***	0.7620
R_1	***1.0000***	0.9812	0.9572	0.6764

Based on the above analysis, the incremental accumulation holographic SDP characteristic fusion method can effectively extract the characteristic of vibration signals, increase the discrimination between signals, and realize accurate diagnosis of ship propulsion shaft bearing faults.

6.6 Conclusion

This chapter proposed an incrementally accumulated holographic SDP characteristic fusion method, which is used in the fault visual diagnosis research of rotating machinery. To address the problem on distinguishing the bearing fault vibration signals, the characteristic parameters in time- and frequency-domains were extracted to describe the change trend of vibration signals and its spectrum. In addition, the incremental accumulation method is adopted to extract the characteristic parameters, so that the changes can be displayed in time. Based on the SDP method, 1D parameters are simultaneously fused to a 2D image, which magnified the difference between the signals and laid the foundation for the fault diagnosis of the bearing.

Chapter 7 Conclusions and future works

7.1 Conclusions

The research on rotating machinery fault diagnosis is of great significance to ensure the safe operation of equipment, reduce the cost of regular maintenance and avoid malignant accidents. In this thesis, the rotating machinery vibration signal containing rich characteristic information is selected as the research object, and the signal processing research is carried out for key problems such as strong background noise, weak fault characteristics and complex interference frequency of vibration signal in rotating machinery diagnosis. The noise suppression and feature enhancement methods of weighted kurtosis VMD and improved frequency-weighted energy operator are studied; A method of non-stationary vibration signal separation and feature enhancement based on reconstruction adaptive determinate stationary subspace filtering and 1.5-dimensional third-order energy operator is constructed; An adaptive multi-band filtering method for accurately extract the actual rotating frequency in engineering signal is designed; The application of successive incrementally accumulated holographic SDP signal conversion method in rotating machinery fault visual diagnosis is studied. The main conclusions of this thesis are summarized as follows:

1) Aiming at the problems of strong background noise and weak fault characteristics in vibration signal in rotating machinery fault diagnosis, a signal processing method of weighted kurtosis VMD and improved FWEO is proposed. The VMD is employed to decompose signal, and the weighted kurtosis is applied to select the optimal IMFs which carry abundant fault information. The third-order cumulant is introduced into the FWEO to improve the analysis performance, and then the IFWEO is used to further improve the signal SNR and enhance the signal impulse.

2) In order to effectively filter the complex interference frequency components in the vibration signal and improve the fault characteristics, a bearing fault feature enhancement method of Rad-SSF and 1.5-dimensional third-order energy operator is proposed. An adaptive Rad-SSF method is developed for constant speed equipment non-stationary vibration signals with the characteristic of strong background noise and weak bearing fault impulse signal. Rad-SSF can adaptively self-determined reconstructs a trajectory matrix and decompose it into stationary and non-stationary signals to realize the extraction of the weak fault characteristic signal optimally. The improved demodulation method of 1.5D third-order energy spectrum is applied to enhance the impact signal feature caused by rotating machinery fault for its advantages of strengthening the fundamental frequency, and eliminating the non-coupling harmonic components.

3) In view of the difference between the actual rotating frequency and the theoretical value in the vibration signal of rotating machinery, an adaptive multi-band filtering is proposed to accurately extract the rotating frequency and its harmonics. In the adaptive multi-band filtering, a search threshold is designed to accurately extract the actual rotating frequency, and the deflection coefficient is set to ensure that the harmonics are within the optimal extraction range.

4) Aiming at the problem that the discrimination of different images is not obvious when the one-dimensional vibration signal is converted into a two-dimensional image, an incremental accumulation characteristic parameter extraction method is proposed to comprehensively record the characteristic change trend of vibration signals. Then, a holographic SDP characteristic fusion method is proposed to realize the image conversion of vibration signals. By fusing the characteristic parameters into one SDP image, discrimination between bearing fault vibration signals is increased.

7.2 Future works

In this thesis, the signal processing methods such as background noise suppression and fault feature enhancement of vibration signals in rotating machinery faults diagnosis are studied, and applications have been made in low-speed bearings, high-speed bearings, structural abnormalities, bearing visual diagnosis and so on. If conditions permit, future research needs to be further carried out in the following aspects:

1) This thesis mainly studies the processing method of vibration signal of rotating machinery at constant speed. For more complex operating conditions such as variable speed and variable load, it needs to be further studied.

2) This thesis mainly studies the single fault type of rotating machinery. For the compound fault of multi part coupling, the application effectiveness of the method studied in this paper needs to be further studied.

Reference

[1] Lucas C.Brito, Gian Antonio Susto, Jorge N. Brito, et al., “An explainable artificial intelligence approach for unsupervised fault detection and diagnosis in rotating machinery”, *Mechanical Systems and Signal Processing*, 2022, 163: 108105.

[2] Heng Sun, Min Xia, Yawei Hu, et al., “A new sorting feature-based temporal convolutional network for remaining useful life prediction of rotating machinery”, *Computers & Electrical Engineering*, 2021, 95: 107413.

[3] Hao Wei, Qinghua Zhang, Minghu Shang, et al., “Extreme learning Machine-based classifier for fault diagnosis of rotating Machinery using a residual network and continuous wavelet transform”, *Measurement*, 2021, 183: 109864.

[4] Jing Yuan, Ze Yao, Huiming Jiang, et al., “Multi-lifting synchrosqueezing transform for nonstationary signal analysis of rotating machinery”, *Measurement*, 2022, 191: 110758.

[5] Jungho Park, Yunhan Kim, Kyumin Na, et al., “An image-based feature extraction method for fault diagnosis of variable-speed rotating machinery”, *Mechanical Systems and Signal Processing*, 2022, 167: 108524.

[6] Yongbo Li, Shun Wang, Yang Yang, et al., “Multiscale symbolic fuzzy entropy: An entropy denoising method for weak feature extraction of rotating machinery”, *Mechanical Systems and Signal Processing*, 2022, 162: 108052.

[7] Na Lu, Mingliang Li, Guangtao Zhang, et al., “Fault feature extraction method for rotating machinery based on a CEEMDAN-LPP algorithm and synthetic maximum index”, *Measurement*, 2022, 189: 110636.

[8] Zhiqiang Zhang, and Qingyu Yang, “Unsupervised feature learning with reconstruction sparse filtering for intelligent fault diagnosis of rotating machinery”, *Applied Soft Computing*, 2022, 115: 108207.

[9] Guoqiang Li, Jun Wu, Chao Deng, et al., “Parallel multi-fusion convolutional neural networks based fault diagnosis of rotating machinery under noisy environments”, *ISA Transactions*, 2021, online.

[10] Wei Li, Xiang Zhong, Haidong Shao, et al., “Multi-mode data augmentation and fault diagnosis of rotating machinery using modified ACGAN designed with new framework”, *Advanced Engineering Informatics*, 2022, 52: 101552.

[11] Fuming Zhou, Jun Han, and Xiaoqiang Yang, “Multivariate hierarchical multiscale fluctuation dispersion entropy: Applications to fault diagnosis of rotating machinery”, *Applied Acoustics*, 2021, 182(1-2): 108271.

[12] Pengfei Liang, Chao Deng, Jun Wu, et al., “Intelligent fault diagnosis of rotating machinery via wavelet transform, generative adversarial nets and convolutional neural network”, *Measurement*, 2020, 159: 107768.

[13] Jingli Yang, Yongqi Chang, Tianyu Gao, et al., “Failure prediction of the rotating machinery based on ceemdan-apen feature and ar-ukf model”, *Applied Sciences*, 2020, 10(6): 2056.

[14] Yongbo Li, Xianzhi Wang, Shubin Si, et al., “A new intelligent fault diagnosis method of rotating machinery under varying-speed conditions using infrared thermography”, *Complexity*, 2019, 2019(5): 1-12.

[15] Yiwei Cheng, Manxi Lin, Jun Wu, et al., “Intelligent fault diagnosis of rotating machinery based on continuous wavelet transform-local binary convolutional neural network”, *Knowledge-Based Systems*, 2021, 216: 106796.

[16] Shaomin Zhu, Hong Xia, Binsen Peng, et al., “Yingying Jiang, Feature extraction for early fault detection in rotating machinery of nuclear power plants based on adaptive VMD and Teager energy operator”, *Annals of Nuclear Energy*, 2021, 160: 108392.

[17] Yibing Li, Weiteng Zou, and Li Jiang, “Fault diagnosis of rotating machinery based on combination

of Wasserstein generative adversarial networks and long short-term memory fully convolutional network", *Measurement*, 2022, 191: 110826.

[18] Dong Zhang, and Zhipeng Feng, "Enhancement of time-frequency post-processing readability for nonstationary signal analysis of rotating machinery: Principle and validation", *Mechanical Systems and Signal Processing*, 2022, 163: 108145.

[19] Kaixuan Liang, Ming Zhao, Jing Lin, et al., "Maximum average kurtosis deconvolution and its application for the impulsive fault feature enhancement of rotating machinery", *Mechanical Systems and Signal Processing*, 2021, 149: 107323.

[20] Yongxing Song, Jingting Liu, Ning Chu, et al., "A novel demodulation method for rotating machinery based on time-frequency analysis and principal component analysis", *Journal of Sound and Vibration*, 2019, 442: 645-656.

[21] Wei Li, Zhencai Zhu, Fan Jiang, et al. "Fault diagnosis of rotating machinery with a novel statistical feature extraction and evaluation method", *Mechanical Systems and Signal Processing*, 2015, 50 - 51: 414 - 426.

[22] Chuan Li, Diego Cabrera, José Valente de Oliveira, et al., "Extracting repetitive transients for rotating machinery diagnosis using multiscale clustered grey infogram", *Mechanical Systems and Signal Processing*, 2016, 76: 157 - 173.

[23] Lei Wang, Zhiwen Liu, Qiang Miao, et al., "Time-frequency analysis based on ensemble local mean decomposition and fast kurtogram for rotating machinery fault diagnosis", *Mechanical Systems and Signal Processing*, 2018, 103: 60 - 75.

[24] Liuyang Song, Huaqing Wang, and Peng Chen, "Vibration-based intelligent fault diagnosis for roller bearings in low-speed rotating machinery", *IEEE Transactions on Instrumentation and Measurement*, 2018, 67(8): 1887 - 1899.

[25] Myungyon Kim, Jin Uk Ko, Jinwook Lee, et al., "A domain adaptation with semantic clustering (dasc) method for fault diagnosis of rotating machinery", *ISA Transactions*, 2022, 120: 372 - 382.

[26] Jinwook Lee, Myungyon Kim, Jin Uk Ko, et al., "Asymmetric inter-intra domain alignments (AIIDA) method for intelligent fault diagnosis of rotating machinery", *Reliability Engineering & System Safety*, 2022, 218: 108186.

[27] Yuanhong Chang, Jinglong Chen, Haixin Lv, et al., "Heterogeneous bi-directional recurrent neural network combining fusion health indicator for predictive analytics of rotating machinery", *ISA Transactions*, 2021, 122: 409 - 423.

[28] Yaowei Shi, Aidong Deng, Xue Ding, et al., "Multisource domain factorization network for cross-domain fault diagnosis of rotating machinery: An unsupervised multisource domain adaptation method", *Mechanical Systems and Signal Processing*, 2022, 164: 108219.

[29] Shangjun Ma, Wei Cai, Kaiwen Liu, et al., "A lighted deep convolutional neural network-based fault diagnosis of rotating machinery", *Sensors*, 2019, 19(10): 2381.

[30] Ruonan Liu, Boyuan Yang, Enrico Zio, et al., "Artificial intelligence for fault diagnosis of rotating machinery: A review", *Mechanical Systems and Signal Processing*, 2018, 108: 33 - 47.

[31] Feng Jia, Lei Yaguo, Jing Lin, et al., "Deep neural networks: A promising tool for fault characteristic mining and intelligent diagnosis of rotating machinery with massive data", *Mechanical Systems and Signal Processing*, 2016, 72-73: 303 - 315.

[32] Min Xia, Teng Li, Lin Xu, et al., "Fault diagnosis for rotating machinery using multiple sensors and convolutional neural networks", *IEEE/ASME Transactions on Mechatronics*, 2017, 23(1): 101 - 110.

[33] Guangyao Zhang, Yi Wang, Xiaomeng Li, et al., "Enhanced symplectic geometry mode decomposition and its application to rotating machinery fault diagnosis under variable speed conditions", *Mechanical Systems and Signal Processing*, 2022, 170: 108841.

[34] Yanli Ma, Junsheng Cheng, Ping Wang, et al., "Rotating machinery fault diagnosis based on multivariate multiscale fuzzy distribution entropy and Fisher score", *Measurement*, 2021,179:

109495.

[35] Xiaowang Chen, and Zhipeng Feng, “Order spectrum analysis enhanced by surrogate test and Vold-Kalman filtering for rotating machinery fault diagnosis under time-varying speed conditions”, *Mechanical Systems and Signal Processing*, 2021, 154: 107585.

[36] Yahui Zhang, Taotao Zhou, Xufeng Huang, et al., “Fault diagnosis of rotating machinery based on recurrent neural networks”, *Measurement*, 2021, 171: 108774.

[37] Xiaoli Zhao, and Minping Jia, “A new Local-Global Deep Neural Network and its application in rotating machinery fault diagnosis”, *Neurocomputing*, 2019, 366: 215 - 233.

[38] Lei Wang, Zhiwen Liu, Hongrui Cao, et al., “Subband averaging kurtogram with dual-tree complex wavelet packet transform for rotating machinery fault diagnosis”, *Mechanical Systems and Signal Processing*, 2020, 142: 106755.

[39] Lei Xiao, Junxuan Tang, Xinghui Zhang, et al., “Weak fault detection in rotating machineries by using vibrational resonance and coupled varying-stable non-linear systems”, *Journal of Sound and Vibration*, 2020, 478: 115355.

[40] Peng Zhou, Yang Yang, Hong Wang, et al., “The relationship between fault-induced impulses and harmonic-cluster with applications to rotating machinery fault diagnosis”, *Mechanical Systems and Signal Processing*, 2020, 144: 106896.

[41] Brandon Van Hecke, Jae Yoon, and David He, “Low speed bearing fault diagnosis using acoustic emission sensors,” *Applied Acoustics*, 2016, 105: 35 - 44.

[42] Henry Omoregbee, and Stephan Heyns, “Fault Classification of Low-Speed Bearings Based on Support Vector Machine for Regression and Genetic Algorithms Using Acoustic Emission,” *Journal of Vibration Engineering and Technologies*, 2019, 7(5): 455 - 464.

[43] Wael Moustafa, Cousinard Olivier, Fabrice Bolaers, et al., “Low speed bearings fault detection and size estimation using instantaneous angular speed,” *Journal of Vibration and Control*, 2016, 22(15): 3413 - 3425.

[44] Lili Bai, Zhennan Han, Jiajun Ren, et al., “Research on feature selection for rotating machinery based on supervision kernel entropy component analysis with whale optimization algorithm”, *Applied Soft Computing*, 2020, 92: 106245.

[45] A Khadersab, and S Shivakumar, “Vibration Analysis Techniques for Rotating Machinery and its effect on Bearing Faults”, *Procedia Manufacturing*, 2018, 20: 247 - 252.

[46] Xunshi Yan, Zhe Sun, Jingjing Zhao, et al., “Fault diagnosis of rotating machinery equipped with multiple sensors using space-time fragments”, *Journal of Sound and Vibration*, 2019, 456: 49 - 64.

[47] Fafa Chen, Baoping Tang, Tao Song, et al., “Multi-fault diagnosis study on roller bearing based on multi-kernel support vector machine with chaotic particle swarm optimization”, *Measurement*, 2014, 47: 576 - 90.

[48] Zhiwei Cheng, and Bin Cai, “Predicting the remaining useful life of rolling element bearings using locally linear fusion regression”, *Journal of Intelligent and Fuzzy Systems*, 2018, 34(6): 1 - 12.

[49] Zehui Hua, Juanjuan Shi, Yang Luo, et al., “Iterative matching synchrosqueezing transform and application to rotating machinery fault diagnosis under nonstationary conditions”, *Measurement*, 2021, 173: 108592.

[50] Masoud Jalayer, Carlotta Orsenigo, and Carlo Vercellis, “Fault detection and diagnosis for rotating machinery: A model based on convolutional LSTM, Fast Fourier and continuous wavelet transforms”, *Computers in Industry*, 2021, 125: 103378.

[51] Zhiliang Liu, Yaqiang Jin, Ming J. Zuo, et al., “ACCUGRAM: A novel approach based on classification to frequency band selection for rotating machinery fault diagnosis”, *ISA Transactions*, 2019, 95: 346 - 357.

[52] Jinde Zheng, Haiyang Pan, Shubao Yuan, et al., “Adaptive parameterless empirical wavelet transform based time-frequency analysis method and its application to rotor rubbing fault diagnosis”, *Signal*

Processing, 2017, 130: 305 - 314.

[53] Ying Zhang, Kangshuo Xing, Ruxue Bai, et al., "An enhanced convolutional neural network for bearing fault diagnosis based on time–frequency image", Measurement, 2020, 157: 107667.

[54] Shan Pang, Xinyi Yang, Xiaofeng Zhang, et al., "Fault diagnosis of rotating machinery with ensemble kernel extreme learning machine based on fused multi-domain features", *ISA Transactions*, 2020, 98: 320 - 337.

[55] Ali Dibaj, Mir Mohammad Ettefagh, Reza Hassannejad, et al., "A hybrid fine-tuned VMD and CNN scheme for untrained compound fault diagnosis of rotating machinery with unequal-severity faults", *Expert Systems with Applications*, 2021, 167: 114094.

[56] Zhiqiang Liao, Xuewei Song, Baozhu Jia, et al., "Bearing Fault Feature Enhancement and Diagnosis Based on Statistical Filtering and 1.5-Dimensional Symmetric Difference Analytic Energy Spectrum," *IEEE Sensors Journal*, 2021, 21(8): 9959 - 9968.

[57] Huaiqian Bao, Zhenhao Yan, Shanshan Ji, et al., "An enhanced sparse filtering method for transfer fault diagnosis using maximum classifier discrepancy," Measurement Science and Technology, 2021, 32(8): 1 - 12.

[58] Moise Avoci Ugwiri, Marco Carratú, Vincenzo Paciello, et al., "Benefits of enhanced techniques combining negentropy, spectral correlation and kurtogram for bearing fault diagnosis", *Measurement*, 2021, 185: 110013.

[59] Xuefang Xu, Zijian Qiao, and Yaguo Lei, "Repetitive transient extraction for machinery fault diagnosis using multiscale fractional order entropy infogram," Mechanical Systems and Signal Processing, 2018, 103: 312 - 326.

[60] Yusuke Kobayashi, Liuyang Song, Masaru Tomita, et al., "Automatic Fault Detection and Isolation Method for Roller Bearing Using Hybrid-GA and Sequential Fuzzy Inference," *Sensors*, 2019, 19(16): 3553.

[61] Xiaohui Gu, Shaopu Yang, Yongqiang Liu, et al., "Rolling element bearing faults diagnosis based on kurtogram and frequency domain correlated kurtosis," *Measurement Science and Technology*, 2016, 27(12): 125019.

[62] Kaixuan Liang, Ming Zhao, Jing Lin, et al., "A Novel Indicator to Improve Fast Kurtogram for the Health Monitoring of Rolling Bearing," *IEEE Sensors Journal*, 2020, 20(20): 12252 - 12261.

[63] Andre A.Silva, ShalabhGupta, Ali M.Bazzi, et al., "Waveletbased information filtering for fault diagnosis of electric drive systems in electric ships," 2018, *ISA Transactions*, 78: 105 - 115.

[64] Kamel Belaid, Abdelhamid Miloudi, and Hadjila Bournine, "The processing of resonances excited by gear faults using continuous wavelet transform with adaptive complex morlet wavelet and sparsity measurement," *Measurement*, 2021, 180(5): 109576.

[65] Qing Xiong, Yanhai Xu, Yiqiang Peng, et al., "Lowspeed rolling bearing fault diagnosis based on EMD denoising and parameter estimate with alpha stable distribution," *Journal of Mechanical Science and Technology*, 2017, 31(4): 1587 - 1601.

[66] Ke Zhang, Tianran Lin, and Xia Jin, "Low speed bearing fault diagnosis based on EMD-CIIT histogram entropy and KFCM clustering," *Journal of Shanghai Jiaotong University (Science)*, 2019, 24(5): 616 - 621.

[67] Liye Zhao, Wei Yu, and Ruqiang Yan, "Rolling bearing fault diagnosis based on ceemd and time series modeling", *Mathematical Problems in Engineering*, 2014, 2014(2014): 1 - 13.

[68] Xuerong Ye, Yifan Hu, Juxian Shen, et al., "An adaptive optimized TVF-EMD based on a sparsity-impact measure index for bearing incipient fault diagnosis", *IEEE Transactions on Instrumentation and Measurement*, 70: 1 - 10.

[69] Yongjian Sun, Shaohui Li, Yaling Wang, et al., "Fault diagnosis of rolling bearing based on empirical mode decomposition and improved manhattan distance in symmetrized dot pattern image," *Mechanical Systems and Signal Processing*, 2021, 159: 107817.

[70] Fuzheng Liu, Junwei Gao, and Liu Huabo, “The feature extraction and diagnosis of rolling bearing based on CEEMD and LDWPSO-PNN”, *IEEE Access*, 2020, 8: 19810 - 19819.

[71] Shuzhi Gao, Quan Wang, Yimin Zhang, “Rolling bearing fault diagnosis based on ceemdan and refined composite multi-scale fuzzy entropy”, *IEEE Transactions on Instrumentation and Measurement*, 2021, 70: 1 - 10.

[72] Lida Liao, Bin Huang, Qi Tan, et al., “Development of an Improved LMD Method for the LowFrequency Elements Extraction from Turbine Noise Background,” *Energies*, 2020, 13(4): 1 - 17.

[73] Yu Zhang, Zhuoyou Fan, Xiaorong Gao, et al., “A Fault Diagnosis Method of Train Wheelset Rolling Bearing Combined with Improved LMD and FK,” *Journal of Sensors*, 2019, 2019(18): 1 - 11.

[74] Lei Wang, Zhiwen Liu, Qiang Miao, et al., “Time–frequency analysis based on ensemble local mean decomposition and fast kurtogram for rotating machinery fault diagnosis,” *Mechanical Systems and Signal Processing*, 2018, 103: 60 - 75.

[75] Jianbo Yu, and Jingxiang Lv, “Weak fault feature extraction of rolling bearings using local mean decomposition-based multilayer hybrid denoising”, *IEEE Transactions on Instrumentation and Measurement*, 2017, 66(12): 3148 - 3159.

[76] Jinbao Zhang, Yongqiang Zhao, Xinglin Li, et al., “Bearing fault diagnosis with kernel sparse representation classification based on adaptive local iterative filtering-enhanced multiscale entropy features”, *Mathematical Problems in Engineering*, 2019, 2019(17): 1 - 17.

[77] Lei Zhao, Yongxiang Zhang, and Danchen Zhu, “Rolling Element Bearing Fault Diagnosis Based on Adaptive Local Iterative Filtering Decomposition and Teager–Kaiser Energy Operator”, *Journal of Failure Analysis and Prevention*, 2019, 2019(4): 1018 - 1022.

[78] Mingyue Yu, and Xiang Pan, “A novel ITD-GSP-based characteristic extraction method for compound faults of rolling bearing,” *Measurement*, 2020, 159: 107736.

[79] Jiansong Zhou, Ka-kit Tung, and King-Fa Li, “Multi-decadal variability in the Greenland ice core records obtained using intrinsic timescale decomposition,” *Climate Dynamics*, 2016, 47(3 - 4): 739 - 752.

[80] Jianbo Yu, and Haiqiang Liu, “Sparse coding shrinkage in intrinsic time-scale decomposition for weak fault feature extraction of bearings”, *IEEE Transactions on Instrumentation and Measurement*, 2018, 67(7): 1579 - 1592.

[81] Ying Zhang, Chao Zhang, Xinyuan Liu, et al., “Fault diagnosis method of wind turbine bearing based on improved intrinsic time-scale decomposition and spectral kurtosis”, *2019 Eleventh International Conference on Advanced Computational Intelligence (ICACI). IEEE*, 2019.

[82] Jiakai Ding, Liangpei Huang, Dongming Xiao, et al., “GMPSOVMD algorithm and its application to rolling bearing fault feature extraction,” *Sensors*, 2020, 20(7): 1946 - 1969.

[83] Xin Li, Zengqiang Ma, De Kang, et al., “Fault diagnosis for rolling bearing based on VMD-FRFT,” *Measurement*, 2020, 155: 1 - 17.

[84] Zipeng Li, Jinglong Chen, Yanyang Zi, et al., “Independence-oriented VMD to identify fault feature for wheel set bearing fault diagnosis of high speed locomotive,” *Mechanical Systems and Signal Processing*, 2017, 85: 512 - 529.

[85] Ali Dibaj, Reza Hassannejad, Mir Mohammad Ettefagh, et al., “Incipient fault diagnosis of bearings based on parameter-optimized VMD and envelope spectrum weighted kurtosis index with a new sensitivity assessment threshold,” *ISA Transactions*, 2021, 114: 413 - 433.

[86] Gang Yao, Yunce Wang, Mohamed Benbouzid, et al, “A Hybrid Gearbox Fault Diagnosis Method Based on GWO-VMD and DE-KELM,” *Applied Sciences*, 2021, 11(4996): 1 - 29.

[87] Xinglong Pei, Xiaoyang Zheng, and Jinliang Wu, “Intelligent bearing fault diagnosis based on Teager energy operator demodulation and multiscale compressed sensing deep autoencoder”, *Measurement*, 2021, 179, 109452.

[88] Maosen Cao, Wei Xu, Wieslaw Ostachowicz, et al, “Damage identification for beams in noisy conditions based on Teager energy operator-wavelet transform modal curvature”, *Journal of Sound and Vibration*, 2014, 333(6): 1543 - 1553.

[89] Ming Liang, and I. Soltani Bozchalooi, “An energy operator approach to joint application of amplitude and frequency-demodulations for bearing fault detection”, *Mechanical Systems and Signal Processing*, 2010, 24(5): 1473 - 1494.

[90] A. Gałęzia, and K. Gryllias, “Application of the combined Teager-Kaiser envelope for bearing fault diagnosis”, *Measurement*, 2021, 182: 109710.

[91] Tian Han, Qiannan Liu, Li Zhang, et al., “Fault feature extraction of low speed roller bearing based on Teager energy operator and CEEMD,” *Measurement*, 2019, 138: 400 - 408.

[92] John M. O'Toole, Andriy Temko, and Nathan Stevenson, “Assessing instantaneous energy in the EEG: a non-negative, frequencyweighted energy operator”, *In 2014 36th Annual International Conference of the IEEE Engineering in Medicine and Biology Societypp*, 2014, 3288 - 3291.

[93] Yuanbo Xu, Fan Fan, and Xiangkui Jiang, “A fast iterative filtering decomposition and symmetric difference analytic energy operator for bearing fault extraction”, *ISA Transactions*, 2021, 108: 317 - 332.

[94] H. Faghidi, and Ming Liang, “Bearing fault identification by higher order energy operator fusion: A non-resonance based approach”, *Journal of Sound and Vibration*, 2016, 381: 83 - 100.

[95] Yacine Imaouchen, Mourad Kedadouche, and Rezak Alkama, “A frequency-weighted energy operator and complementary ensemble empirical mode decomposition for bearing fault detection”, *Mechanical Systems and Signal Processing*, 2017, 82: 103 - 116.

[96] Xiaoxi Ding, Quanchang Li, Lun Lin, et al., “Fast time-frequency manifold learning and its reconstruction for transient feature extraction in rotating machinery fault diagnosis”, *Measurement*, 2019, 141: 380 - 395.

[97] Chang Liu, “A tacholess order tracking method based on inverse short time Fourier transform and singular value decomposition for bearing fault diagnosis”, *Sensors*, 2019, 20: 6924.

[98] Zhihao Chen, Jian Cen, Jianbin Xiong, et al., “Rolling bearing fault diagnosis using time-frequency analysis and deep transfer convolutional neural network”, *IEEE Access*, 8: 150248 - 150261.

[99] Xin Zhang, Zhiwen Liu, Jiaxu Wang, et al., “Time–frequency analysis for bearing fault diagnosis using multiple Q-factor Gabor wavelets”, *ISA Transactions*, 2018, 82: 225 - 234.

[100] Pravin Singru, Vishnuvardhan Krishnakumar, and Dwarkesh Natarajan, “Bearing failure prediction using Wigner–Ville distribution, modified Poincare mapping and fast Fourier transform”, *Journal of Vibroengineering*, 2018, 20: 127 - 137.

[101] Hongwei Fan, Sijie Shao, Xuhui Zhang, et al., “Intelligent fault diagnosis of rolling bearing using FCM clustering of EMD-PWVD vibration images”, *IEEE Access*, 2020, 8: 145194 - 145206.

[102] Attoui Issam, Fergani Nadir, Boutasseta Nadir, et al., “A new time-frequency method for identification and classification of ball bearing faults”, *Journal of Sound and Vibration*, 2017, 397: 241 - 265.

[103] Miao He, and David He, “Deep learning based approach for bearing fault diagnosis”, *IEEE Transactions on Industry Applications*, 2017, 53(3): 3057 - 3065.

[104] Yiwei Cheng, Manxi Lin, Jun Wu, et al., “Intelligent fault diagnosis of rotating machinery based on continuous wavelet transform-local binary convolutional neural network”, *Knowledge-Based Systems*, 2021, 216(1): 106796.

[105] Hosseini Sadegh, Ahmadi Najafabadi Mehdi, and Akhlaghi Mehdi, “Classification of acoustic emission signals generated from journal bearing at different lubrication conditions based on wavelet analysis in combination with artificial neural network and genetic algorithm”, *Tribology International*, 2016, 95: 426 - 434.

[106] Israel Ruiz Quinde, Jorge Chuya Sumba, Luis Escajeda Ochoa, et al., “Bearing fault diagnosis based

on optimal time-frequency representation method", *IFAC-PapersOnLine*, 2019, 52(11): 194 - 199.

[107] Cheng Yang, Zhinong Li, Jin Yuan, et al., "Fractional-order smoothed pseudo wigner-ville distribution and its applications in machinery fault diagnosis", *2017 Prognostics and System Health Management Conference (PHM-Harbin). IEEE*, 2017.

[108] Hui Wang, Jiawen Xu, Ruqiang Yan, et al. "A new intelligent bearing fault diagnosis method using SDP representation and SE-CNN", *IEEE Transactions on Instrumentation and Measurement*, 2020, 69: 2377 - 2389.

[109] Yongjian Sun, Shaohui Li, and Xiaohong Wang, "Bearing fault diagnosis based on EMD and improved Chebyshev distance in SDP image", *Measurement*, 2021, 176: 109100.

[110] Miyazaki Shuuji, Xuewei Song, Zhiqiang Liao, et al., "Low-speed bearing fault diagnosis based on improved statistical filtering and convolutional neural network", *Measurement Science and Technology*, 2021, 32(11): 115009.

[111] Syahril Ramadhan Saufi, Zair Asrar Bin Ahmad, Mohd Salman Leong, et al., "Low-speed bearing fault diagnosis based on ARSSAE model using acoustic emission and vibration signals", *IEEE Access*, 2019, 7: 46885 - 46897.

[112] Sharma, Rahul, Sircar Pradip, and Pachori Ram Bilas, "Automated focal EEG signal detection based on third order cumulant function", *Biomedical signal processing and control*, 2020, 58:101856.1 - 101856.8.

[113] Xiaoan Yan, Minping Jia, and Ling Xiang, "Compound fault diagnosis of rotating machinery based on OVMD and a 1.5-dimension envelope spectrum", *Measurement Science and Technology*, 2016, 27(7): 075002 - 075020.

[114] Erhao Meng, Shengzhi Huang, Qiang Huang, et al., "A hybrid VMD-SVM model for practical streamflow prediction using an innovative input selection framework", *Water Resources Management*, 2021, 1 - 17.

[115] Guangyi Chen, Changfeng Yan, Jiadong Meng, et al., "Improved VMD-FRFT based on initial center frequency for early fault diagnosis of rolling element bearing", *Measurement Science and Technology*, 2021, 32(11): 115024.

[116] Ramakrishna Thirumuru, and Anil Kumar Vuppala, "Application of non-negative frequency-weighted energy operator for vowel region detection", *International Journal of Speech Technology*, 2018, 21(2): 1 - 13.

[117] Xiaojiao Gu, Changzheng Chen, and Hyeong Joon Ahn, "Rolling bearing fault signal extraction based on stochastic resonance-based denoising and VMD", *International Journal of Rotating Machinery*, 2017, 2017: 531 - 544.

[118] Yi Qin, Lei Jin, Aibing Zhang, et al., "Rolling bearing fault diagnosis with adaptive harmonic kurtosis and improved bat algorithm", *IEEE Transactions on Instrumentation and Measurement*, 2020, 70: 1 - 12.

[119] Dehao Wu, Li Sheng, and Donghua Zhou, "Dynamic stationary subspace analysis for monitoring nonstationary dynamic processes", *Industrial & Engineering Chemistry Research*, 2020, 59(47): 20787 - 20797.

[120] Zhiqiang Liao, Liuyang Song, Peng Chen, et al., "An automatic filtering method based on an improved genetic algorithm—with application to rolling bearing fault signal extraction", *IEEE Sensors Journal*, 2017, 17(19): 6340 - 6349.

[121] Shilun Zuo, and Zhiqiang Liao, "Bearing fault dominant symptom parameters selection based on canonical discriminant analysis and false nearest neighbor using GA filtering signal", *Mathematical Problems in Engineering*, 2020, 8: 1 - 13.

[122] Wanke Yu, Chunhui Zhao, and Biao Huang, "Stationary Subspace Analysis-Based Hierarchical Model for Batch Processes Monitoring", *IEEE Transactions on Control Systems Technology*, 2020, 29(1): 444 - 453.

[123] Junhao Chen, and Chunhui Zhao, “Exponential stationary subspace analysis for stationary feature analytics and adaptive nonstationary process monitoring”, *IEEE Transactions on Industrial Informatics*, 2021, 99(12): 8345 - 8356.

[124] Xinglong Pei, Xiaoyang Zheng, and Jinliang Wu, “Intelligent bearing fault diagnosis based on Teager energy operator demodulation and multiscale compressed sensing deep autoencoder”, *Measurement*, 2021, 179(6): 109452.

[125] Hongshan Zhao, and Lang Li, “Fault diagnosis of wind turbine bearing based on variational mode decomposition and teager energy operator”, *IET Renewable Power Generation*, 2016, 11(4): 453 - 460.

[126] Andrew Vigoren, and James M. Zavislan, “Optical sectioning enhancement using higher-order moment signals in random speckle-structured illumination microscopy”, *Journal of The Optical Society of America A-optics Image Science and Vision*, 2018, 35(3): 474 - 479.

[127] Yifan Li, Ming Jing Zuo, and Yuejian Chen, “An enhanced morphology gradient product filter for bearing fault detection”, *Mechanical Systems Signal Processing*, 2018, 109: 166 - 184.

[128] Zhaoyi Guan, Peng Chen, Xiao Zhang, et al., “Vibration analysis of shaft misalignment and diagnosis method of structure faults for rotating machinery”, *International Journal of Performability Engineering*, 2017, 13(4): 337 - 347.

[129] Ke Li, Xiong Meng, Fucai Li, et al., “A novel fault diagnosis algorithm for rotating machinery based on a sparsity and neighborhood preserving deep extreme learning machine”, *Neurocomputing*, 2019, 350: 261 - 270.

[130] Xin Shu, Xiaodi Zhang, and Fan Xu, “Automatic diagnosis of microgrid networks’ power device faults based on stacked denoising autoencoders and adaptive affinity propagation clustering”, *Complexity*, 2020, 1 - 24.

[131] Xiaofeng Yuan, Ou Chen, Yalin Wang, et al., “Deep quality related feature extraction for soft sensing modeling: a deep learning approach with hybrid VW-SAE”, *Neurocomputing*, 2020, 396: 375 - 382.

[132] Wei Gao, Rongjong Wai, and Shiqun Chen, “Novel PV fault diagnoses via SAE and improved multi-grained cascade forest with string voltage and currents measures”, *IEEE Access*, 2020, 8: 133144 - 133160.

[133] Manap Mustafa, Nikolovski Srete, Skamyin Aleksandr, et al., “An analysis of voltage source inverter switches fault classification using short time Fourier transform”, *International Journal of Power Electronics and Drive Systems*, 2021, 12(4): 2209 - 2220.

[134] Hamid Reza Ahmadi, Navideh Mahdavi, and Mahmoud Bayat, “A novel damage identification method based on short time Fourier transform and a new efficient index”, *Structures*, 2021, 33(4): 3605 - 3614.

[135] Izat Shahsenov a, Ruslan Malikov a, Peter Cook b, et al., “Prediction of gamma ray data from pre-stack seismic reflection partial angle stacks using continuous wavelet transform and convolutional neural network approach”, *Journal of Applied Geophysics*, 2022, 197: 104523.

[136] Tian Han, and Zhiqiang Chao, “Fault diagnosis of rolling bearing with uneven data distribution based on continuous wavelet transform and deep convolution generated adversarial network”, *Journal of the Brazilian Society of Mechanical Sciences and Engineering*, 2021, 43(9): 425.

[137] Yanping Liu, Zheng Ma, Huiqin Jia, et al., “Seismic signal filtering based on pseudo wigner-ville distribution and catte model”, *Journal of Physics: Conference Series*, 2021, 1894(1): 012058.

[138] Tianji Xu, Bingjie Cheng, Shuangcen Niu, et al., “A microscopic ancient river channel identification method based on maximum entropy principle and Wigner-Ville Distribution and its application”, *Petroleum Exploration and Development*, 2021, 48(6): 1354 - 1366.

Acknowledge

Three years have passed inadvertently, and I'm already in the last year in my Ph.D program. I would like to express my gratitude to all those who helped me during the study life at Mie University.

I gratefully acknowledge the help of my teacher, Prof. Jinyama Ho**,** who has offered me valuable suggestions in the academic studies. He gave me the opportunity to study at Mie University, his profound knowledge, high sense of responsibility, rigorous academic attitude and unique insights gave me great enlightenment. The approachable character and demeanor of the Prof. Jinyama Ho have had a positive impact on me. Here, I would like to extend my sincerest gratitude and highest respect to my teacher.

I would like to express my gratitude to all the teachers and staffs in bio-resoures Mie university for their great help in my three years' study and life.

I would also like to thank everyone in the laboratory for their enthusiastic help during the experimental and thesis stage, and thank you for your joint discussion and sincere help.

Finally, I would like to thank my family who gave me the greatest help, it is your great support that allows me to realize my dream. Thank you for giving me life and health, and giving me the opportunity to learn knowledge. You are my forever strong backing.

XUEWEI SONG

August, 2022